SKB

TECHNICAL REPORT 88-30

Rheological properties of sodium smectite clay

Lennart Börgesson, Harald Hökmark, Ola Karnland

Clay Technology AB, Lund, Sweden

December 1988

SVENSK KÄRNBRÄNSLEHANTERING AB
SWEDISH NUCLEAR FUEL AND WASTE MANAGEMENT CO

BOX 5864 S-102 48 STOCKHOLM
TEL 08-665 28 00 TELEX 13108-SKB

RHEOLOGICAL PROPERTIES OF SODIUM SMECTITE CLAY

Lennart Börgesson, Harald Hökmark, Ola Karnland

Clay Technology AB, Lund, Sweden

December 1988

CONTENTS Page

RHEOLOGICAL PROPERTIES OF SODIUM SMECTITE CLAY

Lennart Börgesson
Harald Hökmark
Ola Karnland

Clay Technology AB
Lund, Sweden

Keywords: Clay, bentonite, smectite, Na-smectite, rheology, mechanical properties, triaxial tests, shear tests, creep tests, oedometer tests, consolidation, swelling, permeability

SUMMARY

The rheological properties of Na-smectite Mx-80 have been investigated by various laboratory tests. The investigations include determination of the hydraulic conductivity, the undrained stress-strain-strength properties, the creep properties, the compression and swelling properties in drained and undrained conditions and the undrained thermomechanical properties. Measurements have been made at different densities, clay/sand mixtures and pore water compositions. The influence of temperature, rate of strain and testing technique has also been considered.

The investigation has led to a supply of basic data for the material models which will be used at performance calculations. The results have also increased the general understanding of the function of smectitic clay as buffer material.

The microstructural behaviour has been considered at the validation of the different test results and the validity of the effective stress theory has been discussed. Comparisons with the properties of Ca-smectite have also been made.

SYMBOLS

a_c	activity
B	bulk modulus
c_v	coefficient of consolidation
D	constrained modulus
e	void ratio
h	height
I_p	plasticity index
k	hydraulic conductivity
K_o	lateral stress ratio at one-dimensional drained compression
I_c	clay content
p	average pressure
S_r	degree of water saturation
u	pore water pressure
w	water ratio
w_L	liquid limit
w_p	plastic limit
α	coefficient of thermal expansion
γ	strain
$\dot{\gamma}$	rate of strain
ν	Poissons' ratio
ρ	density
ρ_m	density at saturation
ρ_s	density of particles
ρ_w	density of water
σ	normal stress
σ'	effective normal stress
$\sigma_1;\sigma_2;\sigma_3$	principal stress
$(\sigma_1-\sigma_3)$	deviatoric stress
$(\sigma_1-\sigma_3)_f$	deviatoric stress at failure
σ_N	normal stress
σ_s	swelling pressure
τ	shear stress
τ_f	shear stress at failure

PREFACE

This investigation is a part of in the Swedish R & D for final disposal of nuclear waste financed by SKB. It has been carried out in the laboratories of Clay Technology AB and most of the employees of the company have been involved in the work.

Except for Harald Hökmark and Ola Karnland, the laboratory work was also made by Stefan Backe. The manuscript was read and improved by Roland Pusch and then edited by Irene Hansen. The figures not drawn by the computer were drawn by Birgitta Hellström. The contributions from these persons and others not mentioned are gratefully acknowledged

The support from Anders Bergström, SKB, with whom we have had many fruitful discussions is also highly appreciated.

The latter goal is somewhat contradictory. It means that the material model must be complex enough to be able to take into account everything that has an important influence on the behaviour of the material. On the other hand, the material model must be simple enough to be used in existing calculation tools (e.g. FEM) and to make the determination of the involved parameters possible.

It can be questioned whether it would be best to make one large model which takes into account everything, or to make small models suited for the special calculation purpose. For the overall understanding of the behaviour of a buffer material one large model would be to prefer, but such a model would probably be too complicated for calculation purposes. The most "effective" model is the model which is strictly suited for the specific calculation and only takes into account the parameters absolutely necessary for the calculation.

In this work the philosophy has been to make simple material models well suited for the specific analysis complemented with various parameter relations for increasing the understanding and making the choice of input data easier. The adaption and application of the material models to the calculations is described in another report [7].

1 INTRODUCTION

According to the Swedish main concept for disposal of radioactive waste, the highly radioactive waste canisters are to be deposited at ≈ 500 m depth in chrystalline rock and embedded by a barrier of smectite rich clay. The purpose of the clay is to minimize water and ion transportation to and from the canisters and to be a mechanical buffer between the rock and the canister. The clay is also of potential use as sealing material in tunnels, shafts and boreholes or special seal-off-zones. Other repository concepts use smectite rich clay as sealing barrier as well.(Very Deep Boreholes, WP-cave).

The functioning of the barrier requires certain mechanical properties such as low water conductivity, high swelling ability and safe protection against rock movements. To be able to judge the functioning of the barrier for safety analyses it is very important to be able to model the mechanical and rheological properties and to calculate different scenarios.

The work described in this report is preceded by work done on Na-bentonite [1],[2],[3],[4],[5] and Ca-bentonite [6]. The work is part of the ongoing research work on these materials and this report is thus not to be considered as a final report. As will be shown, there are still questions to be answered and some of the work must continue.

Other compositions of buffer material are also investigated but not accounted for in this report (mixtures of Na-bentonite and sand, illite, moraine clay). Simultaneous work on different buffer clays is going on in e.g. France (Ca- bentonite) and Canada (50% Na-bentonite - 50% Sand).

The purpose of these investigations is twofold:

1. To increase the general understanding of the behaviour of these materials.
2. To make material models which can be used in calculations of the normal behaviour as well as special scenarios.

An important question is the validity of the effective stress theory. According to this theory the superposed pore pressure does not affect the state and properties of the material. Instead the state and properties are entirely dependent on the effective stress according to Eqn (1).

$$\sigma' = \sigma - u \qquad (1)$$

where σ' = effective stress
σ = total stress
u = pore pressure

This theory is valid for "normal" soils like sand, silt and illitic clays. The theory usually considers mineral-to-mineral contact between the particles and a demand for the validity is that the contact area between the particles is very small. For normal soils with mineral-to-mineral contact this is true. For the swelling smectitic clays the microstructure is more complex. The clay can be considered as being composed of stacks of flaky clay "particles". Inside a stack there is no mineral-to-mineral contact but the "particles" are separated by well structured water strongly bound to the mineral surfaces. According to the most accepted microstructural theory the structured water between the surfaces in water saturated Na-smectite can be 1-3 water molecule layers thick depending on the external pressure. The stacks act like small compressible particles which build up a particle/void structure.

A possible theory is, that at low densities there are very few mineral-to-mineral contacts between the stacks. At increasing density, those contacts increase in number due to increased external pressure. When the contact pressure is high enough, the structured water in the contact areas between the stacks will be squeezed out and either mineral-to-mineral contact will be established over small areas, or a few water molecule layers will be left over large areas.

Before a mineral-to-mineral contact is established between all stacks there may still be three water molecule layers between the clay particle flakes in the stacks, since the contact area between the individual flakes is much larger and thus the pressure much smaller than between

2. GENERAL ASPECTS OF LABORATORY TESTING OF SMECTITE-RICH CLAYS.

The smectite-rich clays that are suitable to use as a barrier in radioactive waste disposal imply a lot of laboratory test problems. These clays deviate from illitic and kaolinitic clay in mainly the following ways:

1. Very low permeability especially at high densities ($k < 10^{-13}$ m/s at $\rho > 2.0$ t/m^3).
2. Very high swelling pressure at high densities ($\sigma_s > 3.0$ MPa at $\rho > 2.0$ t/m^3)
3. Very high swelling potential and high compressibility.
4. The clays are artificial in the sense that they are dried and ground and compacted having an air dry water ratio w=5-10%.

The consequence of the last paragraph is that the sample must be saturated after compaction. The saturation process is time consuming and leads to air being entrapped and dissolved by the water. If water is pressed out of the sample during testing, the air in that water might be released and the measured volume change or pore pressure may be erroneous. This phenomenon can to some extent be avoided by using vacuum suction of the sample before saturation and backpressure on the pore water during testing.

The consequence of the low permeability is that sample preparation, sample saturation and pore pressure equalization are very time consuming. Saturation of a 1 cm thick sample with water entering from one end takes about 1 week. The time for the sample confined in a triaxial cell to reach equilibrium could be several weeks or months. On some occasions you will also find a remaining difference in pore-pressure between the upper and lower end of the sample. To run an active drained triaxial test could take several years.

The consequence of the high swelling pressure is that ordinary test equipments can only be used for low densities ($\rho_m < 1.9$ t/m^3 for triaxial tests). The high compressibility and swelling potential result in large time consuming volume changes even at low changes in effective pressure.

The second condition is more uncertain. There is an obvious risk that the stacks will be deformed and thus that the contact area will be large. On the other hand, if the contact area is very large, the contact pressure will be low and the mineral-to-mineral contact might be replaced by one or several intermediate water molecule layers, bringing us back to condition 1. The final conclusion is thus that the effective stress theory is valid if condition 1 is fulfilled. Fig 2:1 shows an outline of the microstructure at different densities, illustrating how the stacks probably will be deformed at compression.

The only way to settle the matter is to study the behaviour by stress-strain tests in the laboratory. These tests require relevant pore pressure measurements which is very difficult in this extremely low-permeable material. There are two major problems when measuring pore pressure:

1. Air dissolved in the pore water might become free air bubbles when leaving the pores and entering the filter stones in the device. That process takes place either as flow or diffusion. Air bubbles in the closed pore pressure measuring system will make those measurements erroneous. A high backpressure on pore water might solve this problem but if the effective stress theory is not valid, then the backpressure of course will affect the results.

2. The pore pressure is measured in the filterstones outside the sample and not in the pores of the clay. This means, especially at high densities when all the pore water is more or less structured, that it is uncertain whether we really measure the pore pressure. Another problem is the long time for a pore pressure response to propagate from the centre of a sample to the pore pressure gauge.

The validity of the effective stress concept is at present being investigated both in Sweden and in Canada. The Canadian reference material (50% sand and 50% Avonseal bentonite) has a lower sodium smectite content than the Swedish reference material (100% Wyoming bentonite Mx-80) which is favourable in the laboratory tests. According to the Canadian investigations there is a small volume change when the

the stacks. At high densities when the external pressure must be high to maintain equilibrium, the pressure in the structured water between the clay flakes can be high enough to squeeze out one or two water molecule layers.

This means that at low densities there are probably no mineral-to-mineral contacts between any particles and the effective stress theory should be valid provided that the pore pressure is equally distributed to and does not affect the water between the stacks and between the clay flakes in the stacks.

At medium high density when a major part of the stacks are in particle contact but when the external pressure is not high enough to squeeze out the water between the clay flakes (the interlamellar water), the effective stress theory must also be valid, provided that the clay stacks are so stiff that the particle contact zone is kept small in area.

At high density when the external pressure is so high that one or two molecule layers of the interlamellar water is squeezed out, the stacks will increase in density but the effective stress concept will still be valid if the contact area between the stacks is kept small.

The conclusion is that the validity of the effective stress theory requires that the two following conditions are fulfilled:

1. The interlamellar water in the stacks and the structured water in or near the contact zone between the stacks must be unaffected by the pore water pressure

2. The stacks must be stiff enough to withstand the contact pressure at high densities in order to keep the contact area small.

The first condition is probably fulfilled with the exception that a change in an allround acting water pressure will change the stress balance in the clay structure, since the structured water initially can bear shear stresses due to a high viscosity. This means that a change in pore water pressure might create an unbalance, resulting in small creep deformations in the structure.

cell pressure and the pore pressure are increased simultaneously and thus the "effective stress" is kept constant. However, the change in volume is so small (0.1%-0.7% at pressures increasing from 0.2-6 MPa) that the effective stress concept preliminary is being considered valid for their material [8].

Because of the uncertainty of the effective stress concept and because of the difficulties to measure proper pore pressure, the stress-strain-strength properties will be evaluated using total stresses without considering the change in pore pressure during the tests. However, the effective stress theory will be assumed valid, meaning, for example, that the initially applied pore pressure will be taken into account.

Most material models do not need any effective stress considerations and the behaviour would be much simplified if the pore pressure change could be ignored. Such a total stress analysis is usually sufficient for modelling the completely undrained and completely drained behaviour. If the time until equilibrium is of interest or if any partly drained, partly undrained scenario is studied, then the pore pressure change must be taken into account and thus the effective stress or a modified effective stress theory must be applied.

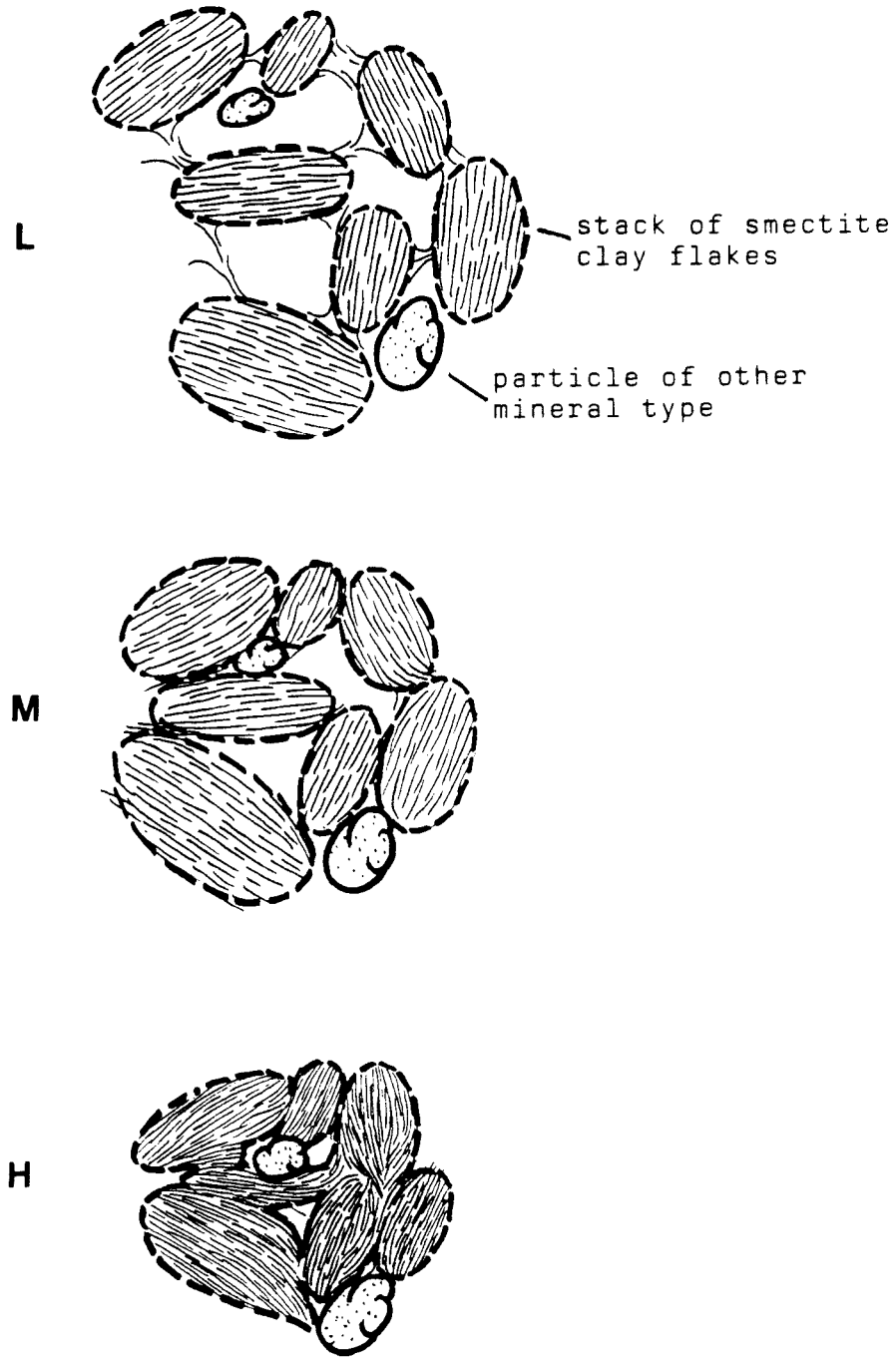

Fig 2:1 An outline of the micro-structure of a Na-smectite at different densities.

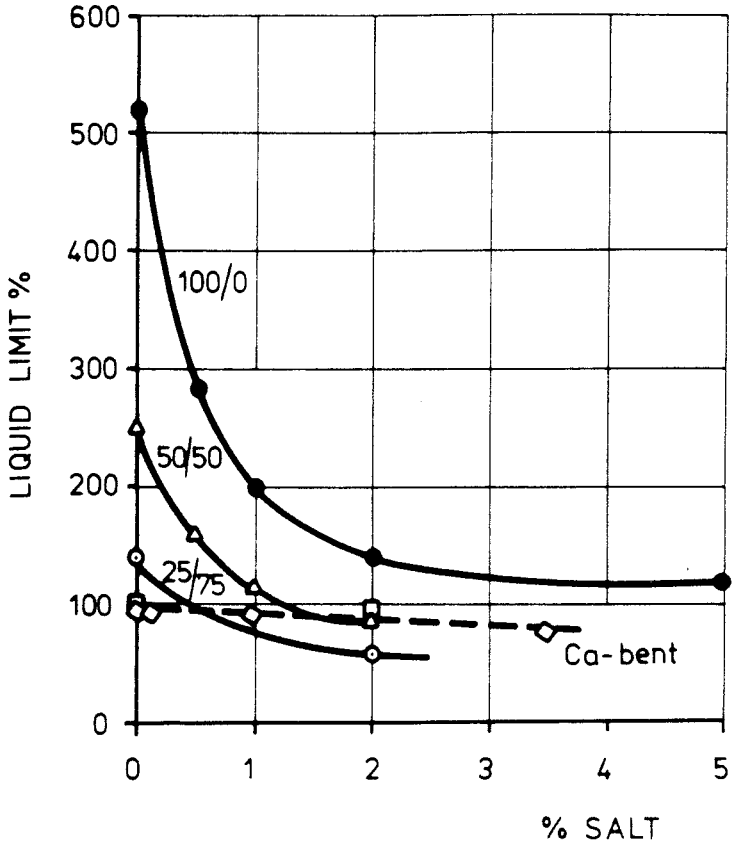

Fig 3:1 The liquid limit of pure Na-bentonite (100/0) and different mixtures of Na-bentonite and quartz filler as a function of the salt content in the added pore water. A Ca-bentonite is also shown for comparison.

also shown, as comparison, the effect of salt ($CaCl_2$) on Ca-bentonite. The same cation has been used for the salt type as the exchangable cation in the bentonite.

It is obvious that while the Na-bentonite is very sensitive to the salt content of the pore water, the influence on the Ca-bentonite is very small. The influence of the salt content can be explained in the following way: In a Na-bentonite the stacks are small and thus the amount of contacts between the stacks are very large. In Ca-bentonite the stacks are much larger and thus the amount of contacts small. This difference in the amount of contacts means that the force that must be taken by each contact is much larger in the Ca-bentonite. This means also

3. GENERAL DESCRIPTION OF THE CLAY

Na-bentonite does not have any well-defined basal properties since those to some extent depend on the origin of the clay. Na-bentonite differs from Ca-bentonite only by having sodium instead of calcium as exchangable cat-ion in the double layer. Since Na-bentonite is rare in nature but Ca-bentonite quite frequent, the cheapest and most frequently used Na-bentonite, at least in Europe, is the sodium treated Ca-bentonite in which the Ca-ions to some extent are changed to Na-ions and the Ca-bentonite thus changed to Na-bentonite.

A Na-bentonite can thus have different properties depending on the composition, the origin and the treatment of the clay. The Swedish reference clay Mx-80 is generally considered to be the best commercially available bentonite. Mx-80 has been used in the tests accounted for in this report. In some diagrammes and comparisons the French reference clay A4 which is a Ca-smectite is referred to. The properties of the French reference clay is described in [6]. Also the Canadian reference clay will be referred to (see reference [8]).

The Mx-80 Na-bentonite studied has a clay content of 80-90 %. The clay fraction has a momtmorillonite content of 80-90 %. Silt is the dominant remaining fraction, mainly containing quartz and feldspars as well as some micas, sulfides and oxides. A closer description of the structure and composition of this clay is given in [9].

The liquid limit determined according to geotechnical standard is w_L = 550% while the plasticity limit is w_p = 70% when destilled water is used for saturating the clay. When NaCl is added to the water, the liquid limit is strongly decreased. The influence of the salt content on the properties of a pure Na-bentonite and mixtures of Na bentonite and quartz filler is illustrated in Fig 3:1. The liquid limit is plotted as a function of the salt concentration in the pore water for a sodium treated bentonite Tixoton. Although this bentonite originally is a Ca-bentonite which has been activated by sodium treatment, it is highly active with a liquid limit almost as high as that of Mx-80. The liquid limit has been determined according to the cone method which for these soils give lower values (15-20 %) than Casagrandes method. In Fig 3:1 is

4. HYDRAULIC PROPERTIES

4.1 General

The hydraulic properties of bentonites differ very much depending on whether they are determined on saturated or unsaturated material. The high suction or osmotic potential of the unsaturated material makes the externally applied gradient of secondary importance, unless it is extremely high ($i>10^4$) or the bentonite very close to saturation.

The hydraulic conductivity can either be measured in a triaxial cell or in an oedometer. The diameter of the tested sample is usually 5 cm in both apparatuses, while the height is 10 cm in the triaxial cell and 2 cm in the oedometer. The technique and difficulties connected to the two methods are described below.

* In the triaxial cell complete equilibrium between the applied cell pressure and the swelling pressure must be reached before the test starts. After equilibrium, a hydraulic gradient is applied by increasing the pore pressure at one end of the sample. The flow of water through the sample is then measured either on the inflow or outflow side of the sample.

However, the increase in pore pressure Δu at one end of the sample results in a decrease in effective stress $\Delta\sigma'$, presupposed that the effective stress theory is valid. $\Delta\sigma'$ varies along the sample from $\Delta\sigma'= 0$ at the outflow end to $\Delta\sigma'= -\Delta u$ at the inflow end. The decrease in effective stress means that the sample swells, resulting in a successive change in density until equilibrium is attained.

The change in effective stress means that the applied increase in pore pressure must be low compared to the swelling pressure. Combined with a high sample this means a low gradient which will make these tests very time consuming.

* In the oedometer the sample height is smaller, and thus a higher hydraulic gradient is reached at the same applied increased pore pressure. Otherwise the effect is similar, with one important

that the effect of the colloid chemistry in the contact points are larger for a Na-bentonite than a Ca-bentonite, since the distance between the particles are smaller in the Ca-bentonite and thus a collapse of the double layer of minor importance.

The effect of adding salt to the adsorbed water is that the extention of the double layer is decreased and consequently also the thickness of the layer of structured water. This means that the ability to adsorb water between the stacks is decreased, which strongly affects the highly swelling Na-bentonite, but not so much the Ca-bentonite.

A rough estimate of the ability to bind water is the activity of the clay minerals a_c.

$$a_c = I_p / l_c = (w_l - w_p)/l_c$$

where I_p = plasticity index
w_l = liquid limit
w_p = plasticity limit
l_c = clay content

The activity of Mx-80 is $a_c = (5.5-0.7)/0.85 = 5.6$ which can be compared to Ca-bentonite which has $a_c \approx 1.0$.

The natural air-dry water ratio w of a clay is primarily a function of the air humidity and the clay mineral composition. Mx-80 normally have $w \approx 10\%$ while the water ratio is lower for Ca-bentonite ($w \approx 5\%$).

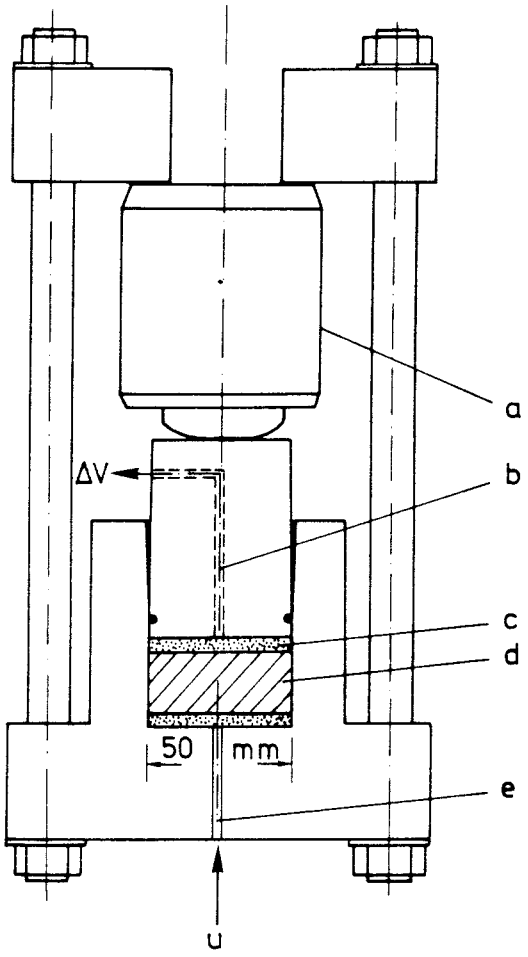

Fig 4:1 Oedometer for determining the hydraulic conductivity and the swelling pressure.

a. Force transducer
b. Water outlet
c. Filter stone
d. Sample
e. Water inlet

The difference between Mx-80 and the French Ca-smectite is very small at densities exceeding ρ_m = 1.7 t/m^3, while the Moosburg[1] Ca-smectite is 3-5 times more permeable. At ρ_m < 1.7 t/m^3 the Ca-smectite is rapidly loosing its tightness with decreasing density, while the Na-smectite still has a

---

[1] a Bavarian not activated Ca-bentonite with a montmorillonite content of 55-70% and a cation exchange capacity of 50-65 meq/100 g

difference being that the sample is totally confined in the oedometer. This means that an applied pore pressure increase Δu at the lower end results in an increased total stress $\Delta\sigma_l = \Delta u_l$ at the inflow end, resulting in an unchanged effective stress σ'. At the upper outflow end the total stress change will be decreased by the friction between the sample and the oedometer ring giving $\Delta\sigma_u = (1-\delta)\Delta u_l$. Since there is no pore pressure change at the upper outflow end ($\Delta u_u = 0$), the effective stress will be increased by $\Delta\sigma' = \Delta\sigma_u$ and thus the sample will be consolidated. After consolidation the density will increase by the distance from the lower inflow end.

The conclusion is that the permeability tests in the oedometer must also be conducted using a pore pressure increase which is considerably lower than the swelling pressure. Another conclusion is that the oedometer is preferable to the triaxial cell since the sample in the oedometer is lower and the gradient thus can be higher. Another advantage of the oedometer is that it is much easier to handle.

The hydraulic conductivity results described in this report are assigned to measurements made in oedometers of the type shown in Fig 4:1. The flow measurements are made on the outflow water. Most tests have been made without any pore water back pressure.

4.2 Water saturated state

After compaction, the samples have been saturated by applying a low pressure close to vacuum at both ends, whereupon deaired water is connected to the two ends. By this procedure, very little air will be entrapped in the sample or filter-stones.

In a test series samples with densities varying between $\rho_m = 1.45$ t/m^3 and $\rho_m = 2.12$ t/m^3, corresponding to water ratios varying between 100 % and 18 % have been tested. The results are shown in Fig 4:2 together with results from tests on two Ca-smectite rich clays. The figure shows that the hydraulic conductivity of Na-smectite Mx-80 is almost a straight line function of the density at saturation in a semi-logarithmic diagram varying from $k = 4\cdot10^{-11}$ m/s at $\rho_m = 1.3$ t/m^3 to $k = 2\cdot10^{-14}$ m/s at $\rho_m = 2.1$ t/m^3.

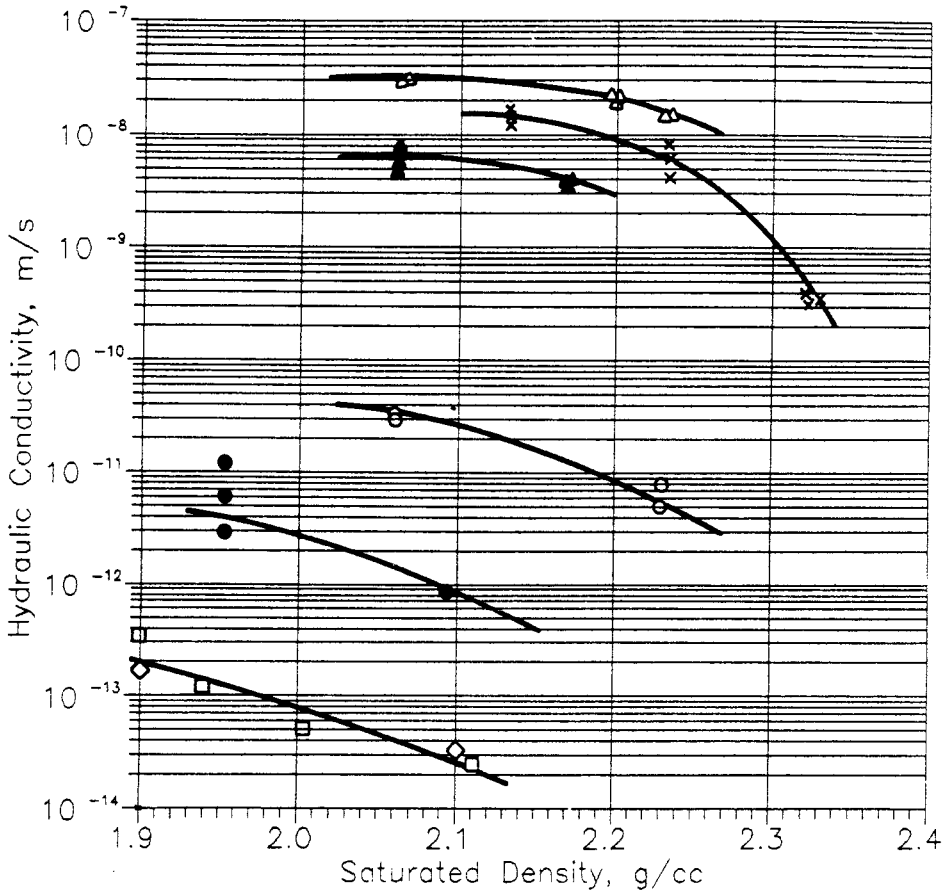

Fig 4:3 The hydraulic conductivity of different mixtures of Na-smectite and sand at different salt contents. The first number refers to the percentage clay. A low salt content means < 0.1 % while a high means ≈ 1.0 %

x 10/90 Low salt cont.

Δ 20/80 High salt cont.

▲ 20/80 Low salt cont.

o 50/50 High salt cont.

● 50/50 Low salt cont.

◊ 100/0 Low salt cont.

□ 100/0 Low salt cont. (Ca-smectite)

diagram shows the obvious influence of the salt content and the amount of ballast material. Forsmark water with a salt content of ≈ 1% and Allard water with a salt content of ≈ 0.1 % were used for the clay/ballast mixtures.

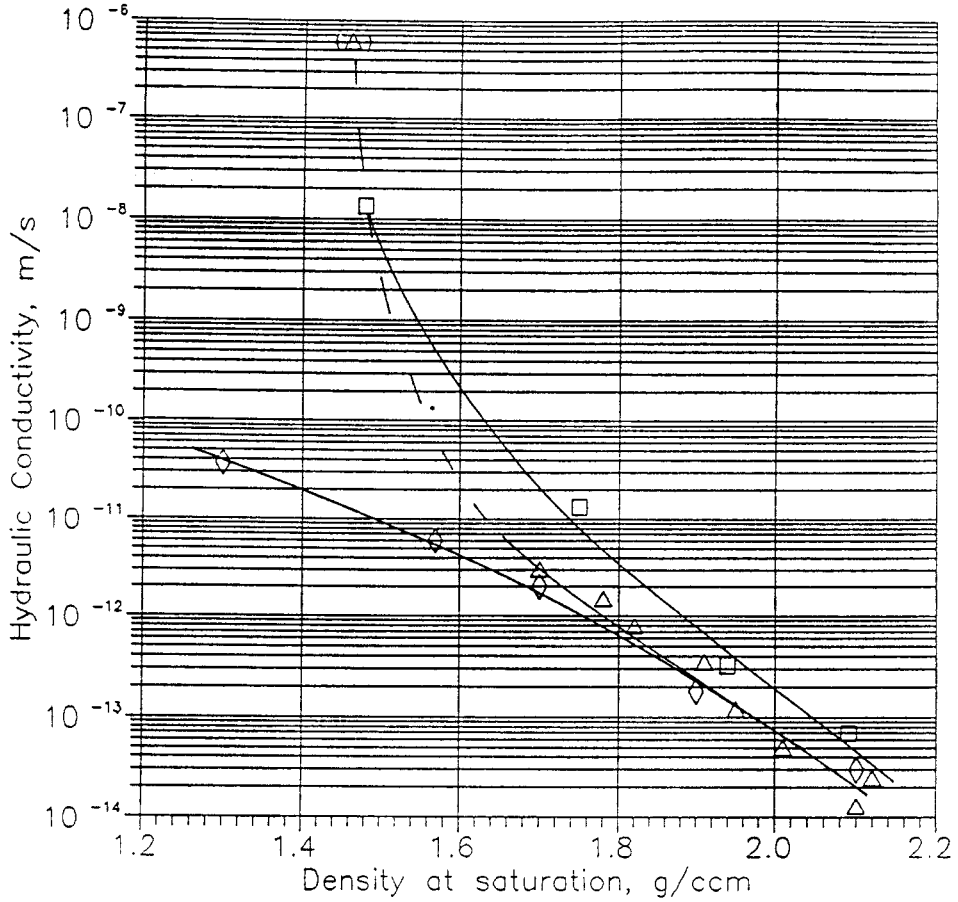

Fig 4:2 Hydraulic conductivity of different bentonites as a function of the density at saturation.

◇ Na-smectite (Mx-80)

□ Ca-smectite (Moosburg)

Δ Ca-smectite (French ref. clay)

very low permeability. The dashed part of the ρ_m-k relation of the French Ca-smectite at $\rho_m < 1.7$ t/m^3 is not relevant since, contrary to the Moosburg Ca-smectite, this clay cannot swell to a lower density than $\rho_m \approx 1.7$ t/m^3 [4].

Influence of pore water composition and ballast admixture

The influence of adding salt to the pore water or mixing the clay with a ballast material was not investigated. However, such tests have been conducted in an earlier investigation [4]. Fig 4:3 summarizes the results from that investigation and the tests made on 100 % Mx-80. The

5. SHEAR PROPERTIES

5.1 General

The shear properties of Na-bentonite have been investigated using three different shear techniques:

* Triaxial shear where the main principal stress σ_1 is increased by constant rate of strain until failure is reached while $\sigma_2 = \sigma_3$ is kept constant.

* Simple shear where the sample is sheared uniformly at a constant normal stress.

* Direct shear where the sample is sheared along one plane at a constant normal stress.

The principles of the different techniques are shown in Fig 5:1. Constant rate of strain (CRS) tests are performed, using the triaxial and simple shear techniques while creep tests or constant load (CL) tests are performed using the triaxial and direct shear technique. The CRS tests are accounted for in this chapter.

5.2 Triaxial tests

Altogether 8 reasonably successful triaxial tests were made. Since the tests are very time- and work consuming, it has been necessary to make "smart" tests with the intention of getting as much information as possible from the tests. This means, for example, that before the samples were sheared to failure, they were used for determining the swelling pressures and tested under constant load in creep tests.

Purpose

The triaxial shear tests had the following purposes:

* Find the general undrained stress-strain-strength relations for the clay

Anisotropy

To investigate if there is any influence of the direction of compaction on the hydraulic conductivity and the swelling pressure of the bentonite, a pair of samples cut parallell and perpendicular to the direction of compression was tested. A sample with the diameter 55 mm and length 100 mm was compacted and saturated in the triaxial saturation device to the density ρ_m = 1.79 t/m^3. After saturation, two samples with the diameter 50 mm and height 22 mm were cut in different directions and mounted into a swelling pressure oedometer. The swelling pressure as well as the hydraulic conductivity were then measured. The results are shown in Table I:

Table I. Results from anisotropy measurements

Flow or press. direction	k m/s	σ_s Kpa
parallel to comp r.	$5.0 \cdot 10^{-13}$	480
perpend. to compr.	$5.0 \cdot 10^{-13}$	650

No difference in hydraulic conductivity and a small but unsignificant difference in swelling pressure could thus be measured.

4.3 Unsaturated state

No special tests have been conducted to study the water uptake or unsaturated flow properties of Mx-80 since these properties have been carefully studied in earlier tests [9],[10]. The conclusions from these tests were that the suction potential of unsaturated smectite-rich clay is so high, that at moderate external hydraulic gradients the effect of that gradient is negligible at high densities. Under those circumstances, the water uptake can be simulated as a diffusion process having the coefficient of water diffusion $D_w = 0.3 \cdot 10^{-9}$. Tests on Ca-bentonite have yielded approximately the same result.

These steps are described in [6]. In some tests a backpressure on the pore water has been applied in order to dissolve air bubbles and thus increase the accuracy of the pore pressure measurements. However, this procedure requires that the effective stress concept is valid, which still has not been proved. There were also considerable difficulties with establishing steady and equal pore pressures at both ends of the samples. Due to the difficulties connected with pore pressure measurements and the uncertainties about the effective stress concept, these tests have primarily been evaluated using total stresses.

The tests are summarized in Table II.

* Column 1 shows the test number.
* Column 2 shows the measured water ratio w after the test.
* Column 3 shows the density ρ of the sample.
* Column 4 shows the degree of saturation S_r calculated from ρ and w assuming the density of the water ρ_w= 1.00 t/m^3 and the particle density ρ_s= 2.70 t/m^3.
* Column 5 shows the applied cell pressure σ_3 before the start of the test. This pressure also corresponds to the swelling pressure.
* Column 6 shows the cell pressure at the start of the test $\sigma_3^{(1)}$. A difference between colums 5 and 6 means that the cell pressure has been changed just before the start of the test.
* Columns 7 and 8 show any new cell pressures $\sigma_3^{(2)}$ and $\sigma_3^{(3)}$ that have been applied during the test.
* Column 9 shows the measured pore pressure at the start of the test.
* Column 10 shows the applied deviatoric creep stress $(\sigma_1-\sigma_3)_{cr}$ before the test.
* Column 11 shows the deviatoric stress at failure $(\sigma_1-\sigma_3)_f$.

Results

The table shows that the degree of saturation is more than 100% at all tests with an average of S_r= 105%. This means that the values ρ_w=1.00 t/m^3 and ρ_s=2.70 t/m^3 used in the calculations probably are erroneous. An accurate measurement of the density of the sample after the test TMX9 confirmed the disagreement. This discrepancy initiated a careful investigation of the relation between ρ_w and ρ_s which was carried out in

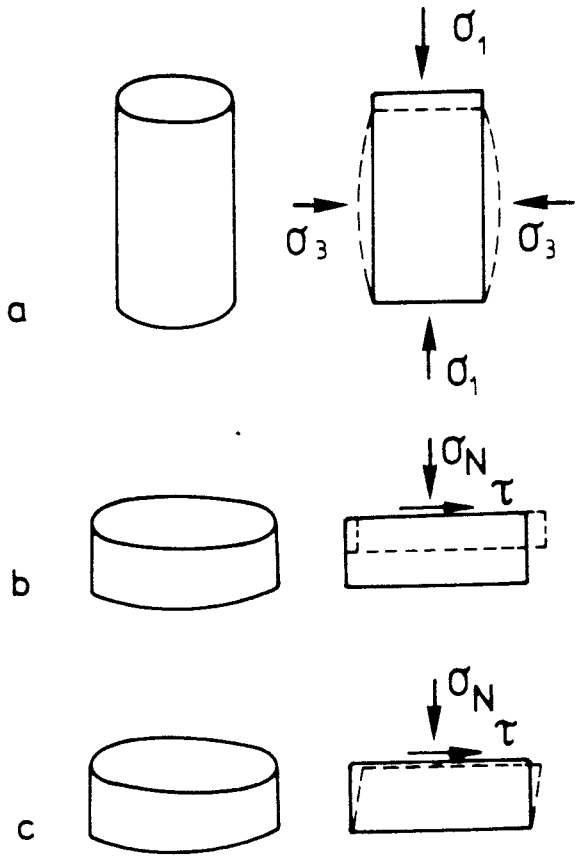

Fig 5:1 Illustration of the different shear-test techniques used: a) triaxial shear, b) direct shear and c) simple shear

* Investigate the influence of quick undrained total stress changes on the stress-strain-strength relation
* Investigate the influence of a preceding applied undrained shear stress on the stress-strain-strength properties
* Study the influence of an increased temperature
* Study the validity of the effective stress theory

Test procedures

The testing proceedures can be divided into three or four steps:

1: Sample preparation and saturation
2: Establishing equilibrium conditions in the cell
3: Any additional pre-failure tests
4: Stress-strain-strength testing

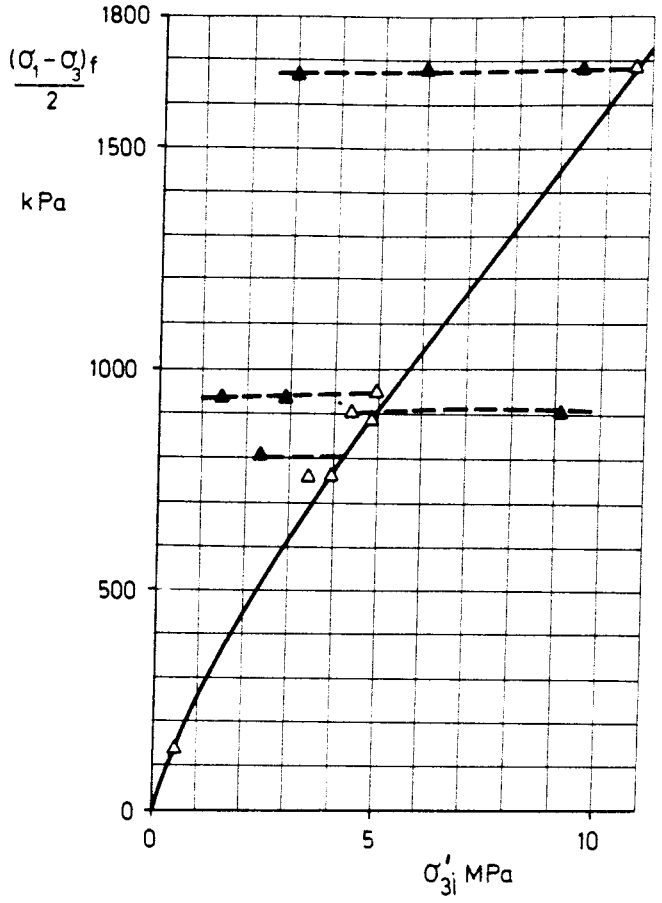

Fig 5:2 Failure stresses at the traxial tests.

Δ Failure stress at cell pressure = swelling pressure

▲ Extrapollated failure stress after change in cell pressure

—— Failure line at cell pressure = swelling pressure

- - Failure line at quick changes in cell pressure

connection with the swelling pressure measurements accounted for in chapter 9.

The results from the triaxial tests are illustrated in Fig. 5:2 where $(\sigma_1-\sigma_3)_f/2$ is plotted as a function of $\sigma_{3i}' = \sigma_3 - u_i$. Any changes in pore pressure during the test have not been considered. The filled triangels represent extrapolated strength values from the tests in which the cell pressure was changed during the test. The strength envelope of the Na-smectite is compared to the earlier derived strength envelope of Ca-smectite in Fig 5:3. The figures show that

Table II - Triaxial tests

1	2	3	4*	5	6	7	8	9	10	11	
Test No.	w	ρ	S_r	σ_3	$\sigma_3^{(1)}$	$\sigma_3^{(2)}$	$\sigma_3^{(3)}$	u_1	$(\sigma_1-\sigma_3)_{cr}$	$(\sigma_1-\sigma_3)_f$	
	%	t/m^3	%	MPa	MPa	MPa	MPa	MPa	MPa	MPa	comments
TMX1	43.2	1.80	102	0.50	0.50	--	--	0.06	0.045	0.268	
TMX2	24.8	2.06	105	10.7	9.65	5.90	2.95	--	0.125	3.30	
TMX3	30.5	2.01	109	4.83	2.40	--	--	0.06	0.400	1.60	
TMX4	28.5	2.01	106	5.00	5.00	2.96	1.40	0.01	0.200	1.88	
TMX5	27.7	1.98	101	4.50	4.50	9.00	--	0.16	0.600	1.80	
TMX6	28.3	2.01	106	4.83	4.83	--	--	1.40	0.400	1.49	60°C
TMX8	28.8	1.99	104	4.83	4.83	--	--	1.03	0.600	1.52	
TMX9	28.1	2.01	105	6.07	6.07	--	--	1.24	1.125	1.77	

* using $\rho_s = 2.70\ t/m^3$

$\rho_w = 1.00\ t/m^3$

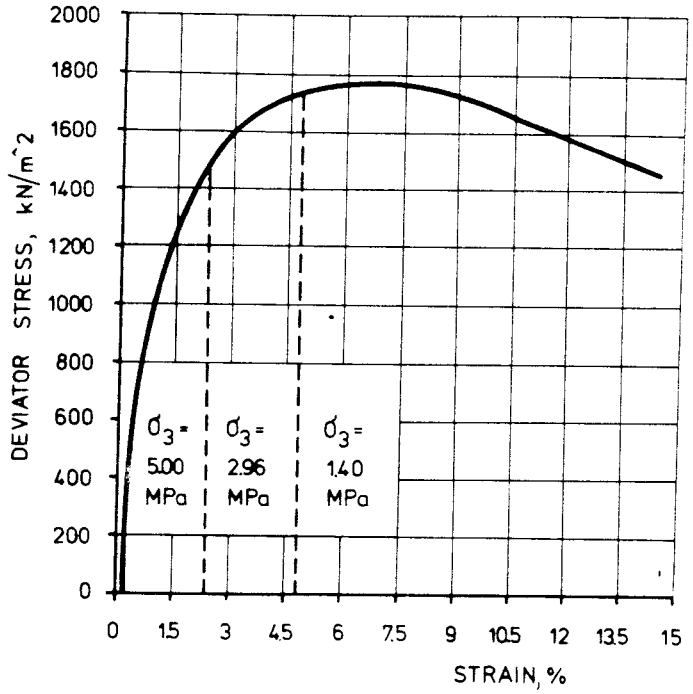

Fig 5:4 Stress-strain relation of the test TMX4 in which the cell pressure has been changed stepwise. ρ_m = 2.01 t/m^3

Mohr-Columbs theory if the failure enevelope is approximated as a straight line giving the values

friction angle ϕ = 7°
cohesion c = 150 kPa

at minor principal stresses exceeding 1000 kPa. A similar evaluation at stresses below 1000 kPa yields

friction angle ϕ = 13°
cohesion c = 0

Effect of a quick change in minor principal stress

In tests TMX2 - TMX5 the minor principal stress σ_3 was changed just

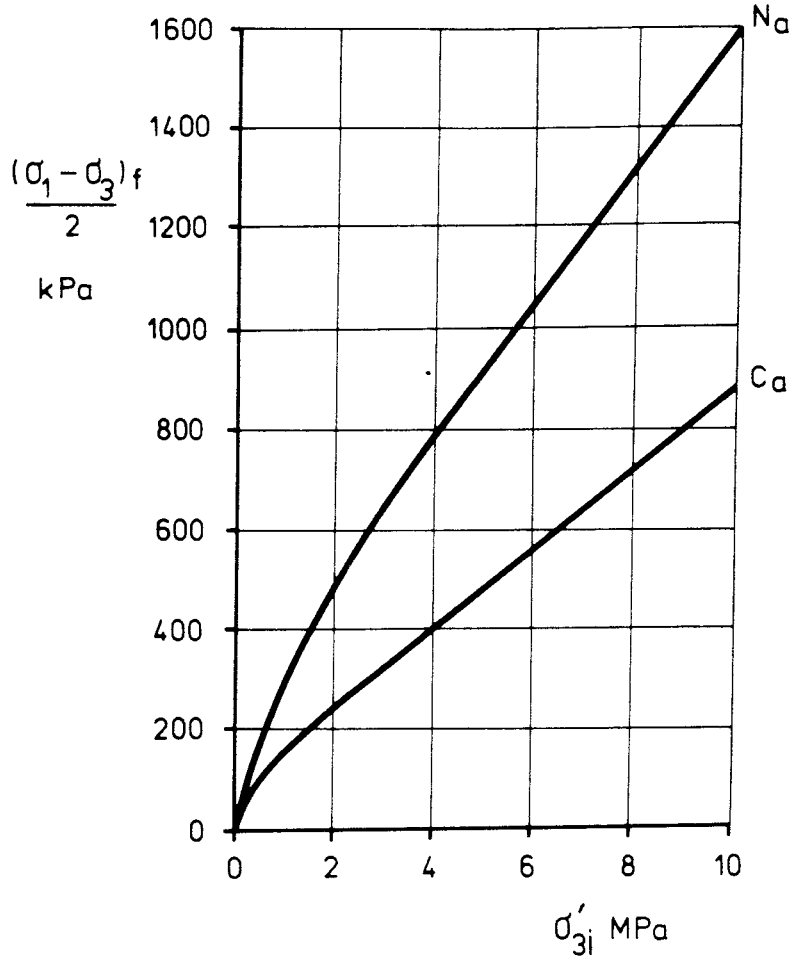

Fig 5:3 Strength envelopes of Na-smectite and Ca-smectite

* the failure envelope is slightly curved
* a quick change in total pressure affects the stress-strain-strength relation very little
* the influence of an increased temperature (T = 60°C) on the shear strength is insignificant.
* the shear strength of Na-bentonite is higher than that of Ca-smectite at high minor principle stresses

The stress-strain relation of all tests is shown in Appendix I.

Evaluation of the failure stresses according to Mohr-Columb

The friction angle and the cohesion can be evaluated according to

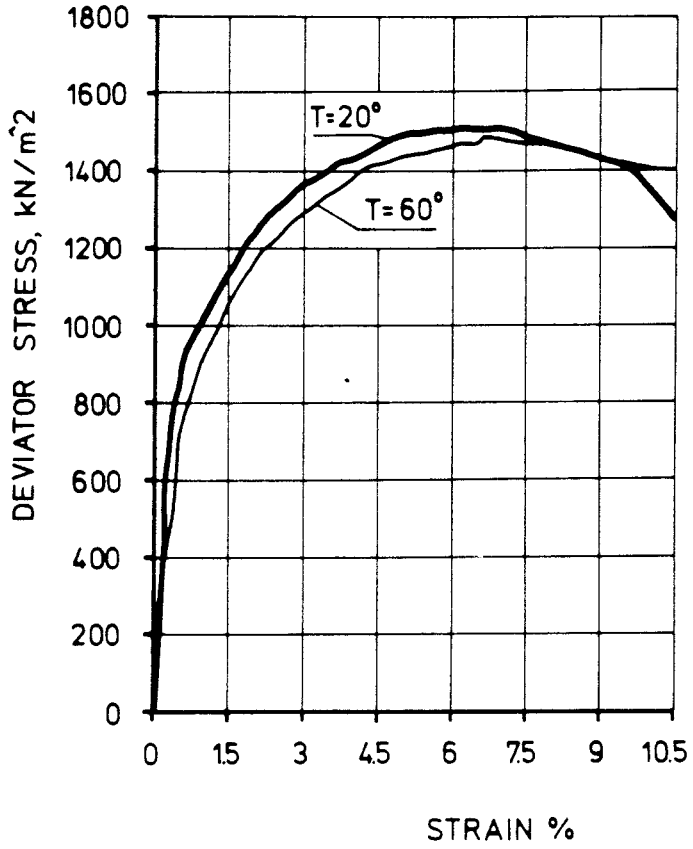

Fig 5:5 Stress-strain relations in tests TMX6 and TMX8 illustrating the insignificant influence of an increased temperature.

Influence of an applied back-pressure

In three of the tests a back-pressure was applied to the pore water in the samples. The stress-strain-strength properties of these samples agree very well with the stress-strain-strength properties of the samples without back-pressure, if the initial effective stress σ'_{3i} = $\sigma_3 - u_i$ is used at the evaluation. These tests support the effective stress concept.

General comments

The general behaviour of the Na-smectite at moderate temperatures is very similar to the behaviour of a Ca-smectite. The properties can be equally modelled but with different strength. The pore pressure change during stress is still unclear and thus not accounted for.

before or during the shearing by changing the cell pressure. The pressure was increased in test TMX5 and decreased in the other three tests. Fig 5:4 shows the stress-strain relation in test TMX4 in which the pressure was decreased in two steps from σ_3= 5.0 Mpa at ε = 0 % to σ_3 = 3.0 Mpa at $\varepsilon \approx$ 2.5 % in the first step and to σ_3= 1.4 Mpa at $\varepsilon \approx$ 4.5 % in the second test. This test is typical for these tests and it clearly shows that a change in total stress has no effect on the stress - strain relation at shearing.

This means that the undrained total stress path does not affect the stress-strain-strength relation. This conclusion is important at the modelling of the soil properties since it means that the stress-strain relation is unique at a given density, provided that the same stress-history of the soil is considered.

This is exactly the effect that the effective stress theory would lead to, since the change in cell pressure would result in a change in pore pressure equal to the change in cell pressure. The effective stress is not changed in such a test. These tests thus support the validity of the effective stress theory.

Influence of temperature

One test was made at the temperature 60°C. Fig 5:5 shows the stress-strain relations at tests 6 and 8 which are identical with the exception of the temperature and a small difference in stress history. Fig 5:5 confirms the conclusion drawn from the tests on Ca-smectite that the influence of a temperature increase to 60-70°C is very small, especially at high densities.

Influence of an undrained stress history

Since the samples have been used for undrained creep tests under different applied deviator stresses before shearing them to failure, the influence of such a stress history can be studied. No significant influence could be found if the applied shear stress is below ≈ 50 % of the shear strength. Above that value, the stiffness at the beginning of the test is increased.

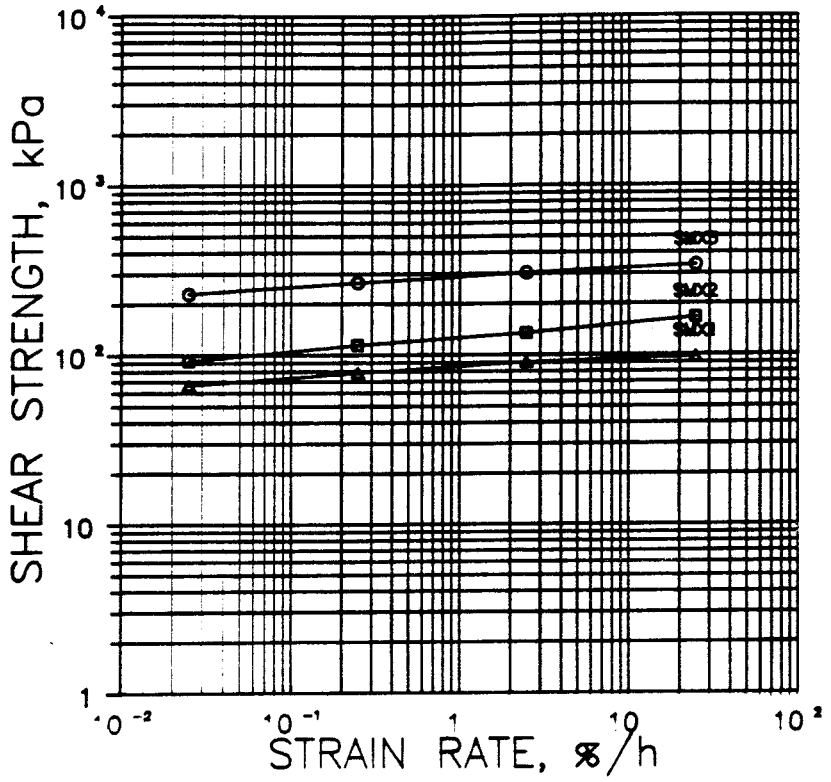

Fig 5:7 The shear strength as a function of the strain rate.

If the stress-strain relations at all strain rates are extrapolated as shown in Fig 5:6 and the strength plotted as a function of the strain rate, a fairly straight line in a double logarithmic diagram is achieved. Fig 5:7 shows this relation for three tests.

The relations in Fig 5:7 can be expressed as in Eqn 3:

$$\tau_f = m\left(\frac{\dot{\gamma}}{\dot{\gamma}_0}\right)^n \qquad (3)$$

where τ = shear strength

$\dot{\gamma}$ = rate of shear strain (1/s)

$\dot{\gamma}_0$ = reference rate of shear strain = 1.0 (1/s)

m = shear stress (or strength) at $\dot{\gamma} = \dot{\gamma}_0$

n = inclination of the straight line in the double logarithmic diagram

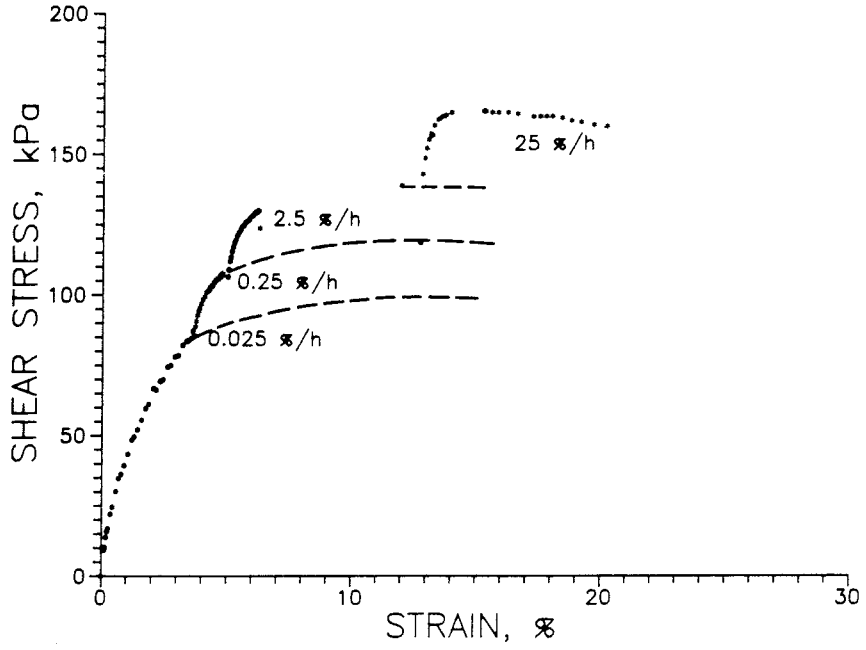

Fig 5:6 Stress-strain relation in shear test SMX2 illustrating the influence of a change in strain rate.

5.3 Simple shear

In order to investigate the influence of the testing technique and the applied rate of strain some shear tests were conducted. The apparatus and the technique used for achieving simple shear is described in [6]. The densities ρ_m = 1.7-1.9 t/m^3 and the strain rates $\dot{\gamma}$ = 0.025-25.0 %/h were used.

The influence of the rate of strain was tested with a technique using the same sample. The tests were started at the low rate 0.025 %/h and then increased 10 times in four steps until 25.0 %/h was achieved. Fig 5:6 shows the stress-strain relation from a test on a sample with the density ρ_m = 1.8 t/m^3. The other tests are accounted for in Appendix II.

The measured and extrapollated failure stresses are summarized in Fig 5:8 together with the range of possible failure stresses from the creep tests. The influence of the rate of strain is clearly seen and the failure envelopes from the slow and fast tests drawn as straight lines differ quite a lot. The failure envelope from tests having the same strain rate as the triaxial tests is illustrated with the dashed line. The Mohr-Coloumbian evaluation of the strength parameters yields

friction angle $\phi = 8.8^{\circ}$

cohesion $c = 40$ kPa

at the stresses 200 kPa $< \sigma_N <$ 2.0 MPa which is in good agreement with the triaxial test results. The failure stresses from the creep tests are a little higher than expected from the triaxial and shear tests which was also the case for the Ca-smectite.

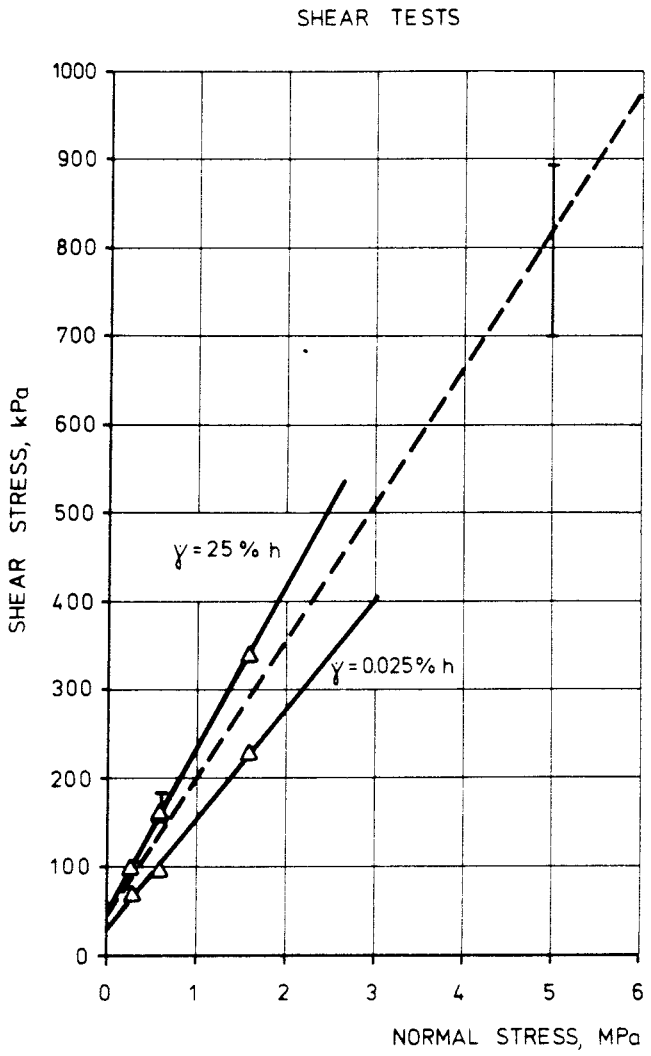

Fig 5:8 The Mohr-Coulumb failure envelopes at the shear tests.

Δ Simple shear tests

I Direct shear creep tests

n thus describes the rate dependence having an average value of

$n = 0.065$

which is of the same order of magnitude as for other clays.

where A, α and n are constants.

Eqn 4 should be normalized and related to a reference time t_r giving:

$$\dot{\gamma}_0 = A e^{\alpha \tau_0} \cdot t_r^{-n} \qquad (6)$$

If the shear stress τ is replaced by the degree of mobilized shear strength τ/τ_f and Eqn (4) is divided by Eqn (6) we arrive at the final Eqn (7)

$$\dot{\gamma} = \dot{\gamma}_0 \cdot e^{\alpha \frac{\tau}{\tau_f}} \cdot e^{-\alpha \frac{\tau_0}{\tau_f}} \cdot \left(\frac{t}{t_r}\right)^{-n} \qquad (7)$$

or

$$log\dot{\gamma} = log\dot{\gamma}_0 - \alpha \frac{\tau_0}{\tau_f} + \alpha \frac{\tau}{\tau_f} - n(logt - logt_r) \qquad (8)$$

Eqn 8 shows that the relation between the strain rate $\dot{\gamma}$ and the elapsed time t is a straight line in a double logarithmic diagram with the inclination n. The relation between the strain rate $\dot{\gamma}$ and the applied degree of mobilized shear stress τ/τ_f is a straight line in a semi-logarithmic diagram. The parameter n can thus be taken from the laboratory determined $\dot{\gamma}$ - t relation while the parameter α is determined from the relation between the rate of strain $\dot{\gamma}$ at the reference time t_r and τ/τ_f.

In order to be able to compare different results, the reference time and the reference degree of mobilized shear strength should be standard values. The following values are chosen:

t_f = 10 000 seconds
τ_0/τ_f = 0.5

If the creep tests are conducted as triaxial tests instead of shear tests, the shear stress τ can be changed to the deviatoric stress $(\sigma_1 - \sigma_3)$. The deviatoric stress is also to be preferred at material

6. CREEP PROPERTIES

6.1 General

The creep properties have been investigated in the triaxial cell and in the direct shear apparatus. In the triaxial cell only one creep load was applied, while in the direct shear apparatus the load was increased stepwise until failure occurred. The main purposes of the creep tests can be summarized in the following 4 points:

* To formulate a creep model which can be used in creep calculations
* To compare the properties measured with the two techniques to see if the much simpler direct shear creep test can replace the much more complicated triaxial creep test
* To compare the creep properties of Ca- and Na-smectite
* To investigate the effect of a change in applied shear stress on the creep rate

Creep theory

There is a number of creep theories derived for soils. The theory by Pusch [6],[11],[13] seems to be the theory that offers the best physical understanding. The theory by Singh & Mitchell [6],[12] is, however, the theory that is best suited for theoretical modelling with a nice concordance between theory and laboratory results.

The theory of Singh & Mitchell will be used at the evaluation of the creep results. The theory states that the strain rate $d\gamma/dt$ can be written as a function of the shear stress τ and the time t according to Eqn 4:

$$\frac{d\gamma}{dt} = Ae^{\alpha\tau}t^{-n} \qquad (4)$$

or

$$\log\dot{\gamma} = \log A + \alpha\tau - n\log t \qquad (5)$$

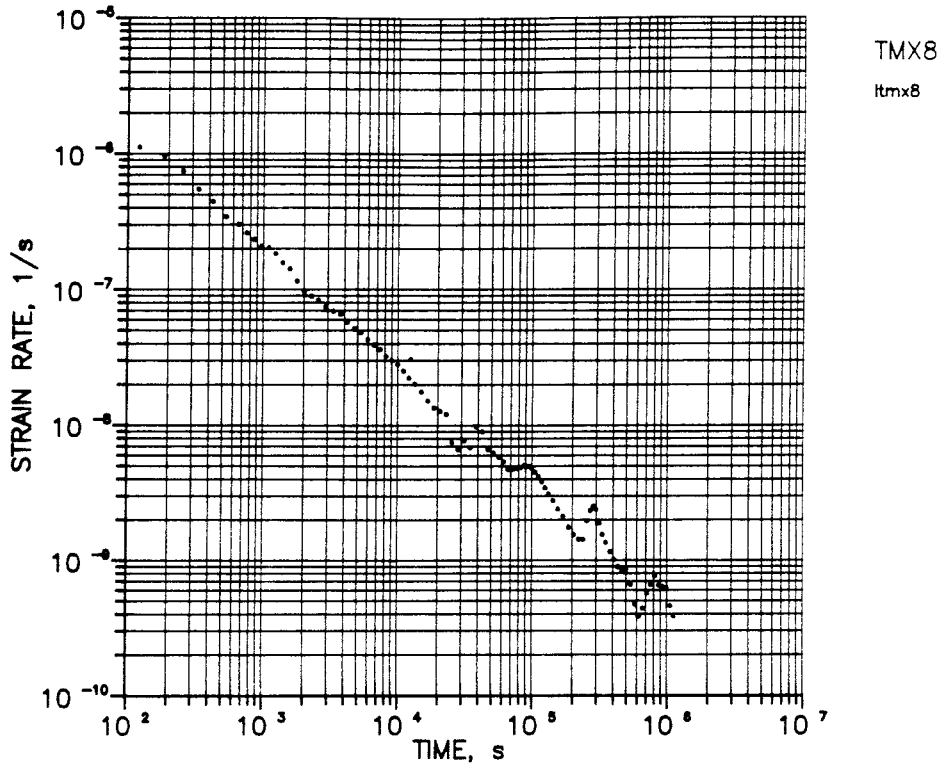

Fig 6:1 The evaluated strain rate as a function of the elapsed time in test TCR8.

Fig 6:1 shows as an example the rate of strain as a function of the elapsed time for creep test TCR8. The inclination of the straight line in the double logarithmic diagram is n = 0.87. As shown in Table III, n is varying from 0.80 to 1.00 with the average value n = 0.91. The other tests are shown in Appendix III.

The rate of strain $\dot{\gamma}$ evaluated at the reference time t_f= 10 000 seconds for all the creep tests can be plotted as a function of the applied deviatoric stress level (column 7 vs column 6 in Table III). That relation is shown in Fig 6:2. As stated in Eqn 8 the relation forms a straight line for the values related to the same density. The result from the test with the increased temperature fits well into the pattern, showing that there is no significant or a very small influence of temperature (T < 70°C) on the creep properties which was also concluded for the Ca-smectite.

models used for FEM calculations.

6.2 Triaxial creep

The triaxial creep tests are summarized in Table III.

Table III - Triaxial creep tests

1 Test No.	2 ρ_m t/m^3	3 σ_3 MPa	4 u_i MPa	5 $\sigma_1-\sigma_3$ MPa	6 $\frac{\sigma_1-\sigma_3}{(\sigma_1-\sigma_3)_f}$	7 $\dot{\gamma}$ 1/s	8 n
TCR1	1.80	0.50	0.06	0.045	0.17	$0.7 \cdot 10^{-8}$	1.00
TCR2	2.06	10.7	---	0.125	0.33	$2.5 \cdot 10^{-8}$	0.93
TCR3	2.01	4.8	0.28	0.400	0.25	$2.0 \cdot 10^{-8}$	0.80
TCR4	2.01	5.00	0.02	0.200	0.11	$0.8 \cdot 10^{-8}$	0.89
TCR5	1.98	4.50	0.06	0.600	0.33	$2.2 \cdot 10^{-8}$	0.81
TCR6*	2.01	4.80	1.00	0.400	0.27	$1.4 \cdot 10^{-8}$	0.94
TCR8	1.99	4.83	0.75	0.600	0.40	$2.8 \cdot 10^{-8}$	0.87
TCR9	2.01	5.14	0.26	1.125	0.64	$9.0 \cdot 10^{-8}$	1.00

* 60°

* Column 1 shows the test number
* Column 2 shows the density at saturation ρ_m
* Column 3 shows the minor principal stress σ_3
* Column 4 shows the initial pore pressure u
* Column 5 shows the applied deviatoric stress $\sigma_1-\sigma_3$
* Column 6 shows the quotient between the applied deviatoric stress and the deviatoric stress at failure $(\sigma_1-\sigma_3)_f$
* Column 7 shows the measured strain rate $\dot{\gamma}$ at the reference time t_r = 10 000 seconds
* Column 8 shows the value n determined according to Eqn 8

In tests 3 - 9 the samples have similar densities (2.0 t/m^3), test 6 is carried out at the temperature 60°C, while the densities in tests 1 and 2 are 1.80 t/m^3 and 2.06 t/m^3, respectively.

Fig 6:2 shows thus that the creep rate is more dependent on the applied degree of mobilized shear strength than the density of the sample or the type of smectite tested. However, since the deviatoric stress at failure is rapidly decreasing with decreasing density, the effect of decreased density is a strongly increased creep rate, which even may lead to failure at a constant shear stress.

At very low or high stress levels ($\tau/\tau_f < 0.1$ or $\tau/\tau_f > 0.9$) the relation is not valid. It is very difficult to do creep tests at such low stresses because of the low creep rate. In a finite element calculation it is, however, necessary to have a model which is valid for all stresses, and a test series investigating the creep rate at $\tau/\tau_f < 0.1$ is in progress.

If the creep model according to Eqn 7 is used and the shear stress is changed to the deviatoric stress, the creep model will be according to Eqn 9:

$$\dot{\gamma} = \dot{\gamma}_0 \cdot e^{\alpha \frac{(\sigma_1-\sigma_3)}{(\sigma_1-\sigma_3)_f}} \cdot e^{-\alpha \frac{(\sigma_1-\sigma_3)_0}{(\sigma_1-\sigma_3)_f}} \cdot \left(\frac{t}{t_r}\right)^{-n} \qquad (9)$$

The reference parameters are

t_f=10 000 seconds

$$\frac{(\sigma_1-\sigma_3)_0}{(\sigma_1-\sigma_3)_f} = 0.5$$

The determined parameters at the density ρ_m= 1.96 t/m^3 will be

$(\sigma_1-\sigma_3)_f$= 1.50 MPa
$\dot{\gamma}_0 = 4.4 \cdot 10^{-8}$ 1/s
$n = 0.91$
$\alpha = 4.15$

The small influence of the density which was shown in Fig 6:2 means that Eqn 9 and the 6 parameters showed above probably can be used at all fairly high densities, with the exception of the deviatoric stress at

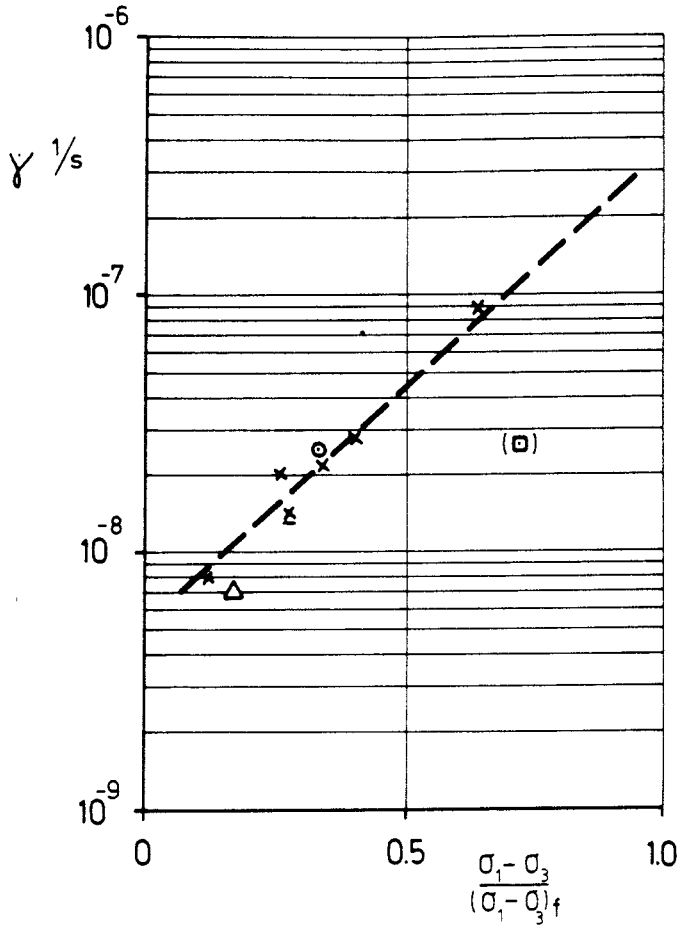

Fig 6:2 The rate of strain at t = 10 000 seconds as a function of the applied stress level

o ρ_m = 2.06 t/m^3

x ρ_m = 2.00 t/m^3 (x 60 °C)

Δ ρ_m = 1.80 t/m^3

□ ρ_m = 1.64 t/m^3 (Ca-smectite)

The two results from the tests made on samples with different densities and one result from a test on Ca-smectite are also included in the figure. It is obvious that the influence of the density is not very great, and if any possible differences between Ca- and Na-smectite are neglected, there seems to be a decreasing rate of strain at decreasing density. However, the amount of tests made on different densities is too small to verify this pattern.

Table IV - Direct shear creep tests

1 Test	2 ρ_m t/m^3	3 σ_N MPa	4 Load step	5 τ kPa	6 τ/τ_f ≈	7 $\dot{\gamma}$ 1/s	8 n
DMX1	2.0	5.0	1	350	0.43	$8.0 \cdot 10^{-8}$	0.80
			2	525	0.64	$1.0 \cdot 10^{-7}$	0.60
			3	700	0.85	$2.6 \cdot 10^{-7}$	0.60
DMX2	2.0	5.0	3	525	0.64	$1.0 \cdot 10^{-7}$	0.66
			4	700	0.85	$2.4 \cdot 10^{-7}$	0.53
DMX3	2.0	5.0	1	525	0.64	$3.1 \cdot 10^{-7}$	0.76
			2	700	0.85	$4.5 \cdot 10^{-7}$	0.60
DMX 4	1.8	0.6	1	5	0.03	$6.5 \cdot 10^{-9}$	0.70
			3	42	0.25	$2.0 \cdot 10^{-8}$	0.58
			5	84	0.51	$3.0 \cdot 10^{-8}$	0.56
			7	127	0.77	$1.2 \cdot 10^{-7}$	0.58

* Column 1 shows the test number.
* Column 2 shows the density at saturation ρ_m.
* Column 3 shows the applied normal stress σ_N.
* Column 4 shows the load step number.
* Column 5 shows the applied shear stress τ
* Column 6 shows the degree of mobilized shear strength τ/τ_f.
* Column 7 shows the measured strain rate $\dot{\gamma}$ at the reference time t_r = 10 000 seconds.
* Column 8 shows the value n according to Eqn 8.

The results from all tests are accounted for in Appendix IV where $\dot{\gamma}$ is plotted as a function of time. The results are examplified in Fig 6:3 where test DMX1 is shown. Test DMX1 is made in 4 steps starting with τ = 350 kPa and ending with τ = 894 kPa. At τ = 894 kPa the sample goes to failure after 3 000 seconds and this step cannot be included in the evaluation.

failure $(\sigma_1-\sigma_3)_f$ which can be seen in Fig 5:3.

It should be noted that the creep model is only valid under undrained conditions. The influence of the drainage condition is yet to be investigated.

6.3 Direct shear creep

Creep testing of clay by direct shear has advantages as well as disadvantages, the main advantage being that the test is much easier and thus much cheaper to perform. The disadvantages are:

1) The shear strain γ is difficult to evaluate since the shear is concentrated to a thin zone with unknown extention.
2) Only drained tests can be performed.
3) The direction and magnitude of the principal stresses are unknown.

A suggestion of a technique for evaluating the shear strain is made in [13]. A comparison with the triaxial creep results will show the relevance of the technique.

The technique for determining the parameters in Eqn 7 or 9 shown in the previous chapter is has the disadvantage that each point in Fig 6:2 requires a virgin sample. If a technique using stepwise loading could be applied, it would be sufficient to use one sample for evaluating all parameters. In order to try to investigate if that technique is applicable, parallel tests using both techniques were carried out.

The shear creep tests are shown in Table IV.

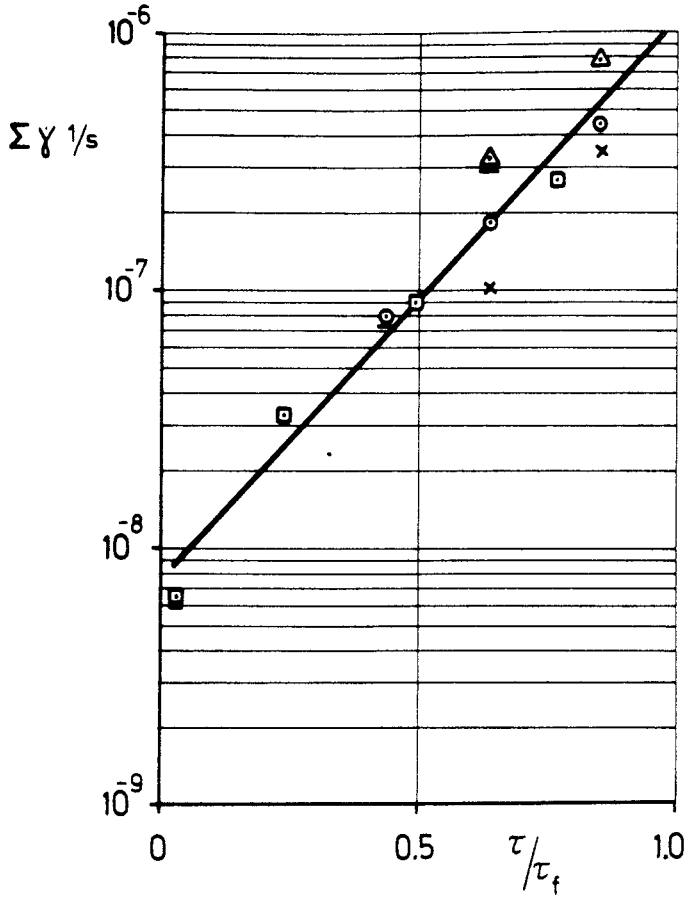

Fig 6:4 The rate of strain at t = 10 000 seconds calculated as the sum of the rates from all previous load steps as a function of the applied stress level. The underlined dots are the first steps.

o DMX1

x DMX2

Δ DMX3

□ DMX4

If these parameters are compared to the parameters evaluated from the triaxial creep tests we can see that $\dot{\gamma}_0$ is higher, n is lower and α approximately the same. This means that the creep rate is overestimated when the shear creep technique is used. The main reson is probably that the evaluation of the strain at the shear creep test is not quite correct. Some influence of the drainage condition could be another reason.

The conclusion must be that direct shear creep tests should only be used for relative comparison and for identification of cementation effects. Further research work is required if this technique is going to be used for other purposes.

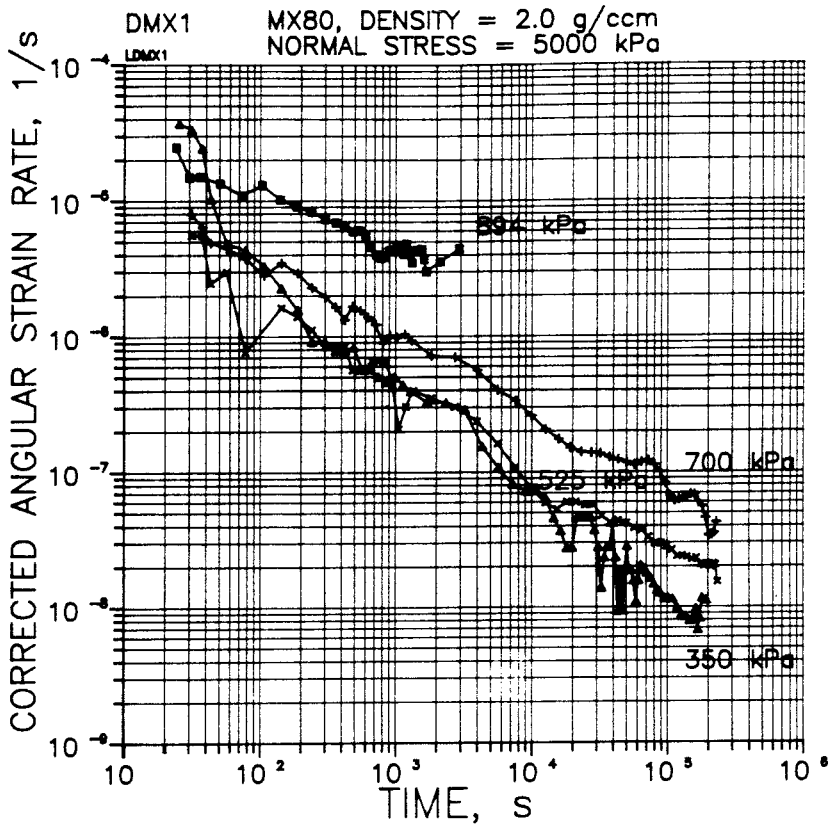

Fig 6:3 The strain rate at the direct shear creep test DMX1 as a function of the elapsed time at the different applied shear stresses.

If the tests are evaluated according to Eqn 7 the strain rate $\dot{\gamma}$ at the reference time t_r can be plotted as a function of the degree of mobilized shear strength τ/τ_f according to Fig 6:4. The underlined dots are the first steps in the tests, while the strain rate at the other dots are evaluated as the sum of the actual strain rate and all the previous strain rates in the test. As can be seen in Fig 6:4, the scatter of the results is too large to enable any satisfactory evaluation of the stepwise technique. If an average straight line, as drawn in the figure, is used and the average value of n from all tests is used, the following parameters from Eqn 7 can be evaluated (t_r= 10 000 seconds, τ_o/τ_f= 0.5):

$\tau_f \approx$ 820 kPa (tests 1-3)
$\dot{\gamma}_o = 9.0 \cdot 10^{-8}$ 1/s
n = 0.63
α = 5.00

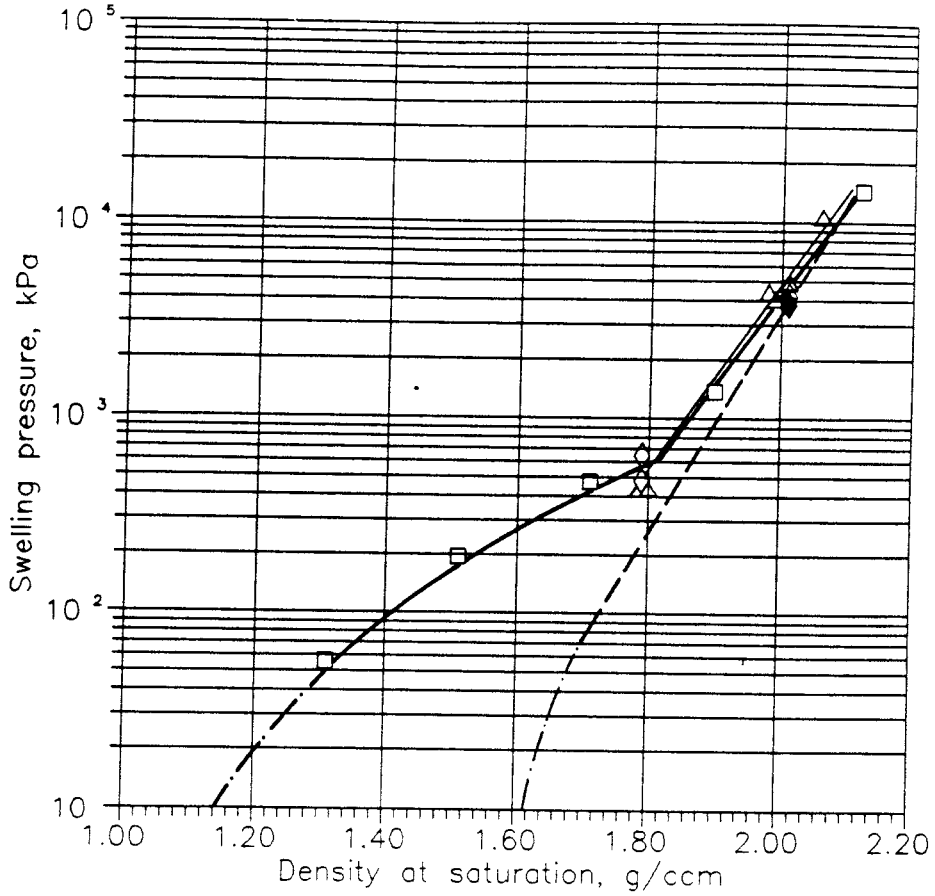

Fig 7:1 Swelling pressure of Na-smectite as a function of the density at saturation measured with the constant volume technique.

Δ measured in the triaxial cell

□ measured in the oedometer

◇ special measurements

◆ 60°C

—— old measurements (thin line)

--- Ca-smectite

-·- Extrapolations

7.2 Swelling pressure at constant volume tests

The swelling pressures measured with the constant volume technique are summarized in Fig 7:1. The results from earlier measurements which were only made on samples with high densities are also shown in Fig 7:1.

7 COMPRESSION AND SWELLING PROPERTIES

7.1 General

The swelling pressure of smectitic clays can either be measured in a triaxial cell or in an oedometer. The difference between these two techniques are that in the triaxial cell the stresses are equal in all three principal stress directions, while in the oedometer only the axial principal stress is measured and the other two principal stresses are unknown.

The swelling pressure can also be measured at at least three different occasions:

1) At the original density without changing the volume of the sample during the measurement. (Constant volume test).

2) After swelling, meaning that the sample has been exposed to a higher pressure at a higher density. (Swelling test)

3) After consolidation, meaning that the sample has had a lower density. (Consolidation test)

It is quite natural that these three different test methods yield different stress-density relations. The magnitude of the swelling or compression as well as the stress path (isotropic or oedometer consolidation) should also influence the stress-density relation.

The low permeability of the smectite-rich clays makes swelling and compression tests very time consuming, since a stepwise loading or deloading requires total pore water pressure dissipation at all steps. In this report, the results from constant volume tests as well as swelling and consolidation tests are described.

The compression and swelling properties in undrained condition have also been investigated. Those properties are required in, for example, thermomechanical calculations.

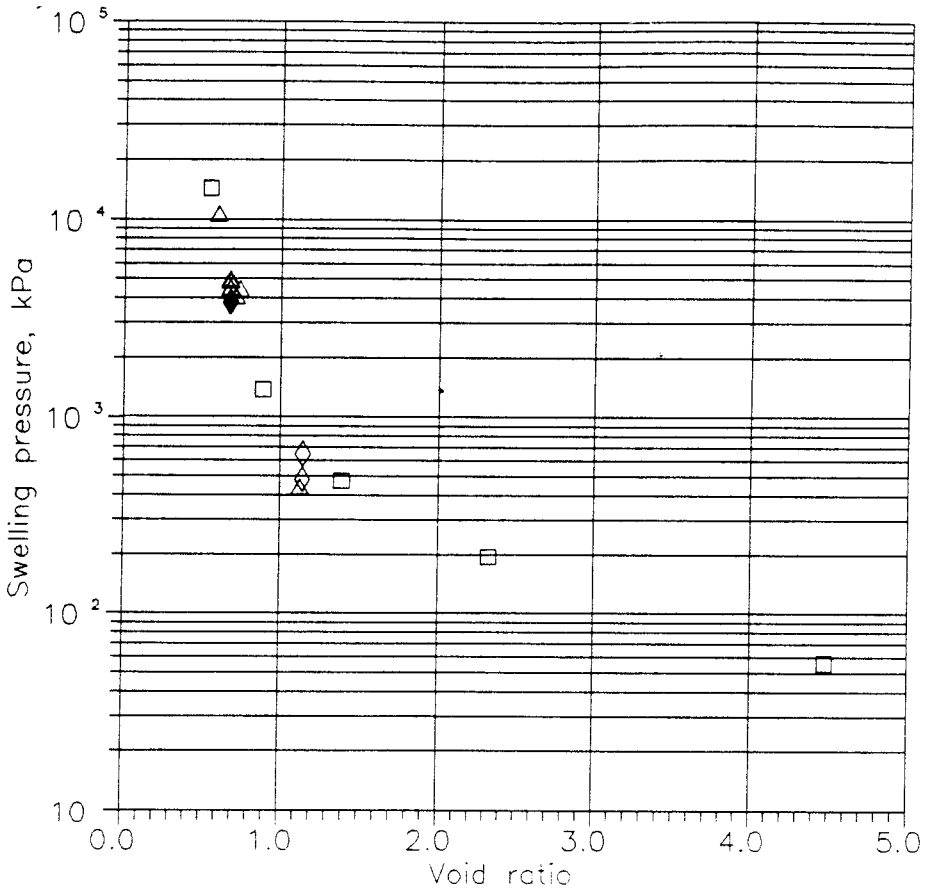

Fig 7:2 Swelling pressure of Na-smectite as a function of the void ratio measured with the constant volume technique.

- Δ measured in the triaxial cell
- □ measured in the oedometer
- ◇ special measurements
- ◆ 60°C

7.3 Drained compression and swelling

The compression and swelling properties have been investigated in an oedometer with a diameter of 5 cm. The sample was prepared from granulated Mx-80 poured into the oedometer at the natural water ratio $w_0 \approx 10$ %. The upper piston was fixed to give the initial low density which was set to be $\rho_m = 1.3$ t/m^3. A vacuum pressure was then applied to the sample and water sucked in by the vacuum. Since the volume occupied by the granulated clay was smaller than the volume at which the piston was fixed, the clay at first swelled until the pre-set

The swelling pressure was measured in both the triaxial cell and the oedometer. In the triaxial cell the cell pressure was adjusted until equilibrium was reached, while the oedometer was equipped with a force transducer for measuring the axial force. In Fig 7:1 the different techniques are marked with different dots. It is obvious from the figure that

1) The new values of the swelling pressure agree quite well with the old measurements.
2) The straight line relation in the semi-logarithmic diagram that was found in the earlier investigations is only valid at high densities. At the densitiy $\rho_m \approx 1.8$ t/m^3 there is a change in direction of the line.
3) The different techniques (oedometer or triaxial cell) give similar values.

The change in swelling pressure behaviour at $\rho_m = 1.8$ t/m^3 agrees well with the microstructural theory. When swelling takes place at high densities $\rho_m > 1.8$ t/m^3 means that mainly the interparticle water layers are filled up until the maximum of three water molecule layers. At about the density 1.8 t/m^3, those layers are filled and the rest of the swelling at lower densities is mainly connected with expanding the voids between the stacks with less structured water.

In Fig 7:1 the probable extrapolation to very low pressure is also indicated. One test was made at high temperature, which yielded a somewhat lower, but not significantly so, swelling pressure.

The measured swelling pressure at constant volume of the French Ca-smectite [4] is also shown in Fig 7:1. The difference is quite small at high densities but at $\rho_m < 1.8$ t/m^3 the difference seems to increase. Further measurements are required at low densities, but the extrapolated line is probable since the swelling pressure and swelling ability of this Ca-smectite is lost at $\rho_m \approx 1.6$ t/m^3.

On some occasions, it is preferable to illustrate the swelling pressure as a function of the void ratio. This is done in Fig 7:2.

$$\sigma'_n = \sigma'_{n-1} + \Delta\sigma - \Delta u = \sigma'_{n-1} \qquad (11)$$

at $t = 0$ when $\bar{U} = 0$ % and

$$\sigma'_n = \sigma'_{n-1} + \Delta\sigma - \Delta u = \sigma'_{n-1} + \Delta\sigma \qquad (12)$$

at $t = t_{100}$ when $\bar{U} = 100$ %

According to Casagrande ([14] and [15]) the time until $\bar{U} = 100$ % at the transition from primary consolidation to secondary can be calculated from the deformation-time curve in a semilogarithmic diagram as the intersection between the straight lines through the inflexion point and the curve of secondary consolidation. The average time for $\bar{U} = 100$ % is for these tests $t = 3 \cdot 10^5$ seconds or 3.5 days.

The coefficient of consolidation can be calculated from Fig 7:3 according to Eqn 13:

$$c_v = 0.197 \cdot \frac{h_{50}^2}{t_{50}} \qquad (13)$$

where h_{50} = half the height of the sample at $\bar{U} = 50$ %
t_{50} = the time at $\bar{U} = 50$ %

c_v evaluated in this way for all load steps can be plotted as a function of ρ_m as shown in Fig 7:4. The coefficient of consolidation of saturated bentonite seems to be of the same order of magnitude as the coefficient of water diffusion in unsaturated bentonite.

The permeability can be estimated from c_v according to Eqn 14

$$k = c_v \cdot \frac{g\rho_w}{D} \qquad (14)$$

where D = the constrained modulus. The permeability estimated according to Eqn 14 will, however, be 5 - 10 times lower than the permeability measured in the ordinary way. The reason for this difference is not quite clear.

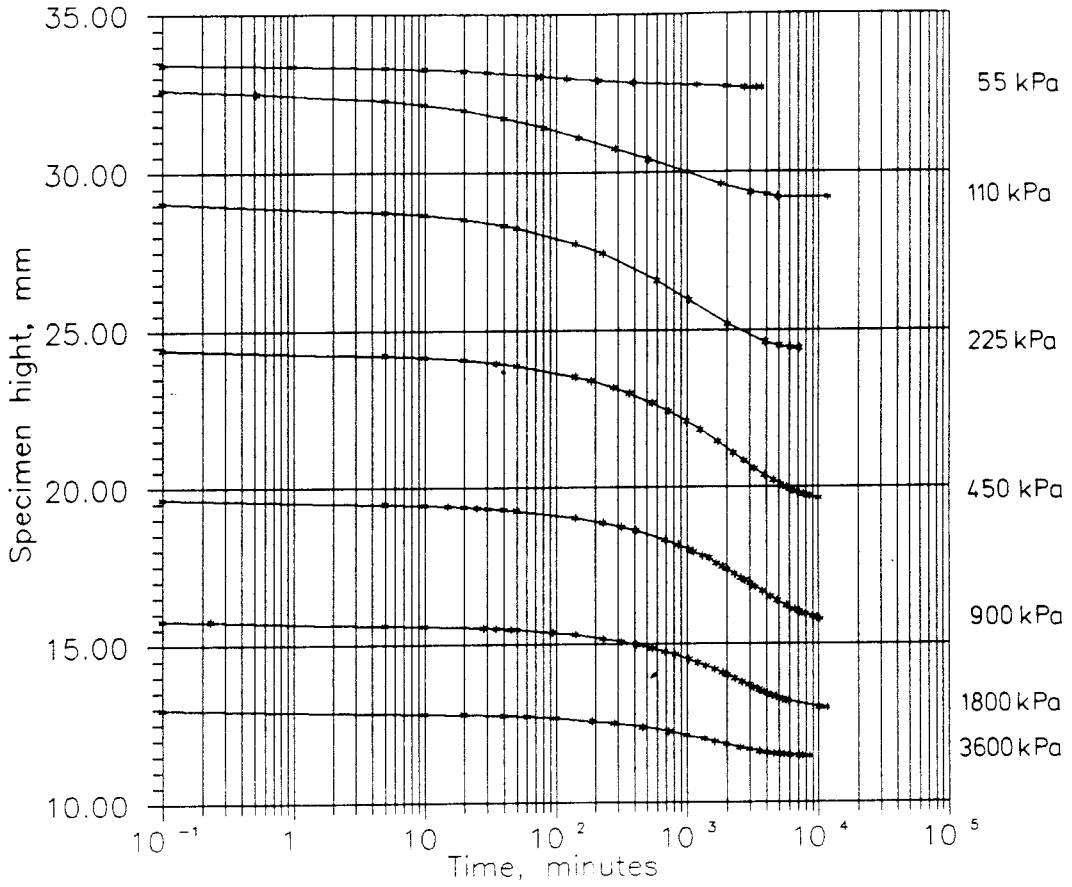

Fig 7:3 Stepwise consolidation of Na-smectite in an oedometer.

volume. After equilibrium, the dead load on the sample was increased by stepwise doubling of the load from ≈ 25 kPa until ≈ 3.6 MPa.

At each load step the compression was measured as a function of time. The successive change in specimen height is shown in Fig 7:3. The results can be analysed using the classical theory of consolidation by Therzaghi (See e.g. [14] and [15]). This theory has the effective stress concept as basis and the results must thus be treated with some caution.

The theory states that the whole additional pressure in a load step is initially carried by the pore water meaning that $\Delta u = \Delta\sigma$ and thus $\Delta\sigma' = 0$. As the pore pressure is declining with time the pressure is successively transmitted to the soil skeleton. At 100 % degree of consoldation ($\bar{U}$ = 100 %) the whole load is carried by the soil skeleton.

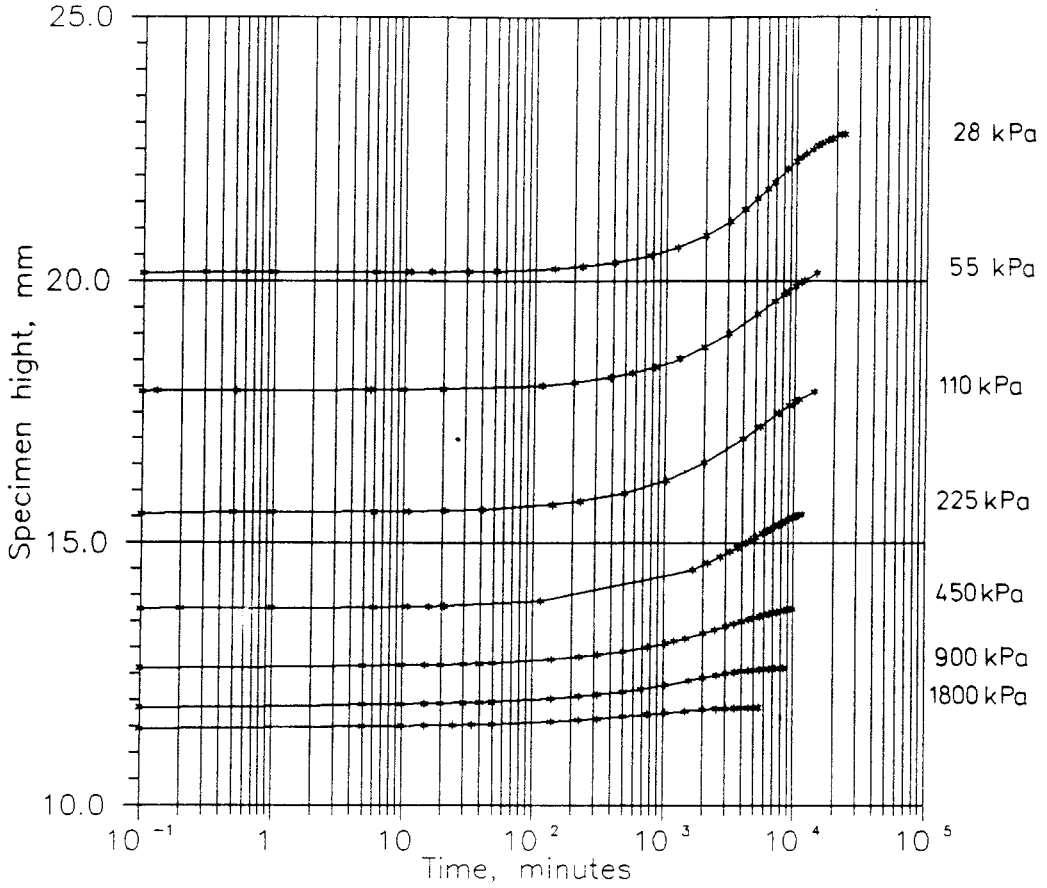

Fig 7:5 Stepwise swelling of Na-smectite in an oedometer.

1. Friction between the sample and the oedometer ring
2. A pre-consolidation behaviour meaning that the maximum applied load at an earlier stage has an influence on the properties
3. The average stress on the sample is higher than the applied vertical pressure at swelling, while the average stress is lower than the applied pressure at compression.

The third factor is probably the most important one. The average stress increase Δp at compression is

$$\Delta p = (\Delta\sigma_1+\Delta\sigma_2+\Delta\sigma_3)/3 = (\Delta\sigma_v+2K_0\Delta\sigma_v)/3 \qquad (15)$$

where $K_0 = \frac{\Delta\sigma_h}{\Delta\sigma_v}$

$\Delta\sigma_v$ = applied vertical stress increase

$\Delta\sigma_n$ = resulting horizontal stress increase at plain strain condition

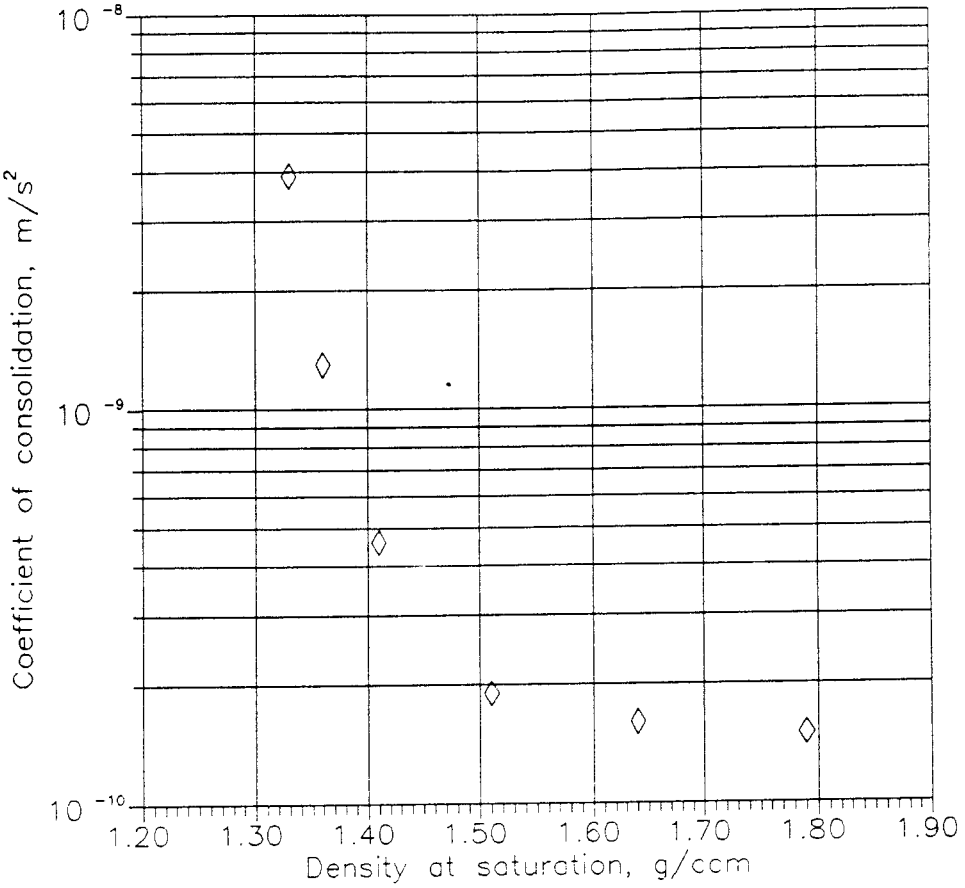

Fig 7:4 The coefficient of consolidation c_v as a function of the density at saturation of Na-smectite.

The swelling at unloading can be plotted in the same way as the consolidation which is shown in Fig 7:5. The swelling was allowed to last for longer time than the compression, but there is no clear transition from a "primary" swelling to "secondary" swelling. The reason might be that the suction potential of the sample is lower than the decrease in load, implying that the swelling will take longer time than the compression.

If the applied pressure at loading and unloading is plotted as a function of the density at saturation ρ_s, it can clearly be seen in Fig 7:6 that the stress path has a decisive influence on the pressure, although the pressure at swelling might be slightly underestimated. The reason for this hysteresis may be the sum of the following factors:

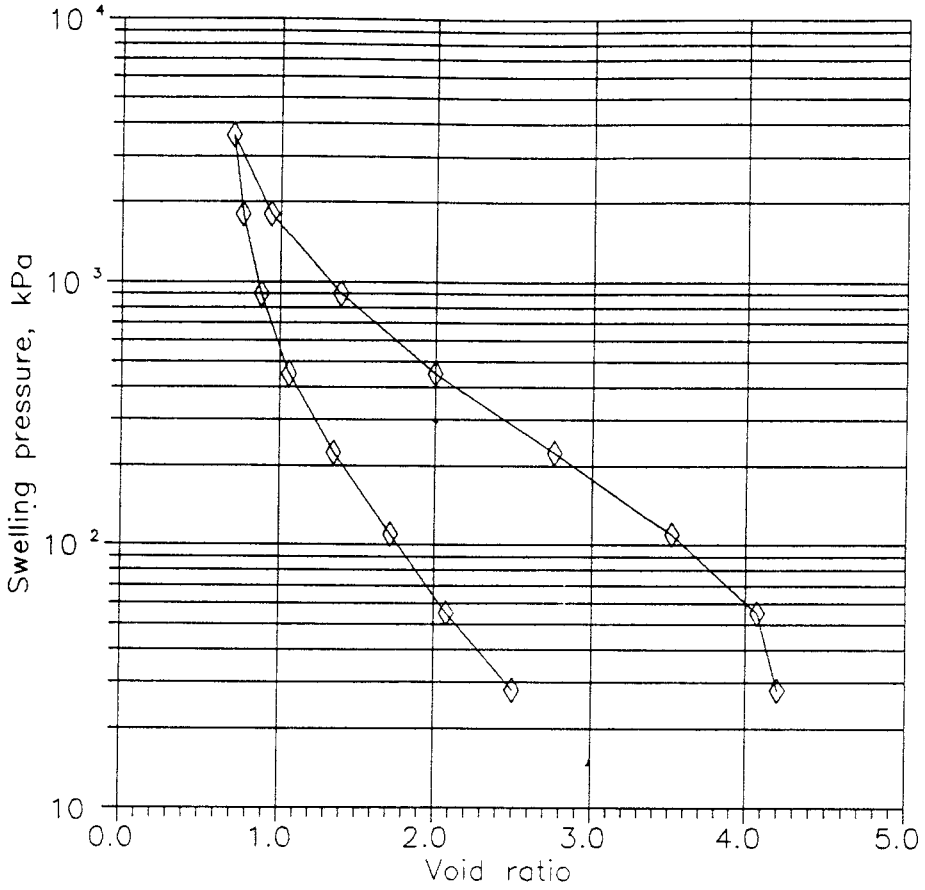

Fig 7:7 Pressure-void ratio relation at loading and unloading

The undrained compression and swelling properties are measured in the very stiff swelling pressure oedometers on 2 cm high samples. After complete saturation of the sample the oedometer is placed in a compression machine and the locked piston released. The deformation of the sample is then measured at fast loading and unloading. Different rates of deformation varying between 0.6% and 24% per hour were used. In spite of the fast rate and the low permeability some of the measured volume change was caused by pore water leaving the sample. Thus the dissipated pore water had to be measured and the volume change corrected. The volume was of course also corrected for the very small deformation of the the apparatus itself. After these corrections the calculated stress strain relations agreed very well, when comparing the results from tests at different strain rates.

Fig 7:9 shows as example the result from a compression test on Mx-80 with a density of ρ = 2.0 t/m^3. The hysteresis is small and the

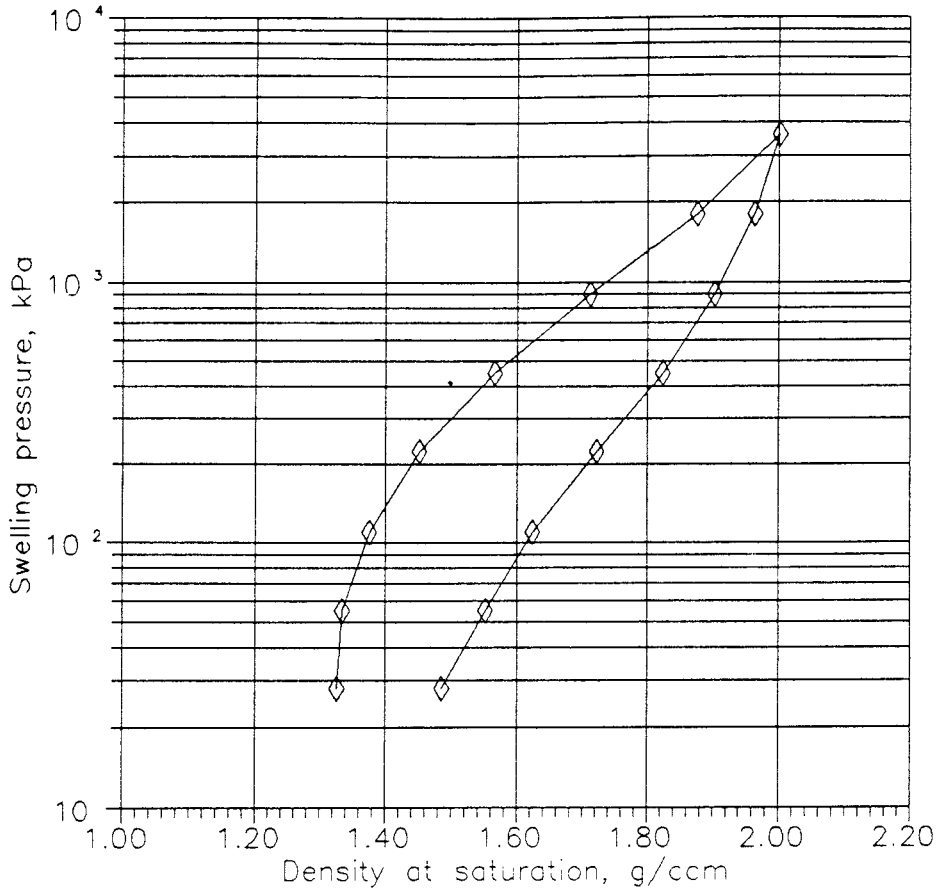

Fig 7:6 Pressure-density relation at loading and unloading

If K_0 is less than 1.0 which is usually the case, then Δp is smaller than $\Delta\sigma_v$. At swelling the result will be the opposite and Δp larger than $\Delta\sigma_v$. A correct material model used in a simulation of an oedometer test must result in the hysteresis shown in Fig 7:6. Fig 7:7 shows the relation between the applied vertical pressure σ_v and the void ratio e, while Fig 7:8 shows the compression, swelling and constant volume tests in one diagram for comparison.

7.4 Undrained compression and swelling

The initial response at loading or unloading is an undrained compression or expansion. If the clay is saturated, the volume change is extremely small compared to the final volume change at the end of the consolidation, which means that the pressure caused by even a small volume change will initially be very high. Such a volume change can, for example, be caused by temperature changes and rock displacements.

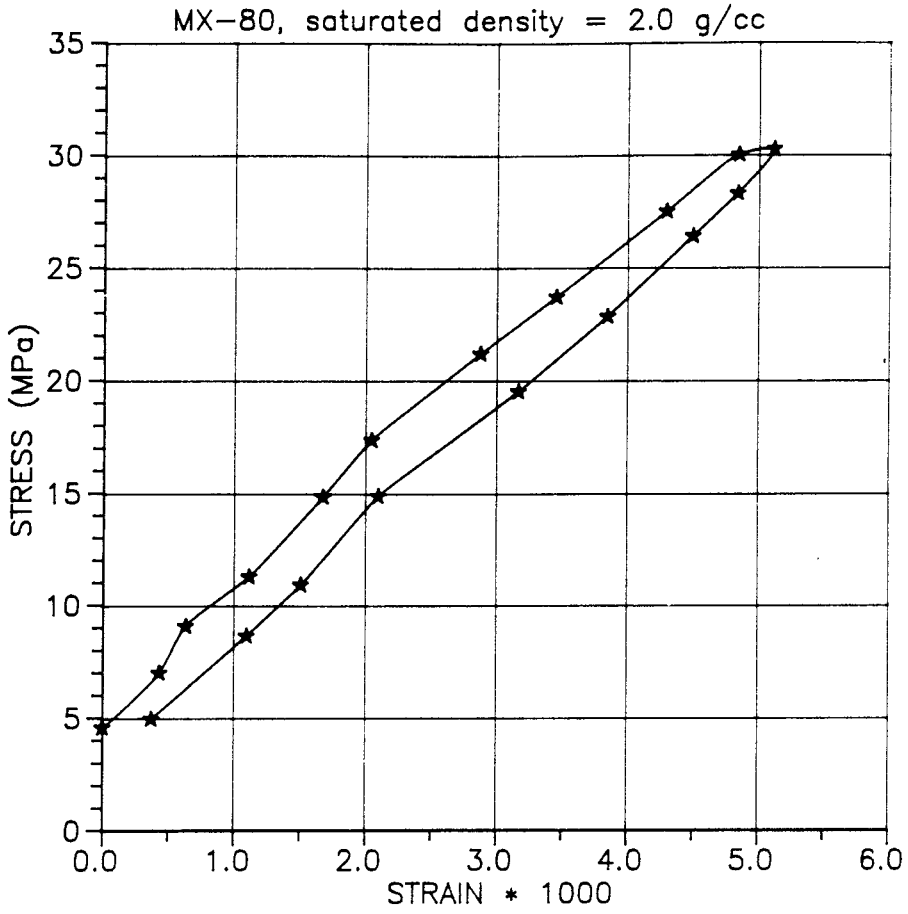

Fig 7:9 Undrained compression and swelling of Na-smectite

Since Poissons ratio $\nu \approx 0.5$ the bulk modulus is equal to the constrained modulus ($B = D$). It is interesting to compare these values to the compressibility of free water which is

$$B_w = 2.1 \cdot 10^3 \text{ MPa}$$

Since the bulk modulus of the clay minerals is a few orders of magnitude higher and since the compressibility of the soil skeleton is a few orders of magnitude lower, it can be assumed that the soil skeleton does not affect the compressibility and that the clay particles are floating as non compressible particles in the water. This assumption leads to that the compressibility of the water in the sample B_w can be calculated according to Eqn 16

$$B_w = B \cdot \frac{1+e}{e} \qquad (16)$$

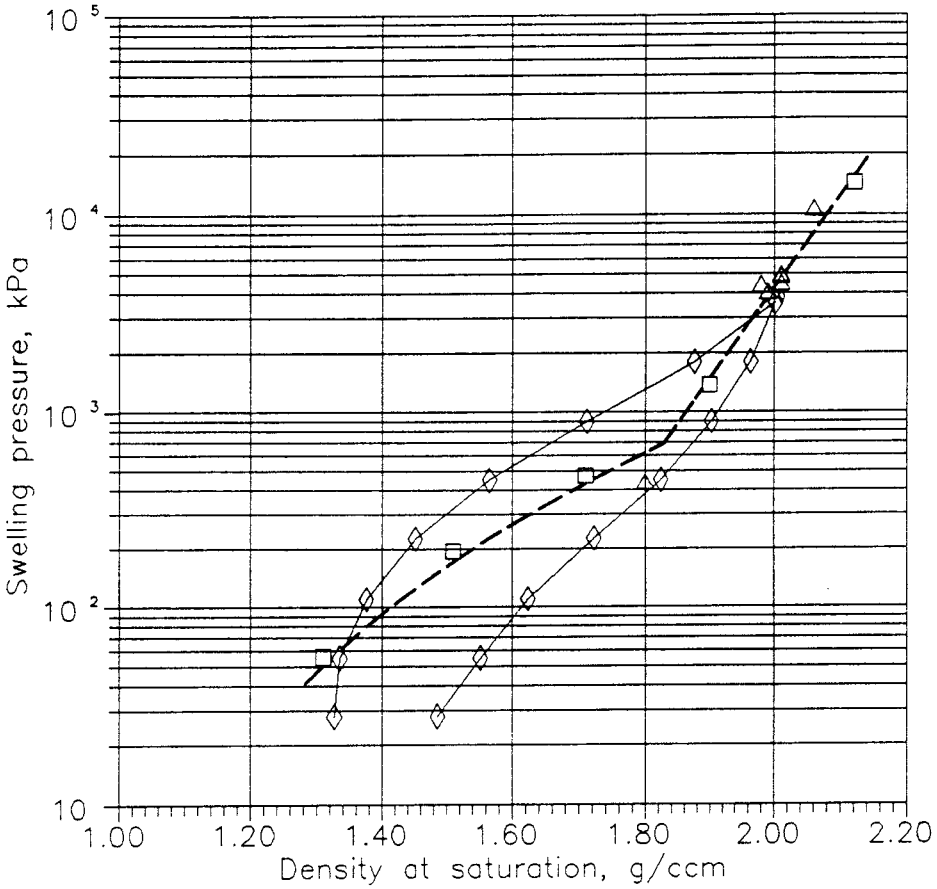

Fig 7:8 Pressure-density relation from all three test methods

stress-strain relation is a straight line which means that it can be described by one single constrained modulus *D*. Fig 7:10 shows the results from compression as well as expansion tests on a sample with the density ρ_m = 2.1 t/m^3. No difference in D-modulus was achieved, neither in the test above the swelling pressure, nor below.

Three densities were tested and the results are summarized in Table V. The measurements from all three densities are shown in Appendix V.

Table V. Results from the undrained compression and expansion tests

ρ_m	*e*	*B*	B_w
t/m^3		MPa	MPa
1.8	1.25	$2.3 \cdot 10^3$	$1.3 \cdot 10^3$
2.0	0.80	$5.0 \cdot 10^3$	$2.2 \cdot 10^3$
2.1	0.64	$6.0 \cdot 10^3$	$2.3 \cdot 10^3$

8. THERMOMECHANICAL PROPERTIES

8.1 General

A thermomechanical calculation in undrained state requires the knowledge of the bulk modulus B and the coefficient of thermal expansion α. B is determined in chapter 7.4, while the determination of α will be described in this chapter. The consequence of drainage after heating is studied in ongoing research work.

8.2 Thermal expansion

The volume change caused by heating has been determined on saturated samples with the densities 1.8 -2.1 t/m^3. The samples were 5 cm high and had a diameter of 5 cm. To prevent water from leaving the sample, the sample was surrounded by a rubber membrane with one steel plate at each end. The volume change was measured after a temperature increase from 20 to 60 degrees. The results are shown in Table VI.

Table VI. The coefficient of thermal expansion α at ΔT = 40°C

ρ_m	e	α	α_w
t/m^3		1/°K	1/°K
1.8	1.25	$3.1 \cdot 10^{-4}$	$5.6 \cdot 10^{-4}$
2.0	0.80	$3.0 \cdot 10^{-4}$	$6.8 \cdot 10^{-4}$
2.1	0.64	$2.2 \cdot 10^{-4}$	$5.6 \cdot 10^{-4}$

α for free water determined in the same temperature interval is

$$\alpha_w = 3.8 \cdot 10^{-4} \ 1/°K$$

An evaluation of α_w for the water in the samples can be made in a similar way as B_w in chapter 7.4. yielding

$$\alpha_w = \alpha \cdot \frac{1+e}{e} \qquad (17)$$

These values are also shown in Table VI. The coefficient of thermal

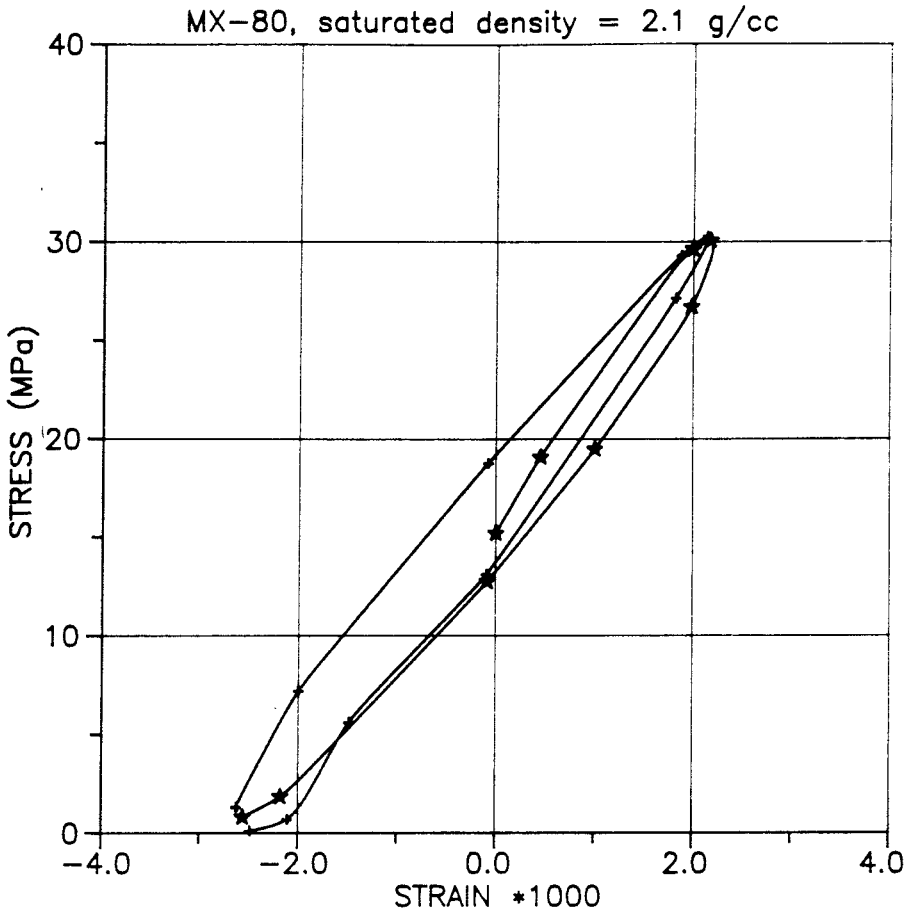

Fig 7:10 Undrained compression and swelling of Na-smectite

if no distinction is made between the internal and external water. B_w, calculated according to Eqn 16, is shown in Table V.

9. MECHANICAL PROPERTIES OF THE PORE WATER

9.1 General

The behaviour of smectitic clay is very much related to the behaviour and state of the pore water in the clay. It is also depending on the distribution of the pore water in internal interlamellar water and external pore water situtated between the clay particle stacks. These questions are mainly treated in other reports and research projects, but rheological and mechanical tests on clay samples can be accompanied by increased understanding of the behaviour of the pore water.

The compressibility and thermal properties of the pore water have been evaluated in chapters 7.4 and 8. The density of the pore water can be evaluated from careful measurements accounted for in chapter 9.2

9.2 Density of the pore water

In a clay sample the degree of saturation S_r, water ratio w, bulk density ρ, clay particle density ρ_s and pore water density ρ_w are related according to Eqn 17:

$$S_r = \frac{w\rho\rho_s/\rho_w}{\rho_s(w+1)-\rho} \qquad (17)$$

Eqn 17 shows that a completely saturated sample (S_r = 100%) with a carefully determined bulk density and a known particle density can be used for finding the density of the pore water. ρ_w and ρ_s have been determined in several investigations with varying results and there is still no final knowledge of the state and density of the pore water in these clays.

The samples used for determining the hydraulic conductivity have been exposed to deaired water flowing through for several months. It must be reasonable to believe that these samples are as saturated as possible. If S_r = 100% is assumed, the density of the pore water can be determined.

The bulk density of the samples was very carefully determined by lowering the samples in liquid paraffin to measure the volume. The water

expansion is about 50 % higher for the water in the samples than for free water. Similar results have been reached by other researchers [16].

REFERENCES

[1] Pusch, R. 1980. Swelling pressure of highly compacted bentonite. SKBF/KBS Technial Report 80-13.

[2] Pusch, R. 1983. Use of clays as buffers in radioactive repositories. SKBF/KBS Technical Report 83-46.

[3] Pusch, R. & Börgesson, L. 1985. Final Report of the Buffer Mass Test - Volume II: Test results. Stripa Project. Technical Report 85-12.

[4] Börgesson, L. & Stenman, U. 1985. Laboratory determined properties of sand/bentonite mixtures for WP-cave. Internal report SGAB IRAP 85511.

[5] Börgesson, L. 1985. Water flow and swelling pressure in non-saturated bentonite-based clay barriers. Eng. Geol., 21:229-237.

[6] Börgesson, L. & Pusch, R. 1987. Rheological properties of a calcium smectite. SKB Technical Report 87-31.

[7] Börgesson, L. 1988. Modelling of buffer material behaviour. Some examples of material models and performance calculations. SKB Technical Report 88-

[8] Graham, J., Sadat, F., Gray, M.N., Dixon, D.A. & Zhang Q-Y. 1988. Strength and volume change behaviour of a sand-bentonite mixture. Draft report. Canada.

[9] Pusch, R., Nilsson, J. & Ramqvist, G. 1985. Final Report of the Buffer Mass Test - Volume 1. Stripa Project. Technical Report 85-11.

[10] Pusch, R. 1983. Stress/strain/time properties of highly compacted bentonite. SKB/KBS Technical Report 83-47.

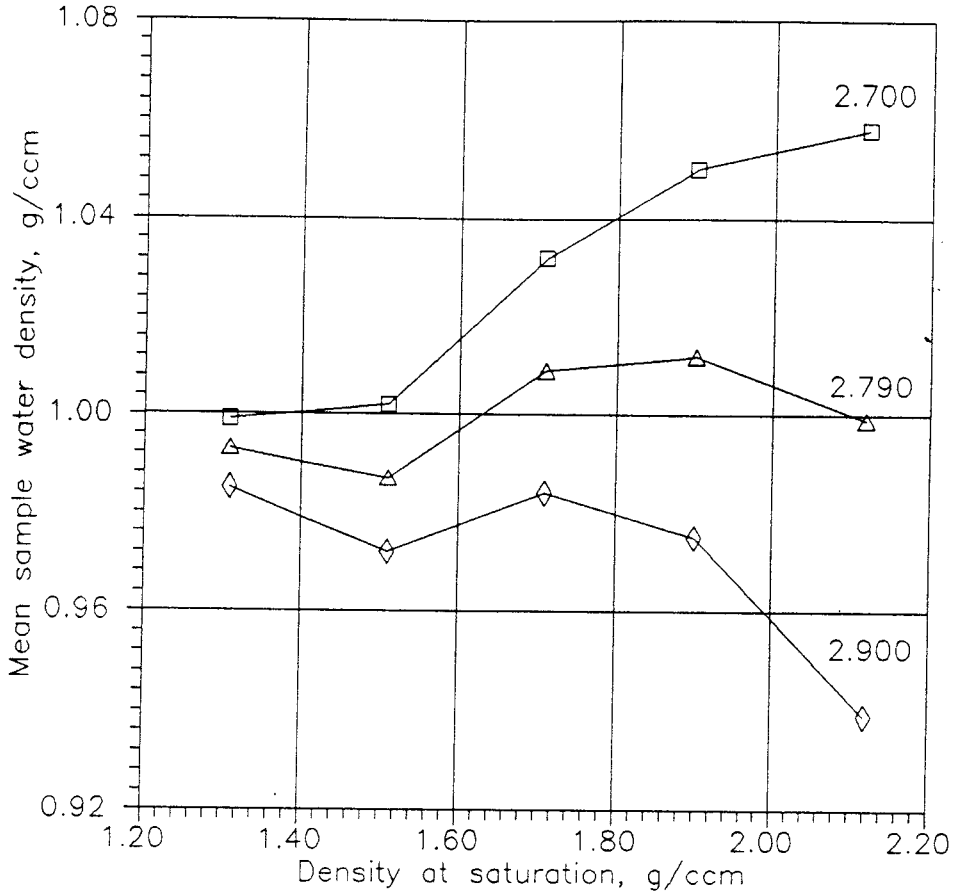

Fig 9:1 Density of pore water as a function of the bulk density at different assumed particle densities (2.70 - 2.90 t/m^3)

ratio was determined by measuring the weight of lost water at the temperature 105°C. ρ_s and ρ_w are thus determined, assuming that all water has disappeared at 105°C. The possible water left is considered to be an integral part of the clay particles.

Fig 9:1 shows the results of the measurements. ρ_w is plotted as a function of ρ_m at different possible clay particle densities ρ_s. ρ_s= 2.9 t/m^3 yields a good concordance with the ρ_w-ρ_m relation determined by Andersson and Low [17] with ρ_w < 1.00 t/m^3 decreasing at increasing ρ_m. ρ_s= 2.79 t/m^3 which was determined by Müller Vonmoos [18] yields $\rho_w \approx$ 1.00 for all bulk densities.

The question of the state of the pore water is still open, but the low values of the water compressibility (decreasing with increasing bulk density) support the ρ_w-ρ_m relation at ρ_s = 2.90 t/m^3.

[11] Pusch, R. 1986. Settlement of canisters with smectite clay envelope in deposition holes. SKB Technical Report 86-23.

[12] Singh, A. & Mitchell, J.K. 1968. General Stress-strain-time function for soils. American Society of Civil Engineers, Proceedings, Vol. 94, No. SM1.

[13] Pusch, R., Börgesson, L. & Erlström, M. 1987. Alteration of isolation properties of dense smectite clay in repository environment as examplified by seven pre-quarternary clays. SKB Technical Report 87-29.

[14] Taylor, D.W. 1948. Fundaments of Soil Mechanics. John Wiley & Sons. New York.

[15] Terzaghi, K. and Peck, R.B. 1967. Soil Mechanics in Engineering Practice, 2nd ed. John Wiley & Sons. New York.

[16] Derjaguin, B.V., Karasev, V.V. and Khromova, E.N. 1986. Thermal expansion of water in fine pores. Journal of Colloid and Interface Science. Vol. 109, No. 2, February 1986.

[17] Anderson, D. and Low, Ph. 1958. The density of water absorbed by lithium-, sodium-, and potassium-bentonite. Soil Science Society of America Proceedings, Vol. 22, No. 2.

[18] Müller-Vonmoos, M. and Kahr, G. 1983. Mineralogische Untersuchungen von Wyoming bentonit MX-80 und Montigel. NAGRA, Technischer Bericht 83-12.

APPENDIX I

Triaxial tests TMX1 - TMX9

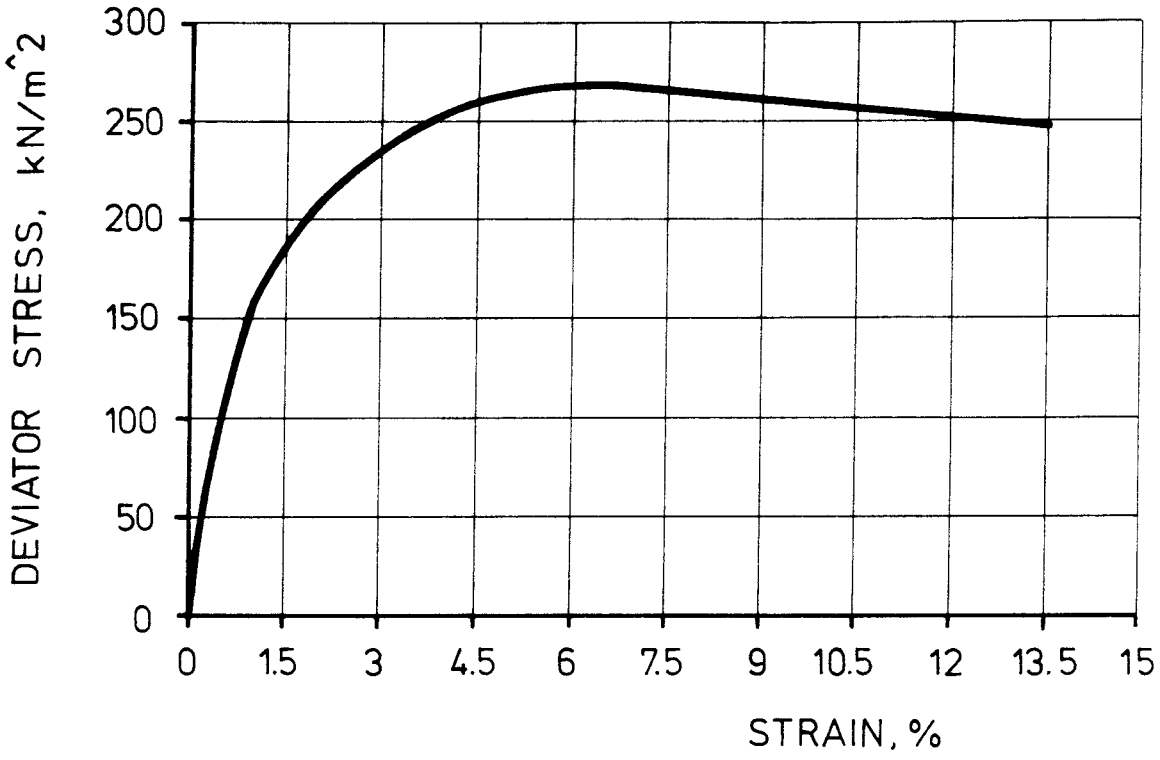
DEVIATOR STRESS, kN/m^2
300
250
200
150
100
50
0
0
1.5
3
4.5
6
7.5
9
10.5
12
13.5
15
STRAIN, %

TEST TMX1

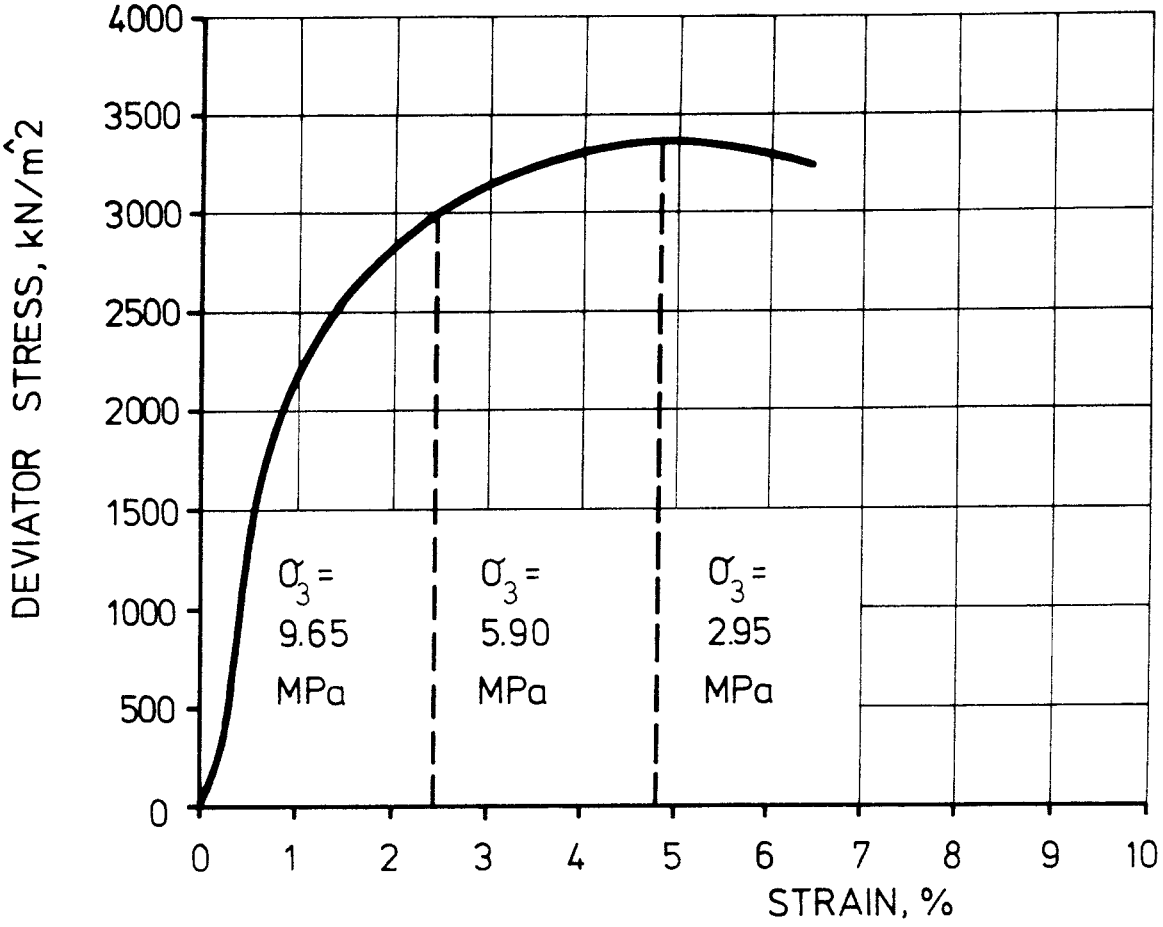
DEVIATOR STRESS, kN/m^2
4000
3500
3000
2500
2000
1500
1000
500
0
0
1
2
3
4
5
6
7
8
9
10
STRAIN, %
σ3 = 9.65 MPa
σ3 = 5.90 MPa
σ3 = 2.95 MPa

TEST TMX2

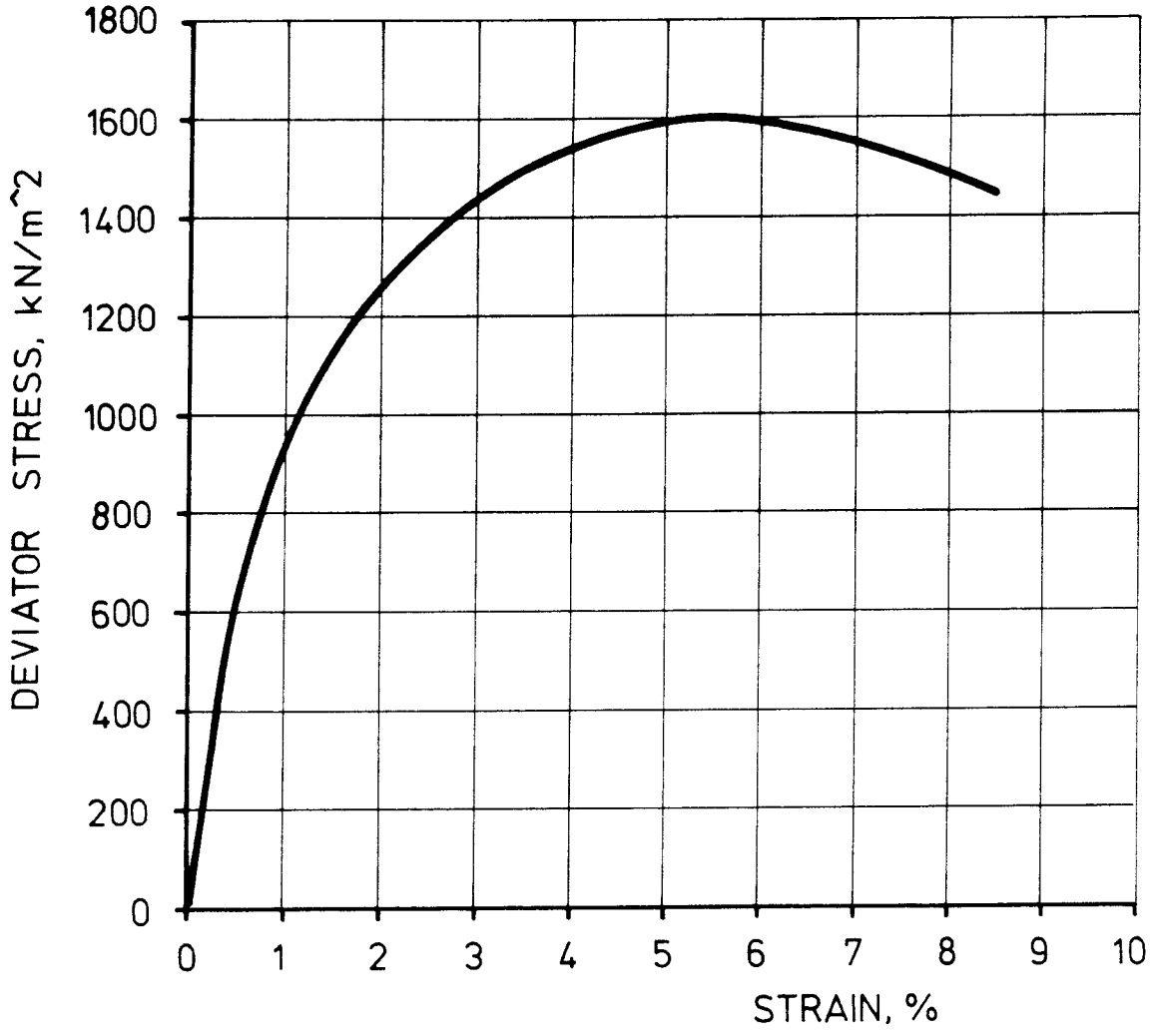
1800
1600
1400
1200
1000
800
600
400
200
0
DEVIATOR STRESS, kN/m^2
0
1
2
3
4
5
6
7
8
9
10
STRAIN, %

TEST TMX3

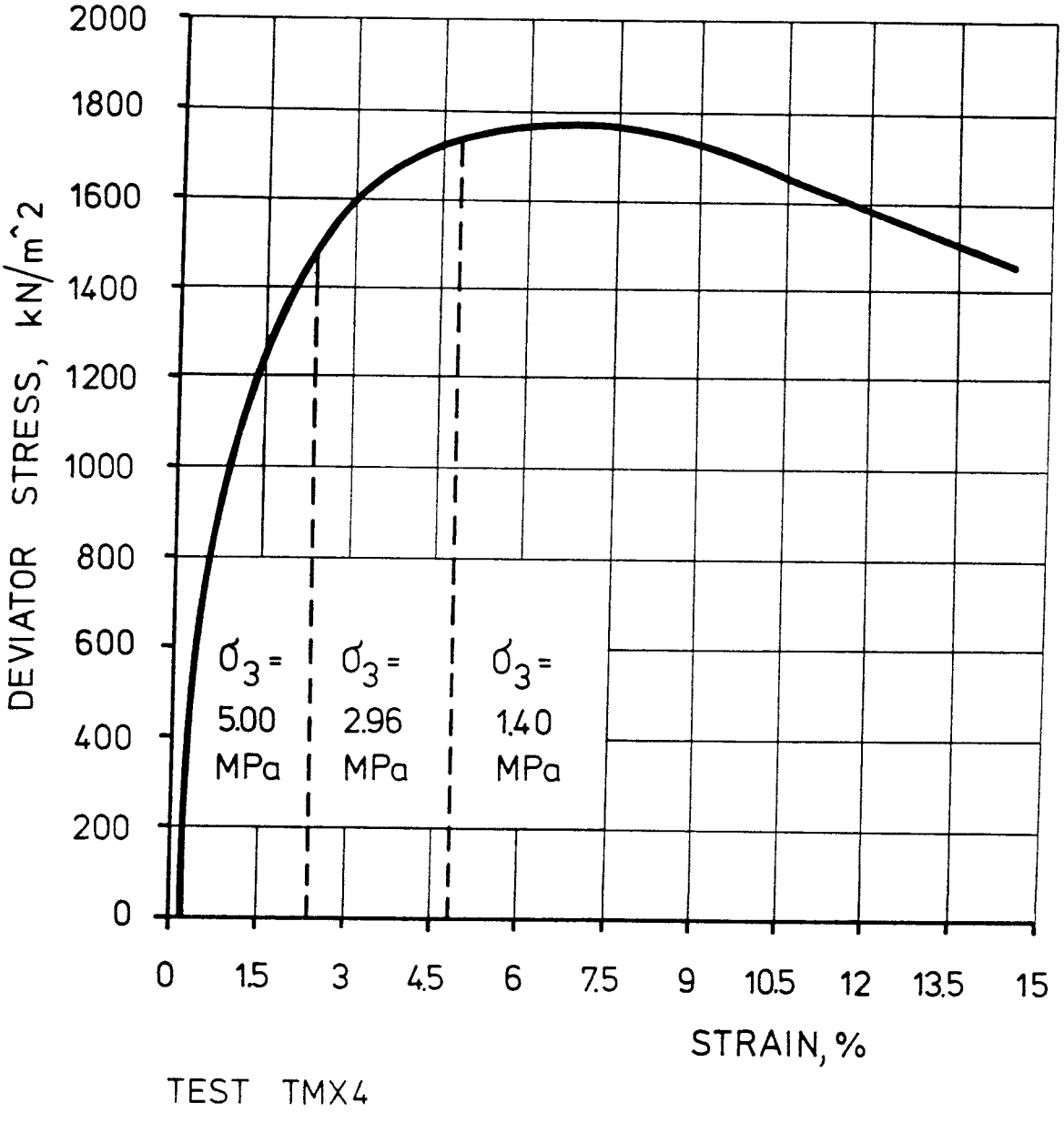
2000
1800
1600
1400
1200
1000
800
600
400
200
0
DEVIATOR STRESS, kN/m^2
σ3 = 5.00 MPa
σ3 = 2.96 MPa
σ3 = 1.40 MPa
0
1.5
3
4.5
6
7.5
9
10.5
12
13.5
15
STRAIN, %

TEST TMX4

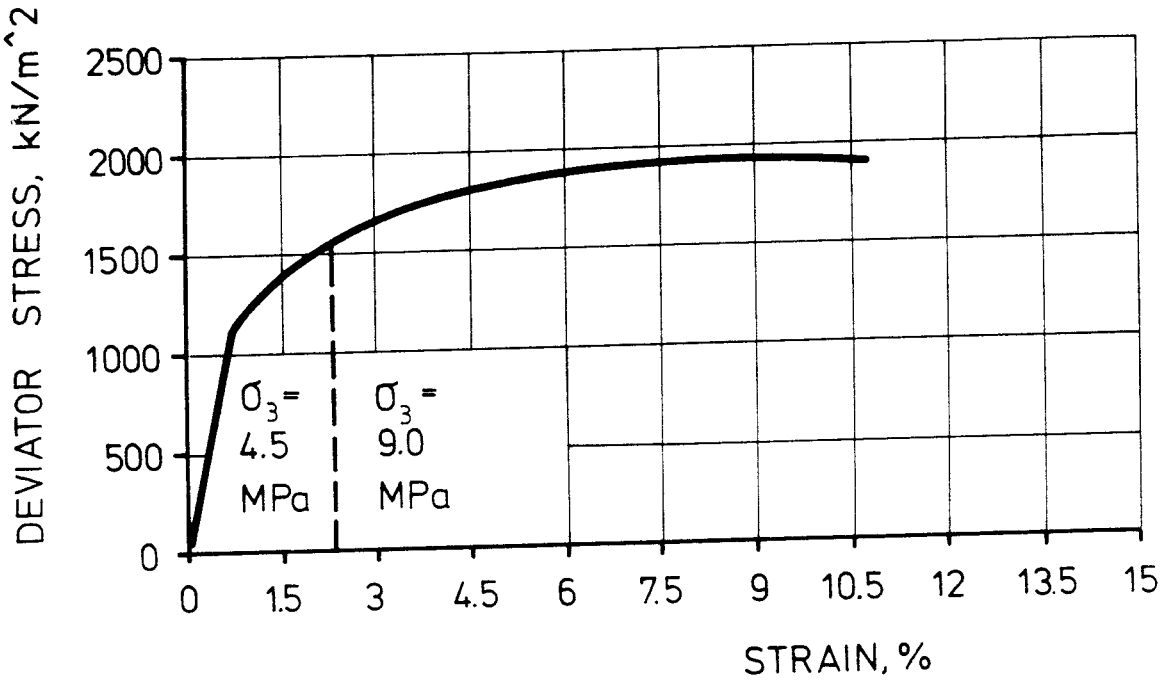
DEVIATOR STRESS, kN/m^2
2500
2000
1500
1000
500
0
0
1.5
3
4.5
6
7.5
9
10.5
12
13.5
15
STRAIN, %
σ3 = 4.5 MPa
σ3 = 9.0 MPa

TEST TMX 5

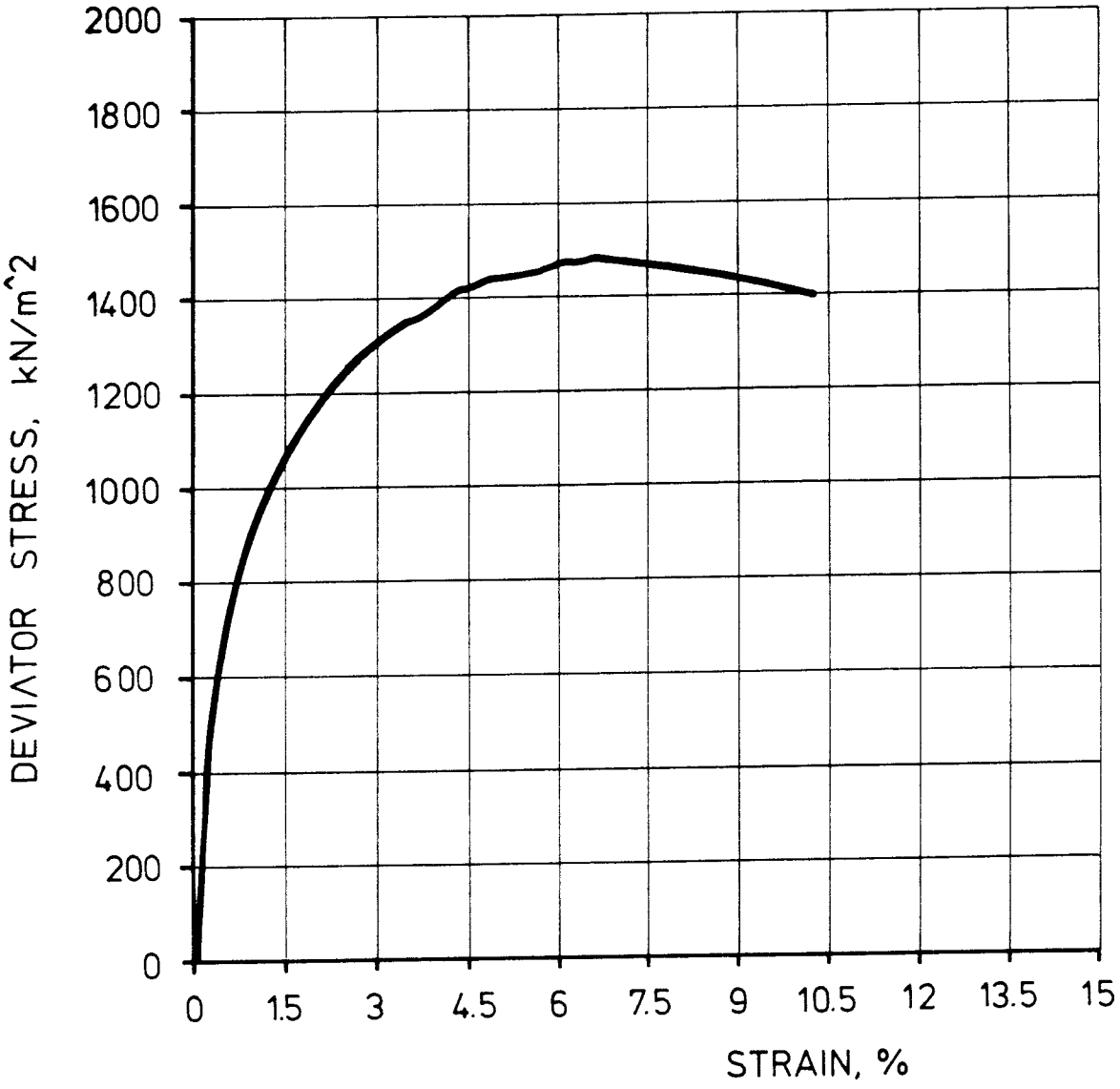
2000
1800
1600
1400
1200
1000
800
600
400
200
0
DEVIATOR STRESS, kN/m^2
0
1.5
3
4.5
6
7.5
9
10.5
12
13.5
15
STRAIN, %

TEST TMX6

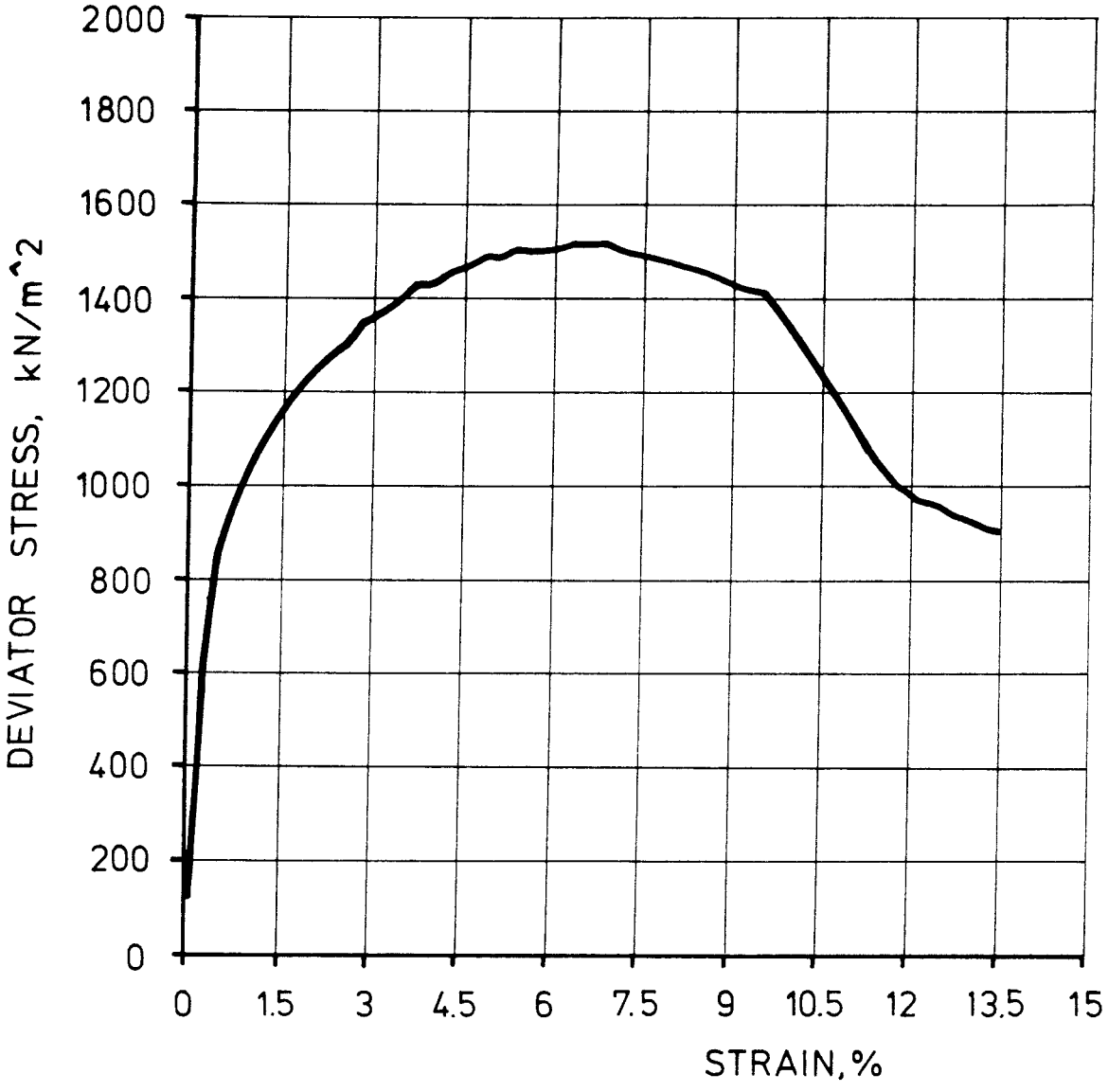
2000
1800
1600
1400
1200
1000
800
600
400
200
0
DEVIATOR STRESS, kN/m^2
0
1.5
3
4.5
6
7.5
9
10.5
12
13.5
15
STRAIN, %

TEST TMX 8

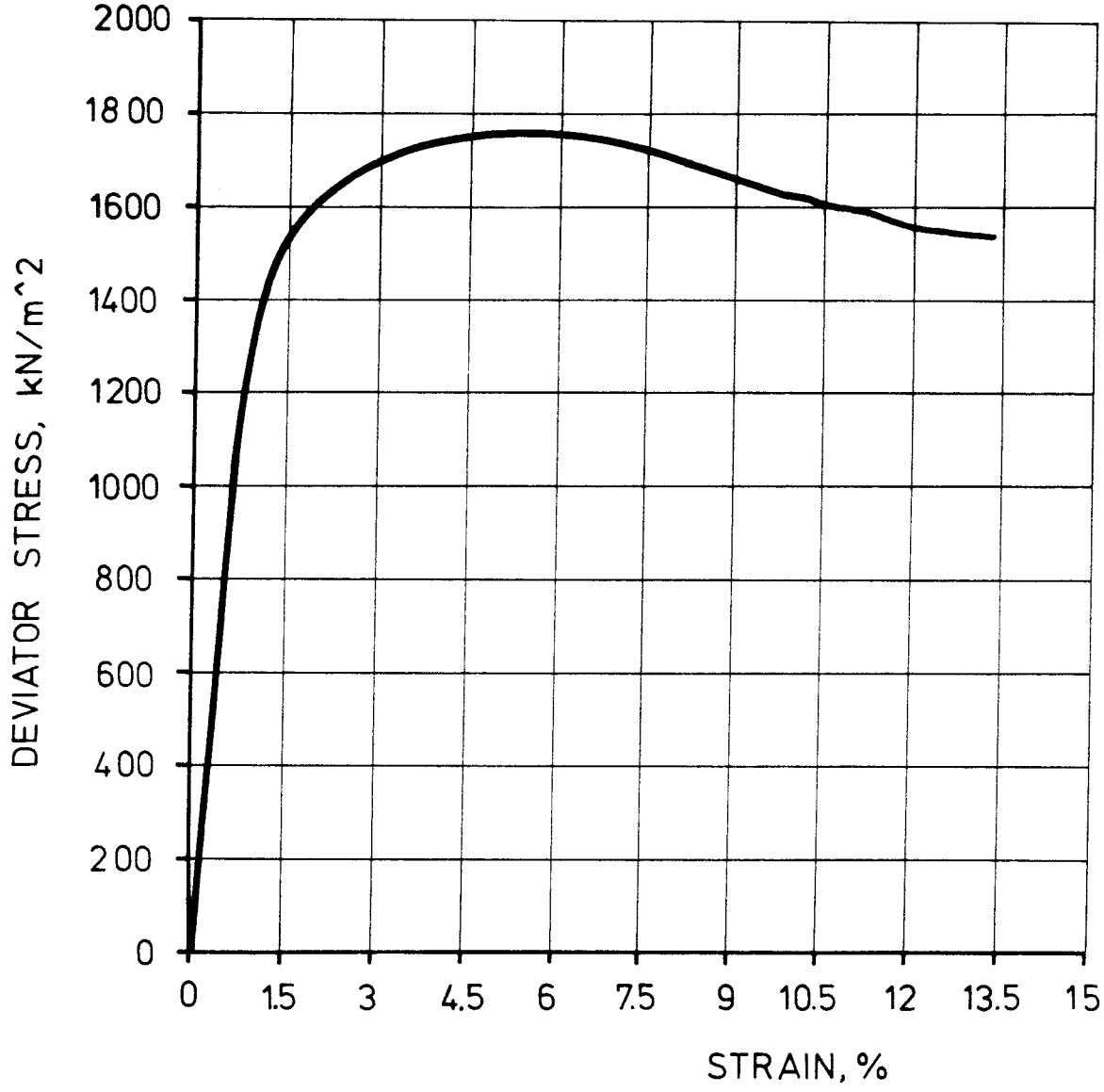
2000
18 00
1600
1400
1200
1000
800
600
400
200
0
DEVIATOR STRESS, kN/m^2
0
1.5
3
4.5
6
7.5
9
10.5
12
13.5
15
STRAIN, %

TEST TMX9

APPENDIX II

Simple shear tests SMX1 - SMX3

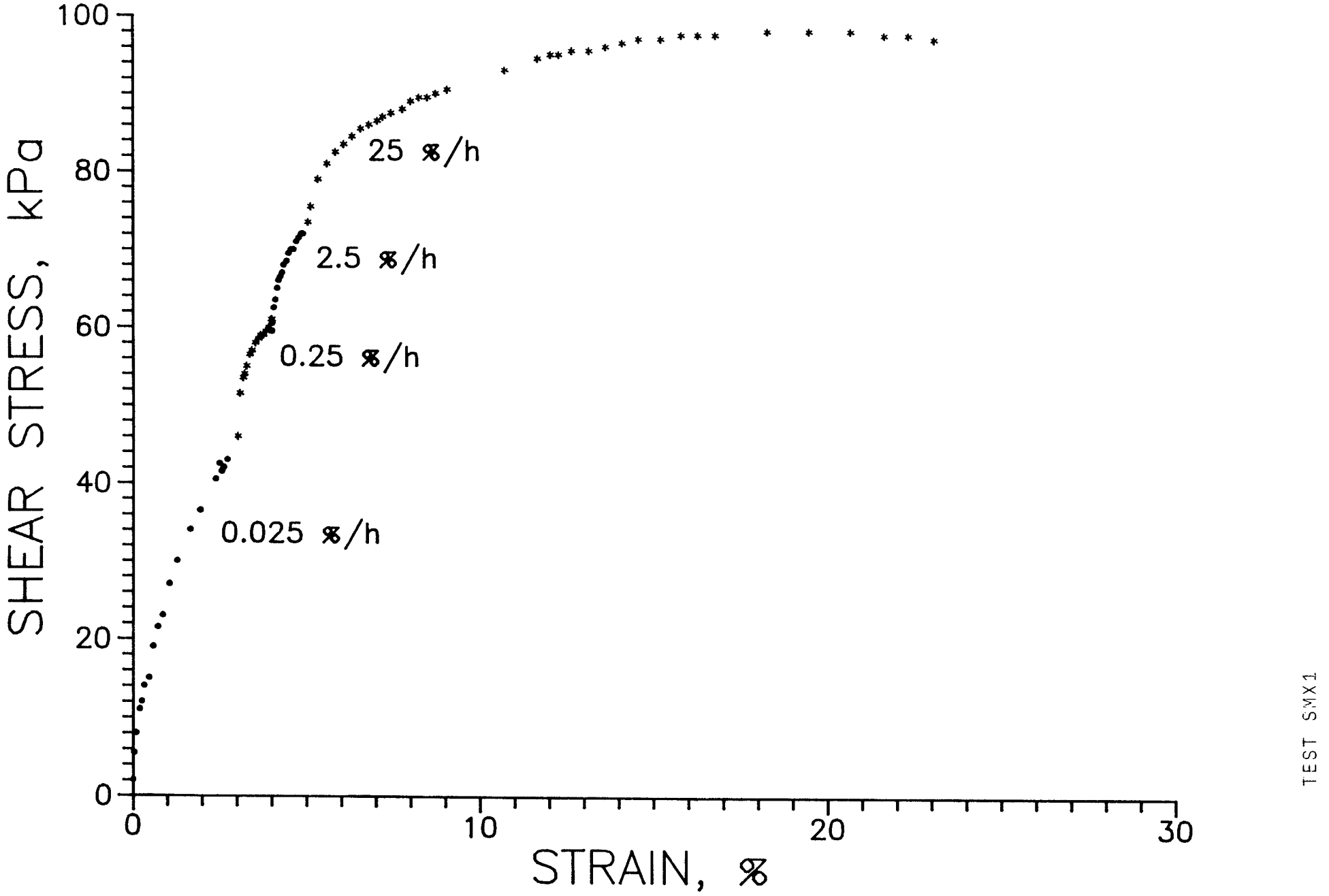
SHEAR STRESS, kPa
100
80
60
40
20
0
0
10
20
30
STRAIN, %
25 %/h
2.5 %/h
0.25 %/h
0.025 %/h
TEST SMX1

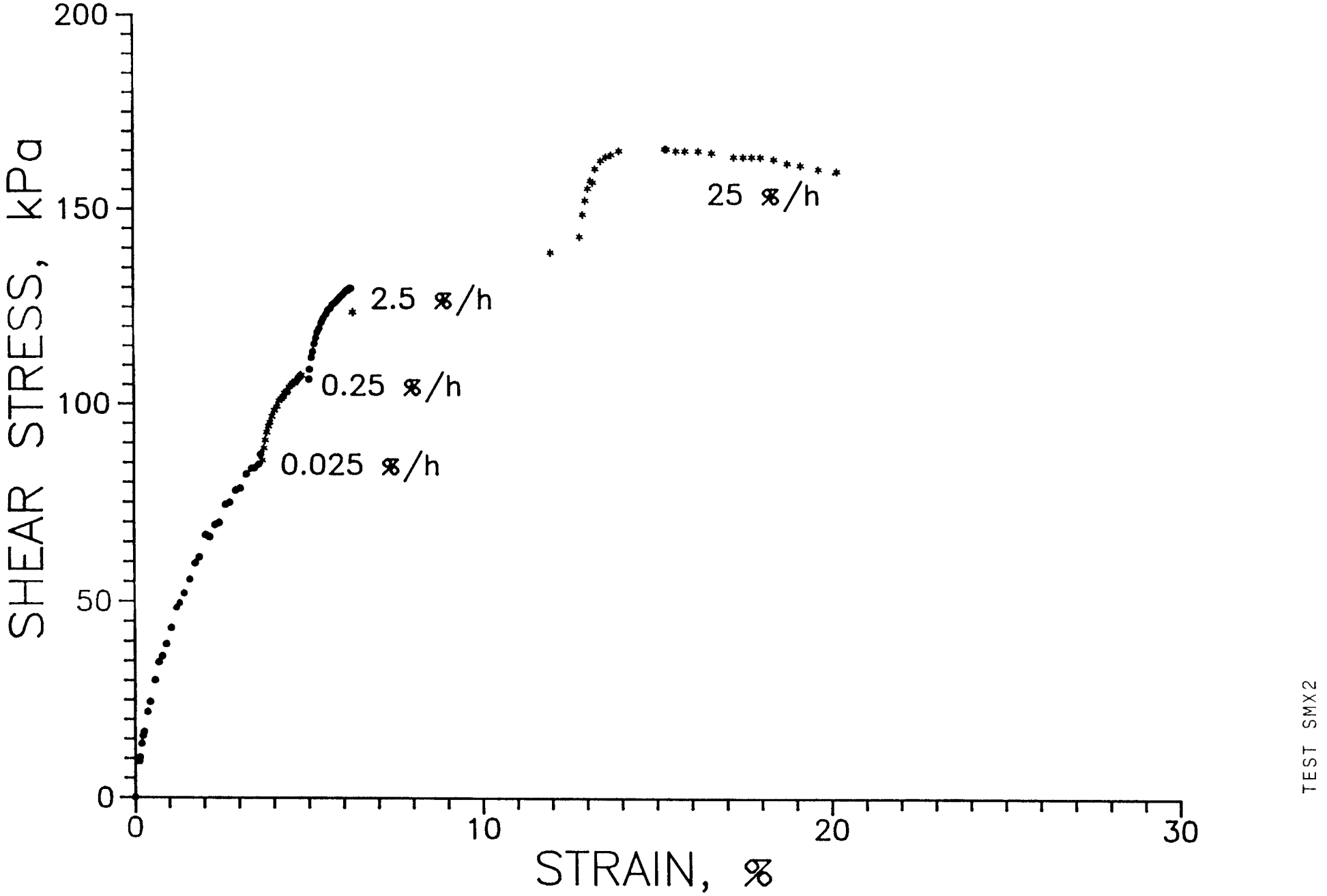
SHEAR STRESS, kPa
200
150
100
50
0
0
10
20
30
STRAIN, %
25 %/h
2.5 %/h
0.25 %/h
0.025 %/h
TEST SMX2

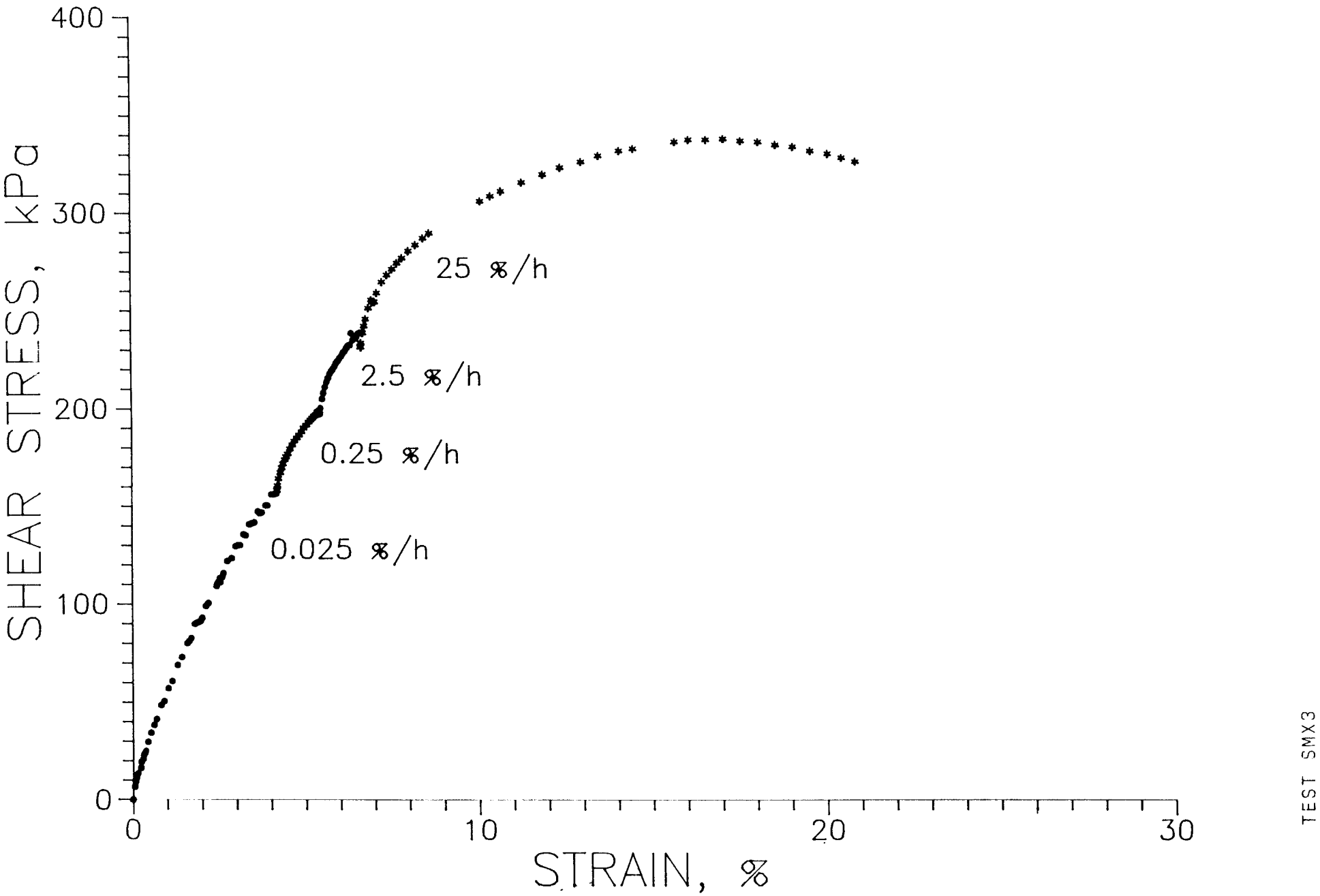
400
300
200
100
0
SHEAR STRESS, kPa
0
10
20
30
STRAIN, %
25 %/h
2.5 %/h
0.25 %/h
0.025 %/h
TEST SMX3

APPENDIX III

Triaxial creep tests TCR1 - TCR9
(TMX1 - TMX9)

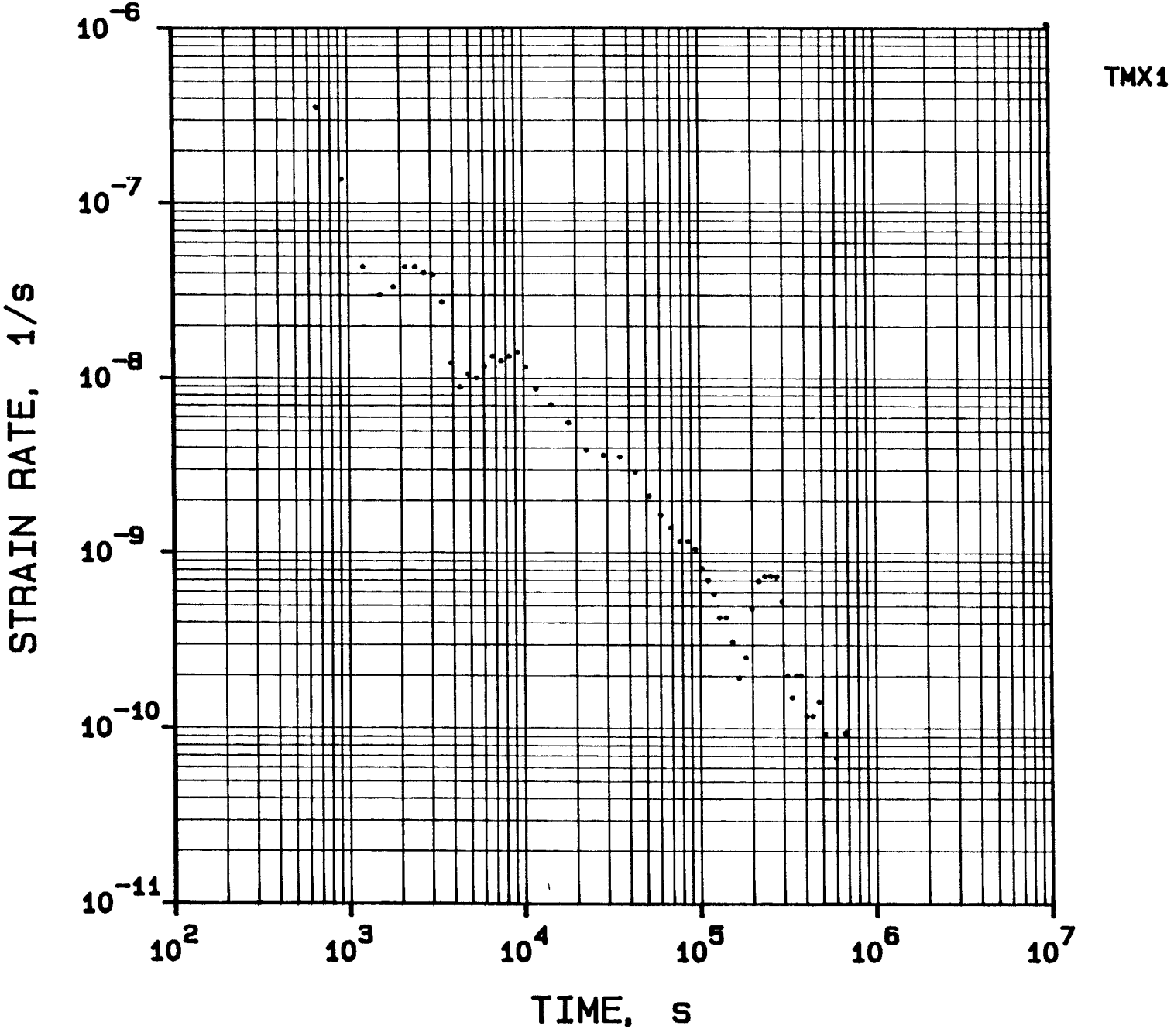
TMX1
STRAIN RATE, 1/s
10^{-6}
10^{-7}
10^{-8}
10^{-9}
10^{-10}
10^{-11}
10^{2}
10^{3}
10^{4}
10^{5}
10^{6}
10^{7}
TIME, s

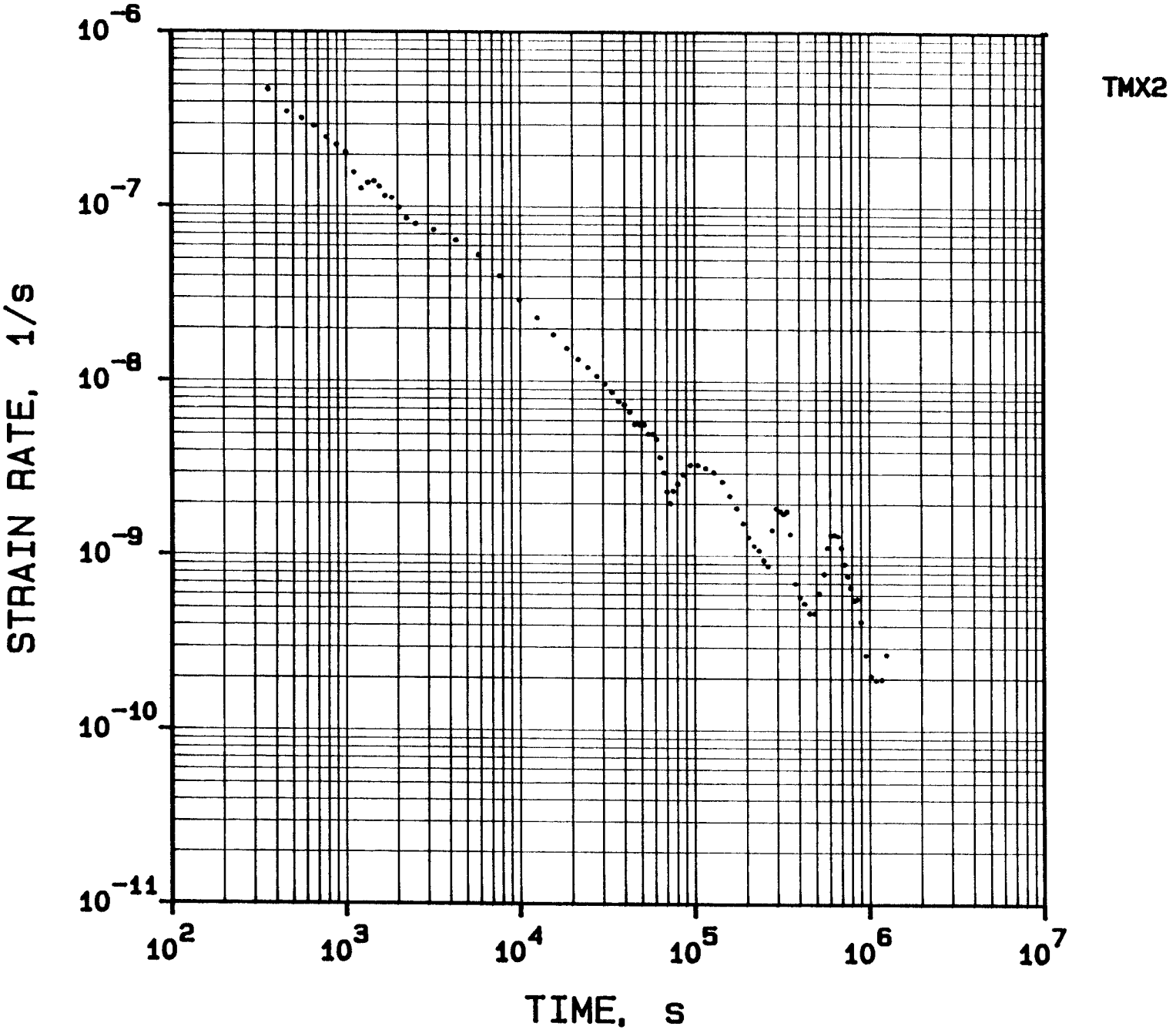
STRAIN RATE, 1/s
10^{-6}
10^{-7}
10^{-8}
10^{-9}
10^{-10}
10^{-11}
10^{2}
10^{3}
10^{4}
10^{5}
10^{6}
10^{7}
TIME, s
TMX2

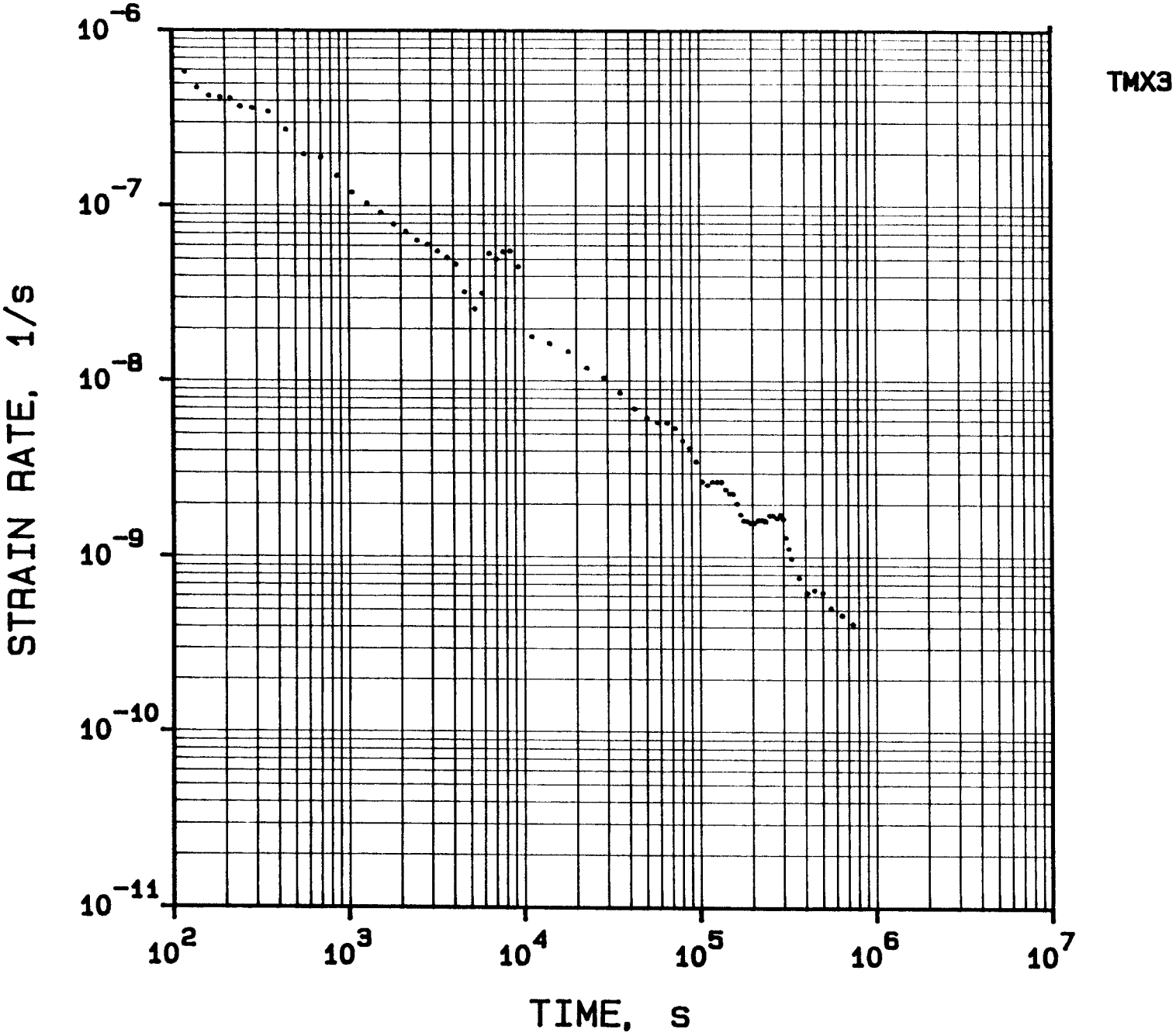
TMX3
STRAIN RATE, 1/s
10^{-6}
10^{-7}
10^{-8}
10^{-9}
10^{-10}
10^{-11}
10^{2}
10^{3}
10^{4}
10^{5}
10^{6}
10^{7}
TIME, s

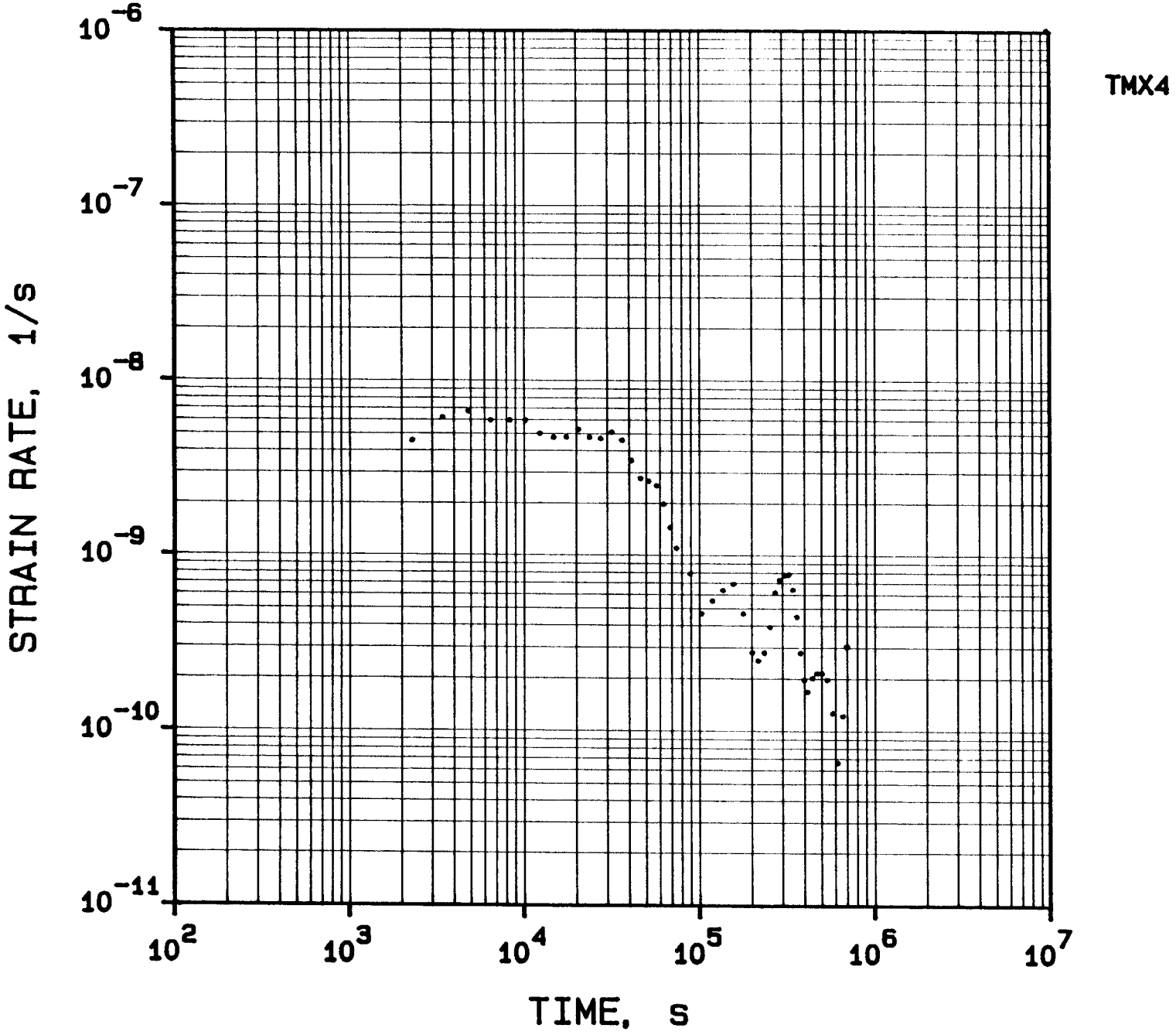
STRAIN RATE, 1/s
10^{-6}
10^{-7}
10^{-8}
10^{-9}
10^{-10}
10^{-11}
10^{2}
10^{3}
10^{4}
10^{5}
10^{6}
10^{7}
TIME, s
TMX4

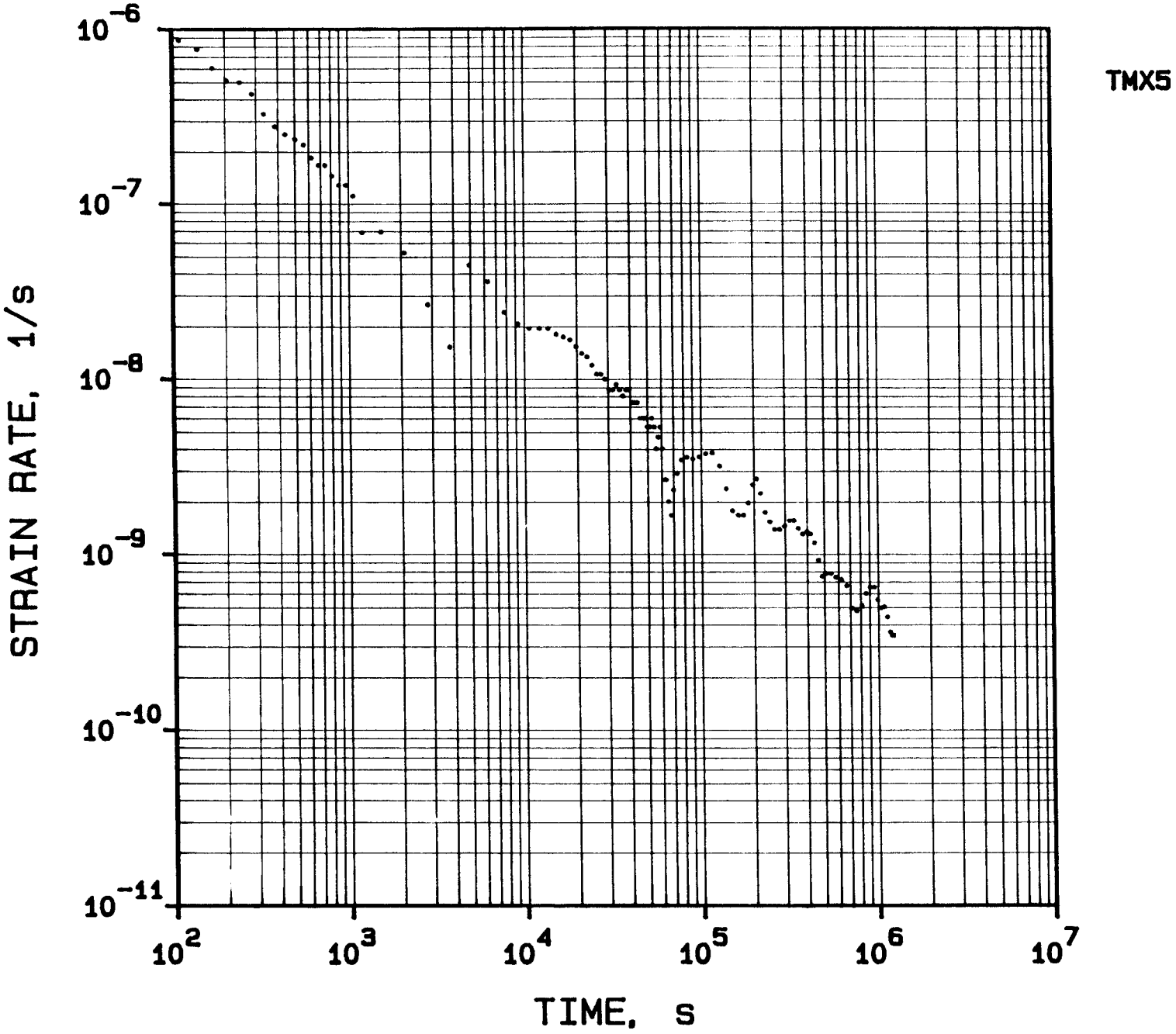
TMX5
STRAIN RATE, 1/s
10^{-6}
10^{-7}
10^{-8}
10^{-9}
10^{-10}
10^{-11}
10^{2}
10^{3}
10^{4}
10^{5}
10^{6}
10^{7}
TIME, s

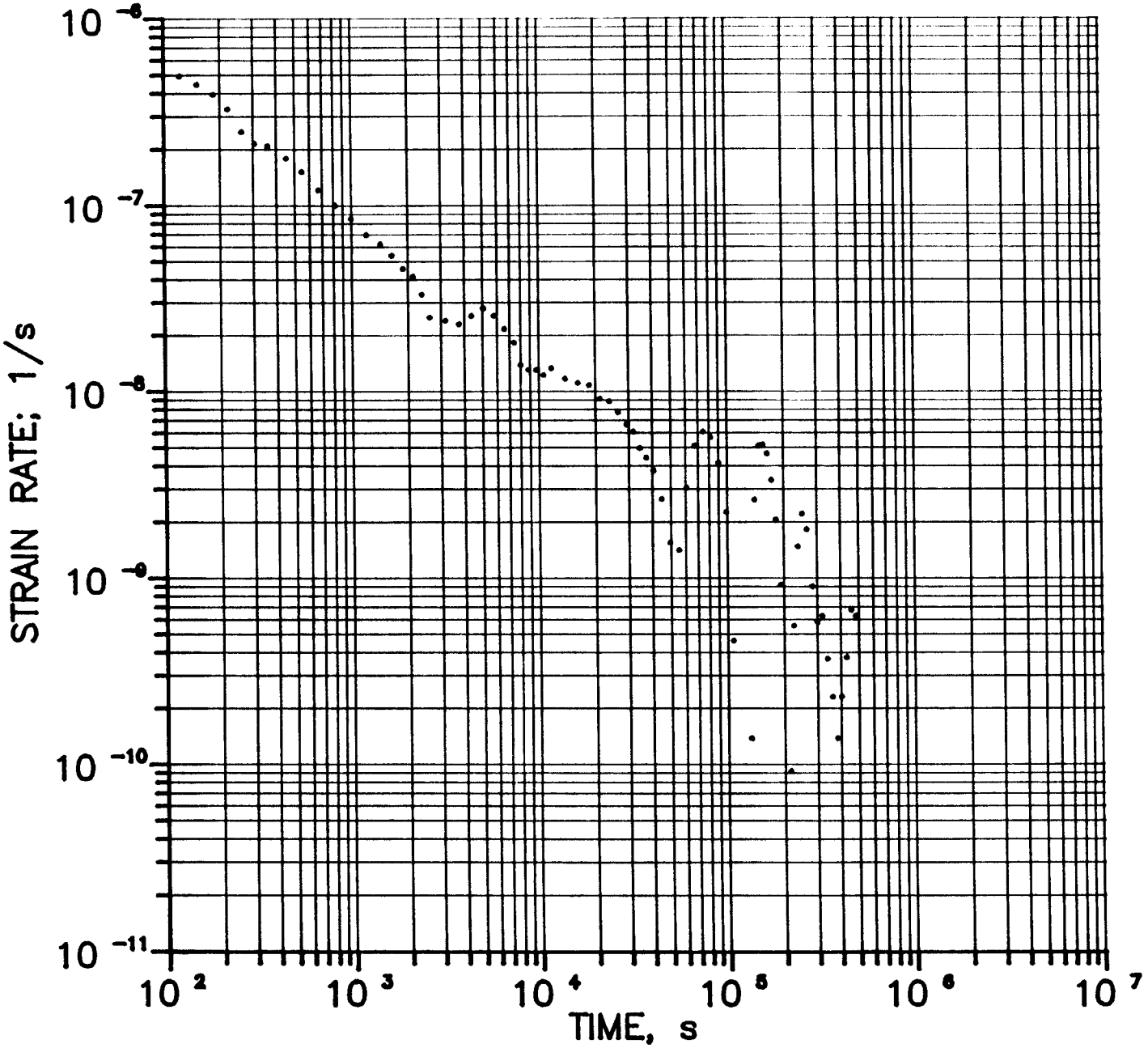
STRAIN RATE; 1/s
10 -6
10 -7
10 -8
10 -9
10 -10
10 -11
10 2
10 3
10 4
10 5
10 6
10 7
TIME, s

TMX6

LTMX6

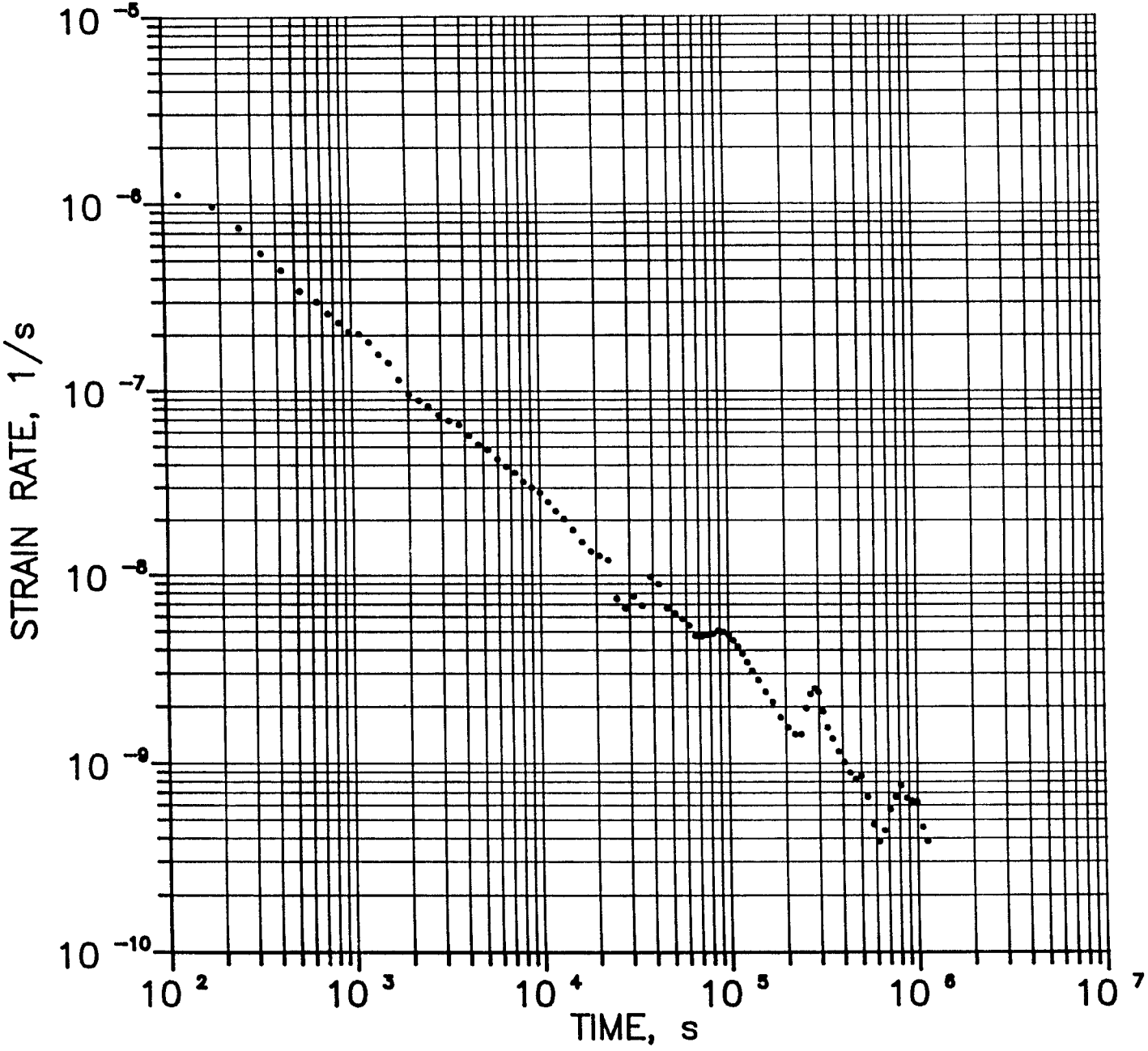
STRAIN RATE, 1/s
10 -5
10 -6
10 -7
10 -8
10 -9
10 -10
10 2
10 3
10 4
10 5
10 6
10 7
TIME, s

TMX8

ltmx8

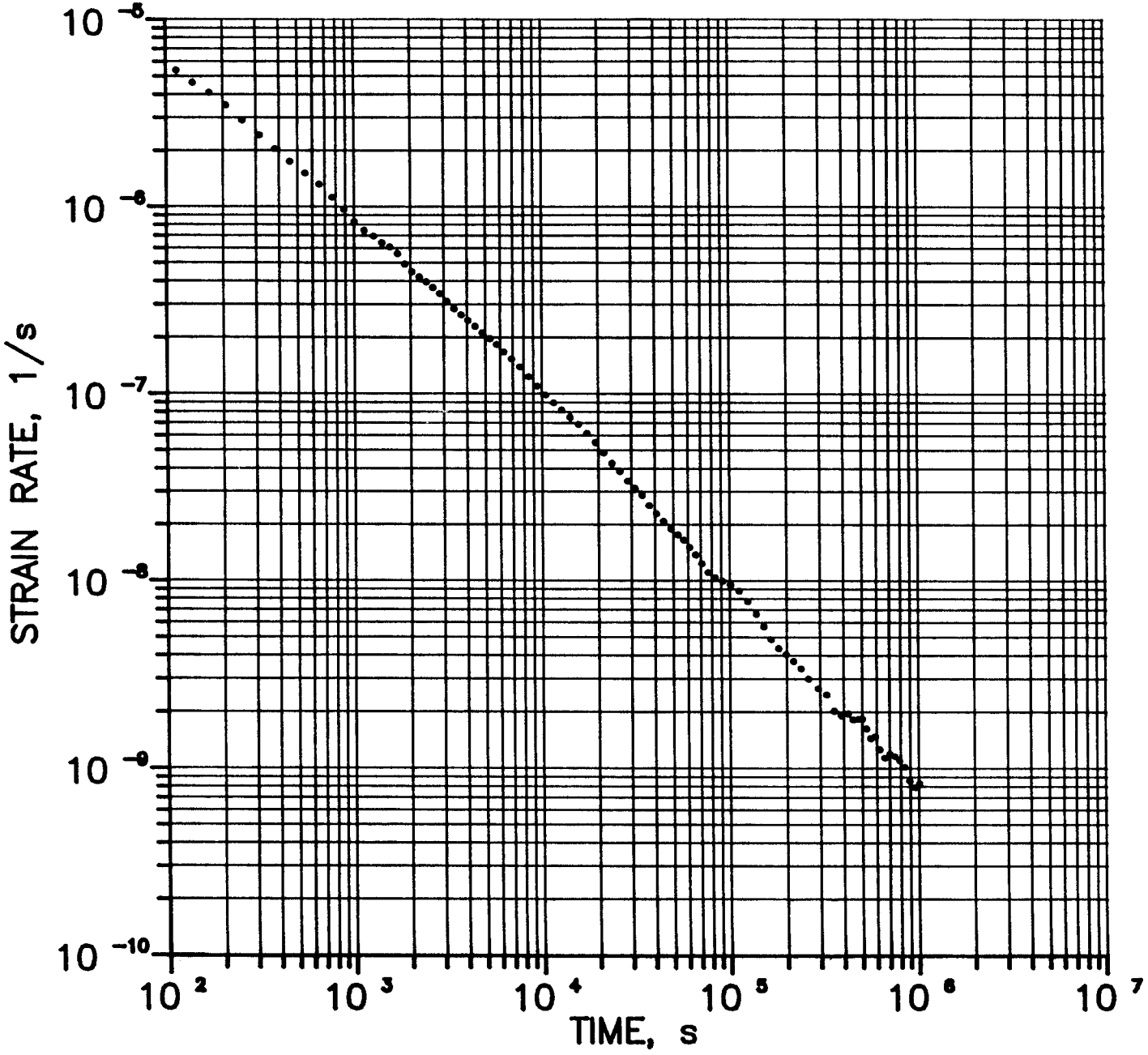
STRAIN RATE, 1/s
10 -5
10 -6
10 -7
10 -8
10 -9
10 -10
10 2
10 3
10 4
10 5
10 6
10 7
TIME, s

TMX9

ltmx9

APPENDIX IV

Direct shear creep tests DMX1 - DMX4

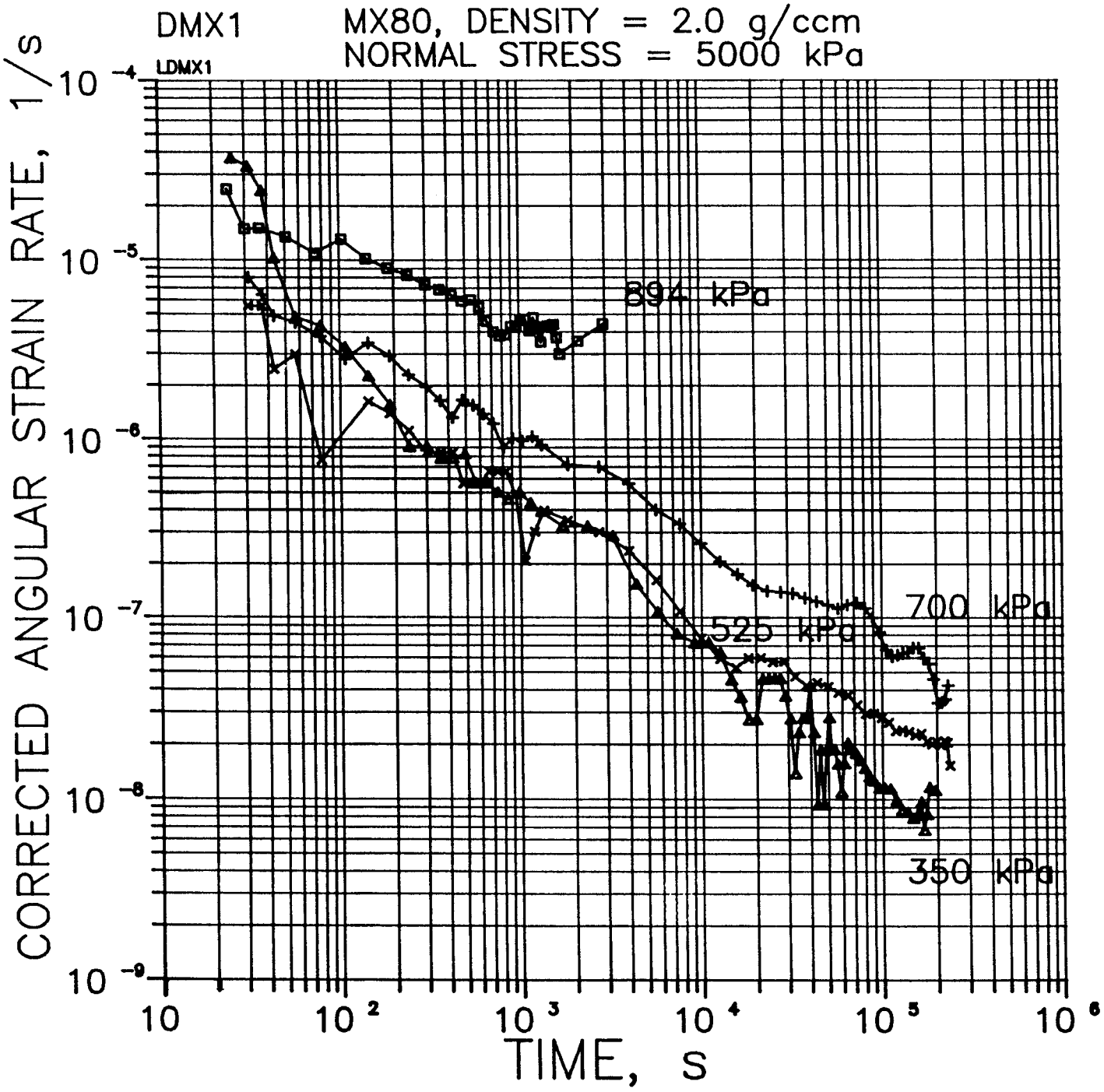
DMX1
LDMX1
MX80, DENSITY = 2.0 g/ccm
NORMAL STRESS = 5000 kPa
CORRECTED ANGULAR STRAIN RATE, 1/s
TIME, s
894 kPa
700 kPa
525 kPa
350 kPa

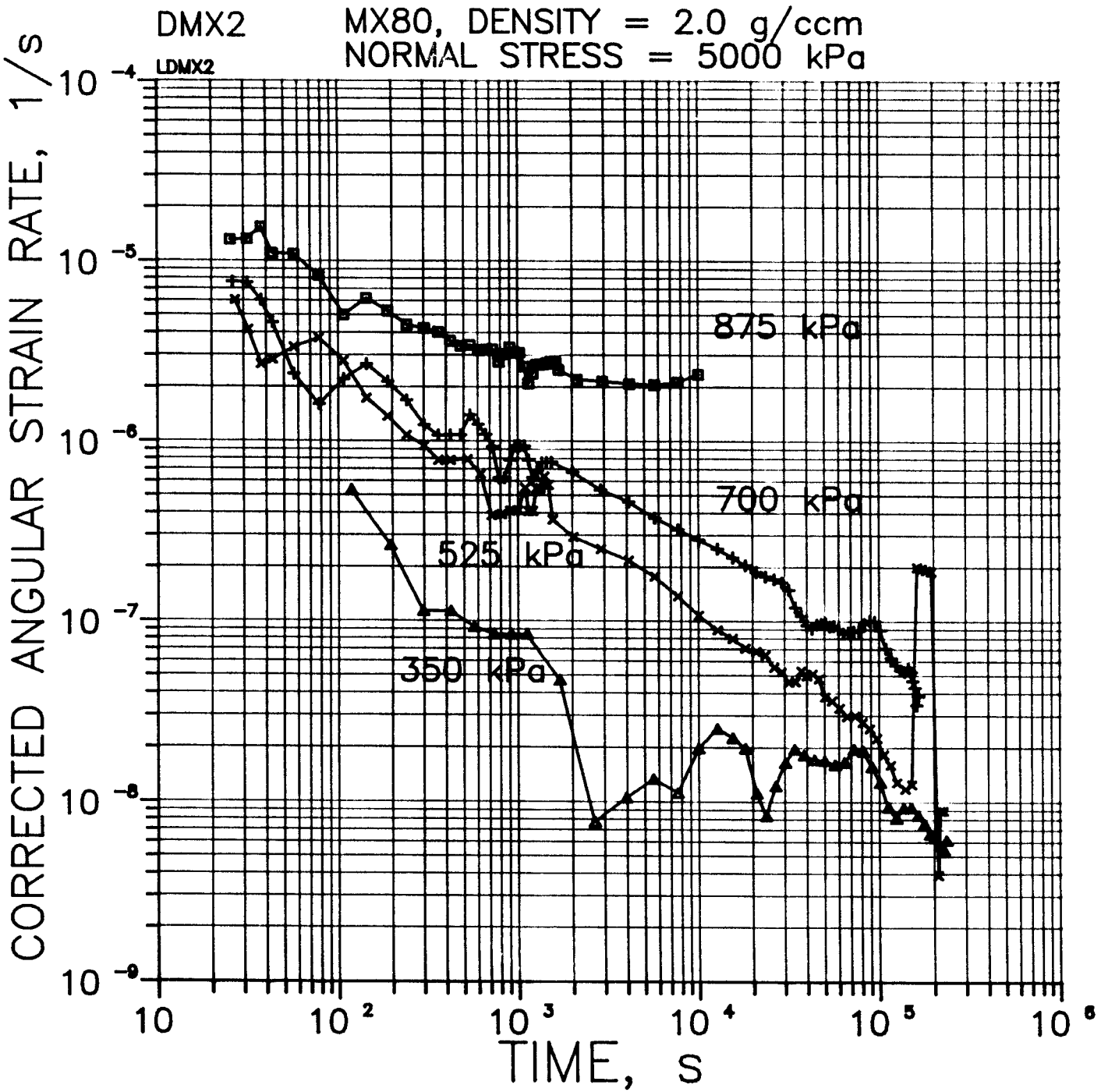
DMX2
LDMX2
MX80, DENSITY = 2.0 g/ccm
NORMAL STRESS = 5000 kPa
875 kPa
700 kPa
525 kPa
350 kPa
CORRECTED ANGULAR STRAIN RATE, 1/s
TIME, s
10 -4
10 -5
10 -6
10 -7
10 -8
10 -9
10
10 2
10 3
10 4
10 5
10 6

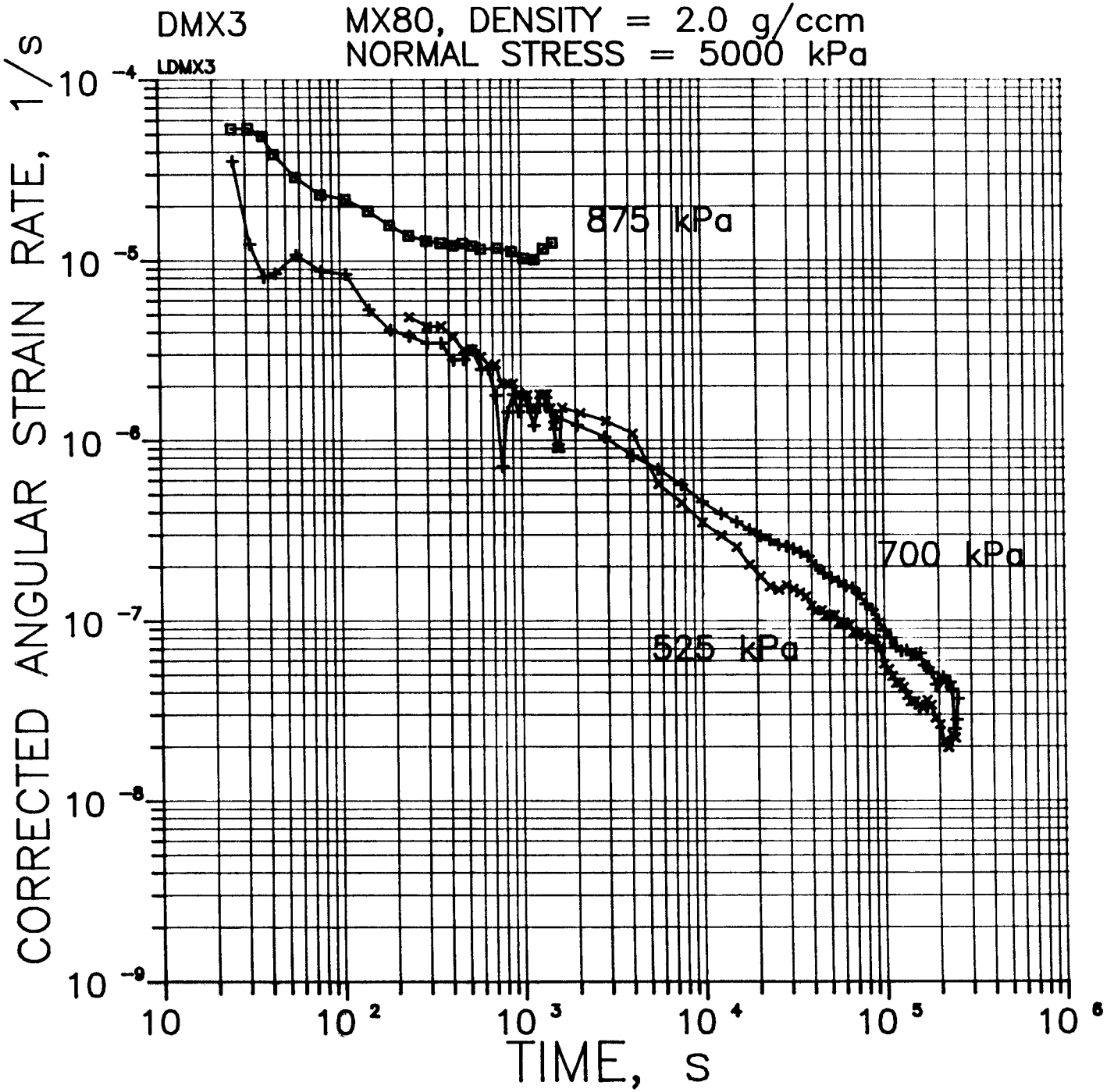
DMX3
LDMX3
MX80, DENSITY = 2.0 g/ccm
NORMAL STRESS = 5000 kPa
875 kPa
700 kPa
525 kPa
CORRECTED ANGULAR STRAIN RATE, 1/s
TIME, s
10 -4
10 -5
10 -6
10 -7
10 -8
10 -9
10
10 2
10 3
10 4
10 5
10 6

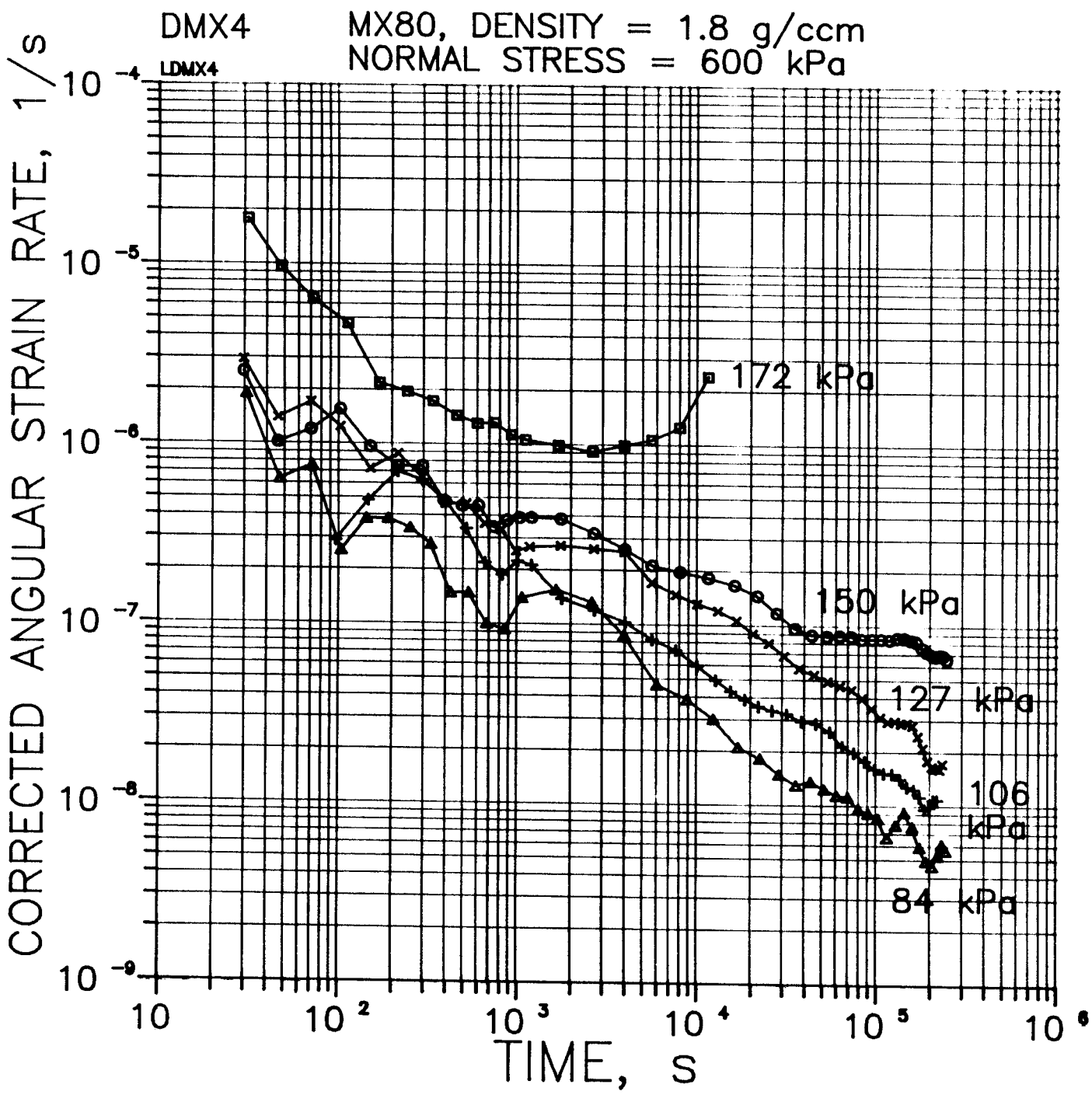
DMX4
LDMX4
MX80, DENSITY = 1.8 g/ccm
NORMAL STRESS = 600 kPa
CORRECTED ANGULAR STRAIN RATE, 1/s
TIME, s
172 kPa
150 kPa
127 kPa
106 kPa
84 kPa

APPENDIX V

Undrained compression and expansion tests

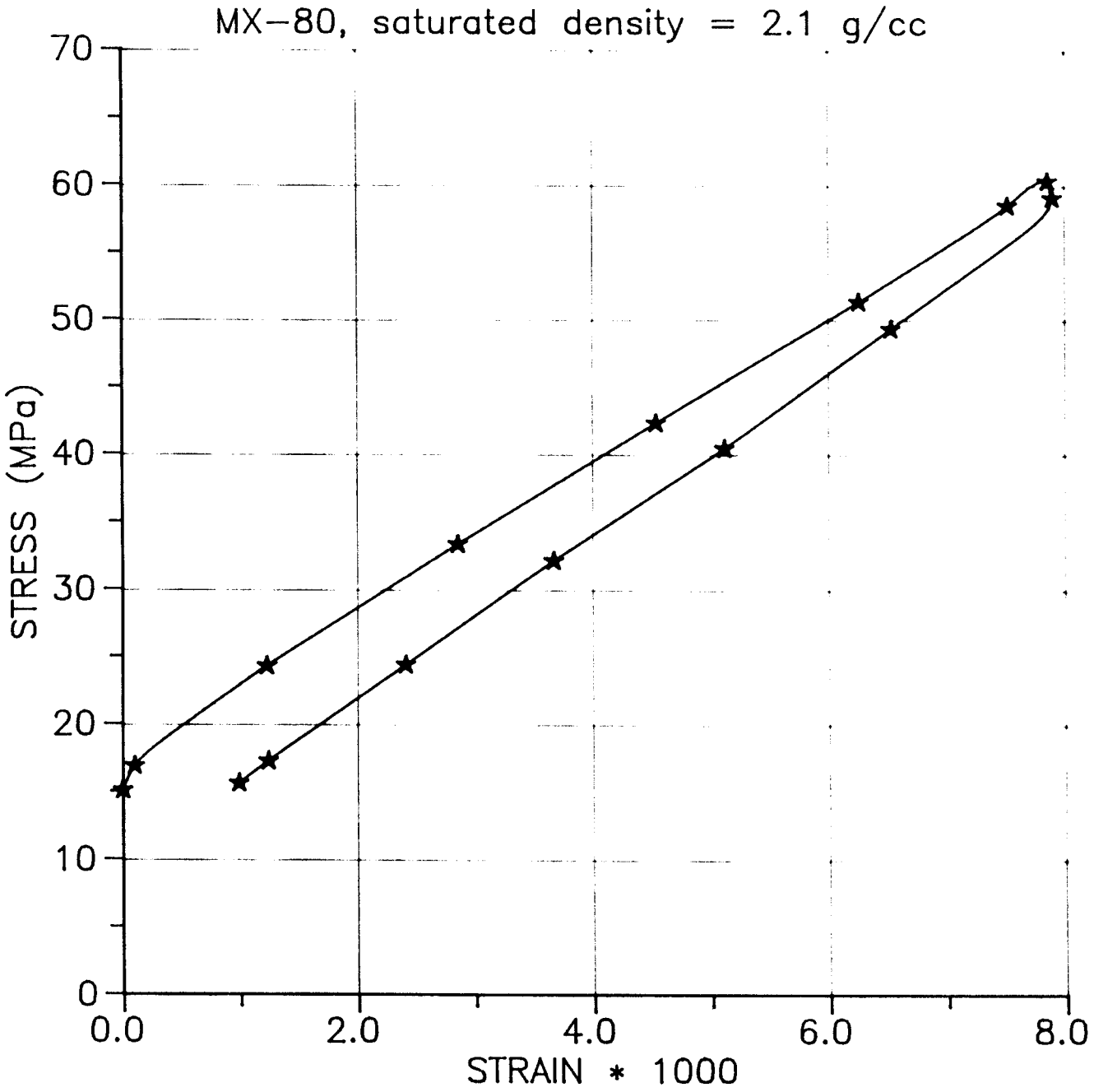
MX–80, saturated density = 2.1 g/cc
70
60
50
40
30
20
10
0
STRESS (MPa)
0.0
2.0
4.0
6.0
8.0
STRAIN * 1000

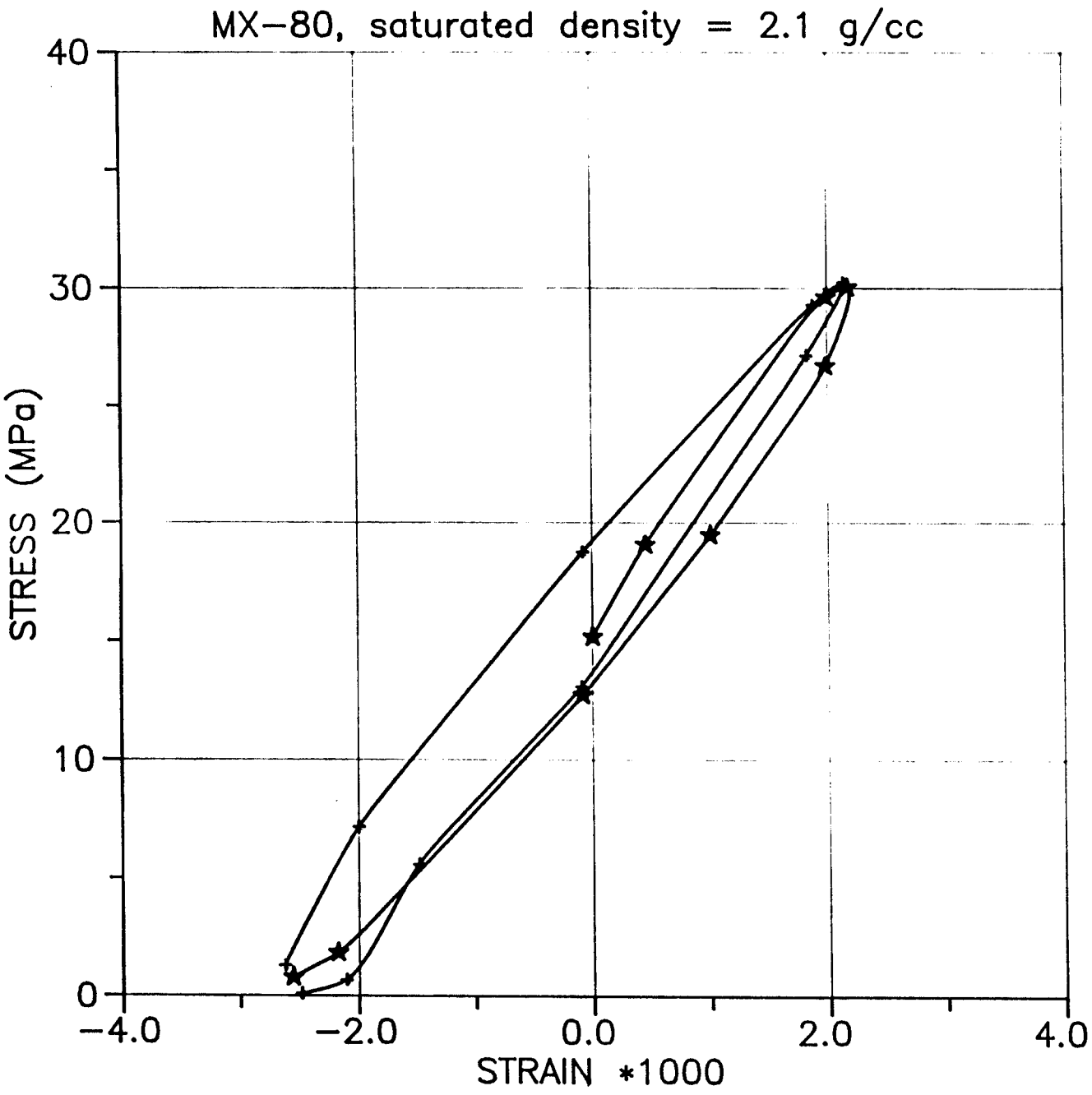
MX–80, saturated density = 2.1 g/cc
40
30
20
10
0
STRESS (MPa)
–4.0
–2.0
0.0
2.0
4.0
STRAIN *1000

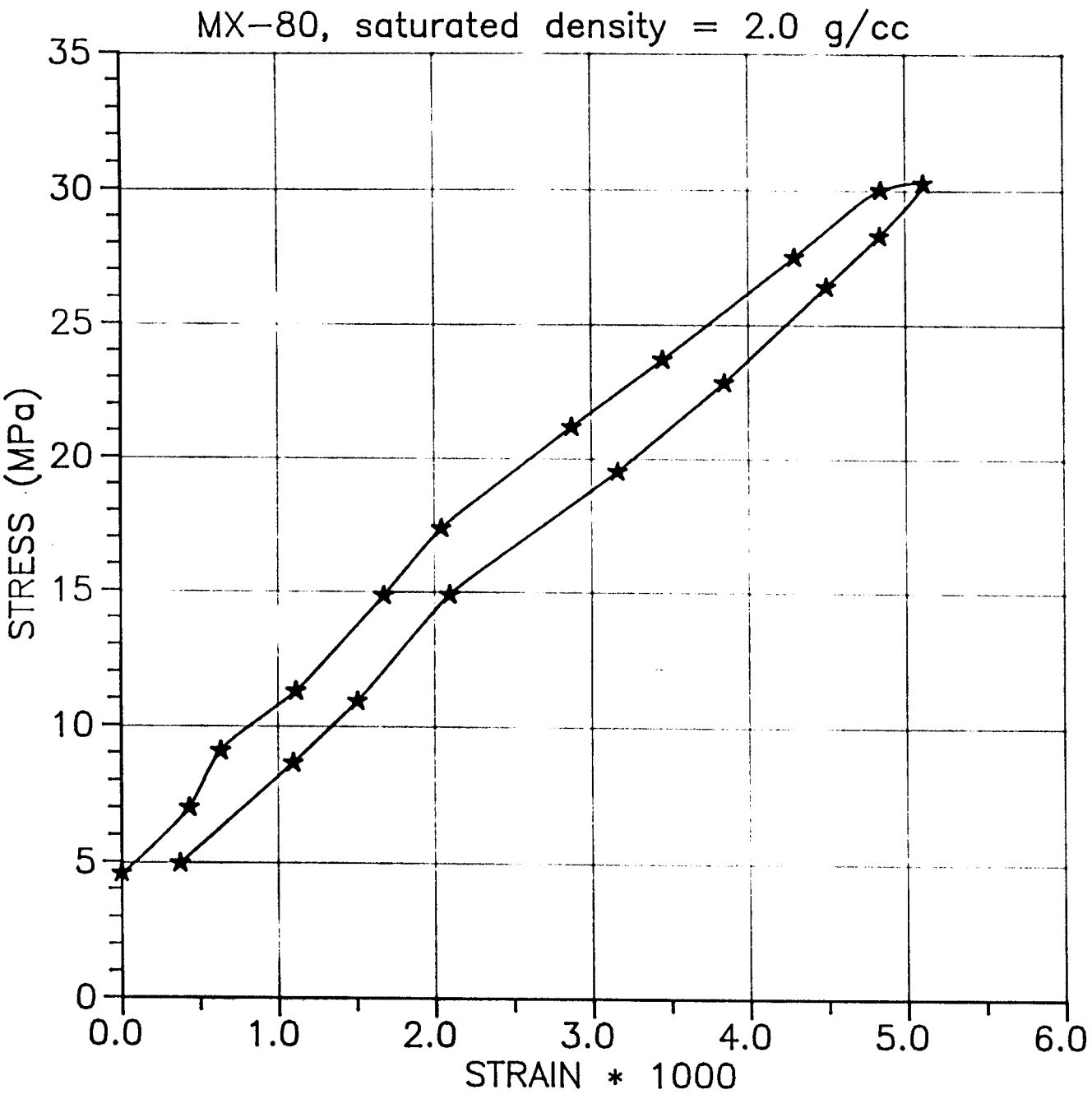
MX–80, saturated density = 2.0 g/cc
STRESS (MPa)
0
5
10
15
20
25
30
35
0.0
1.0
2.0
3.0
4.0
5.0
6.0
STRAIN * 1000

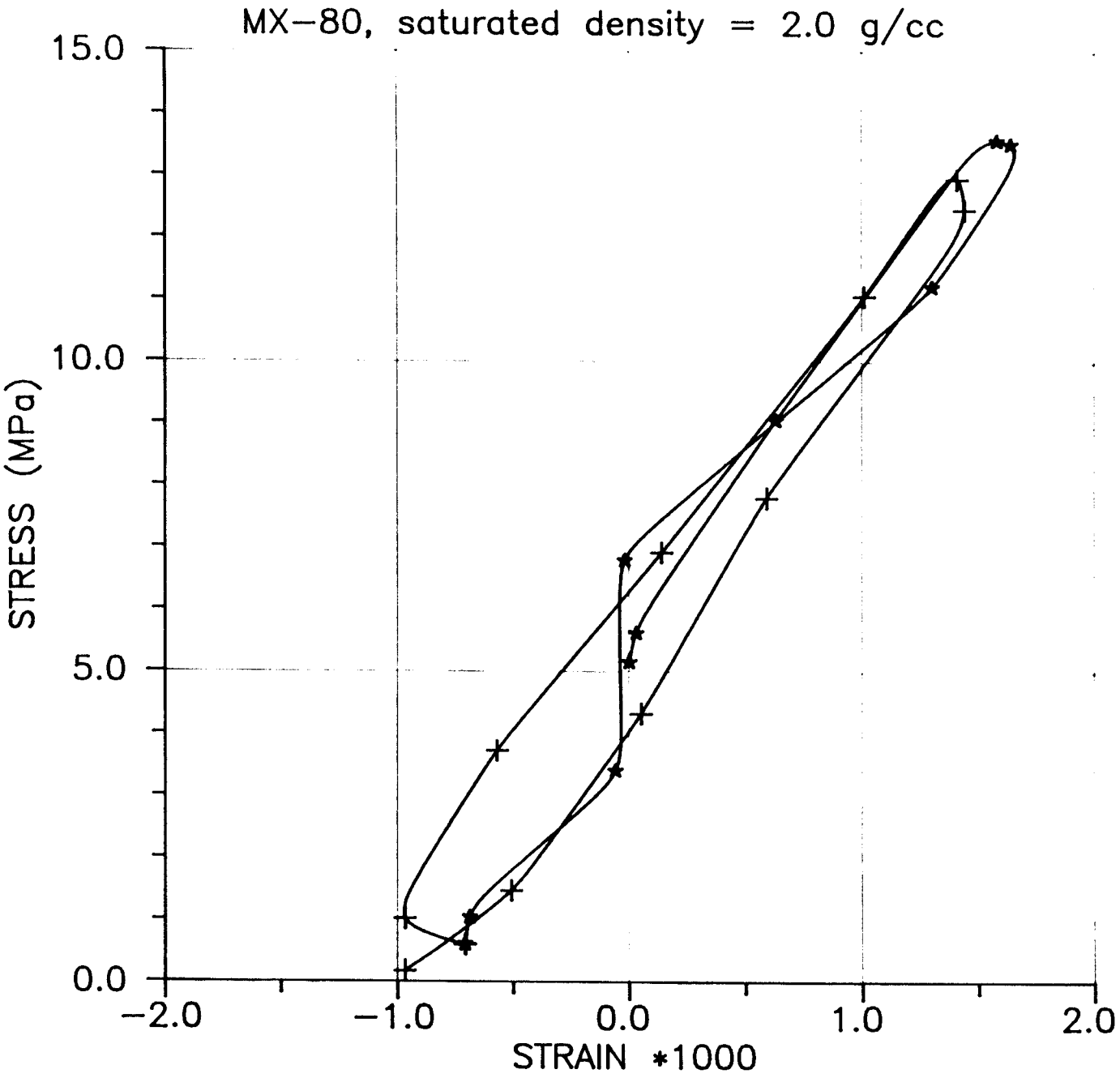
MX–80, saturated density = 2.0 g/cc
15.0
10.0
5.0
0.0
STRESS (MPa)
–2.0
–1.0
0.0
1.0
2.0
STRAIN *1000

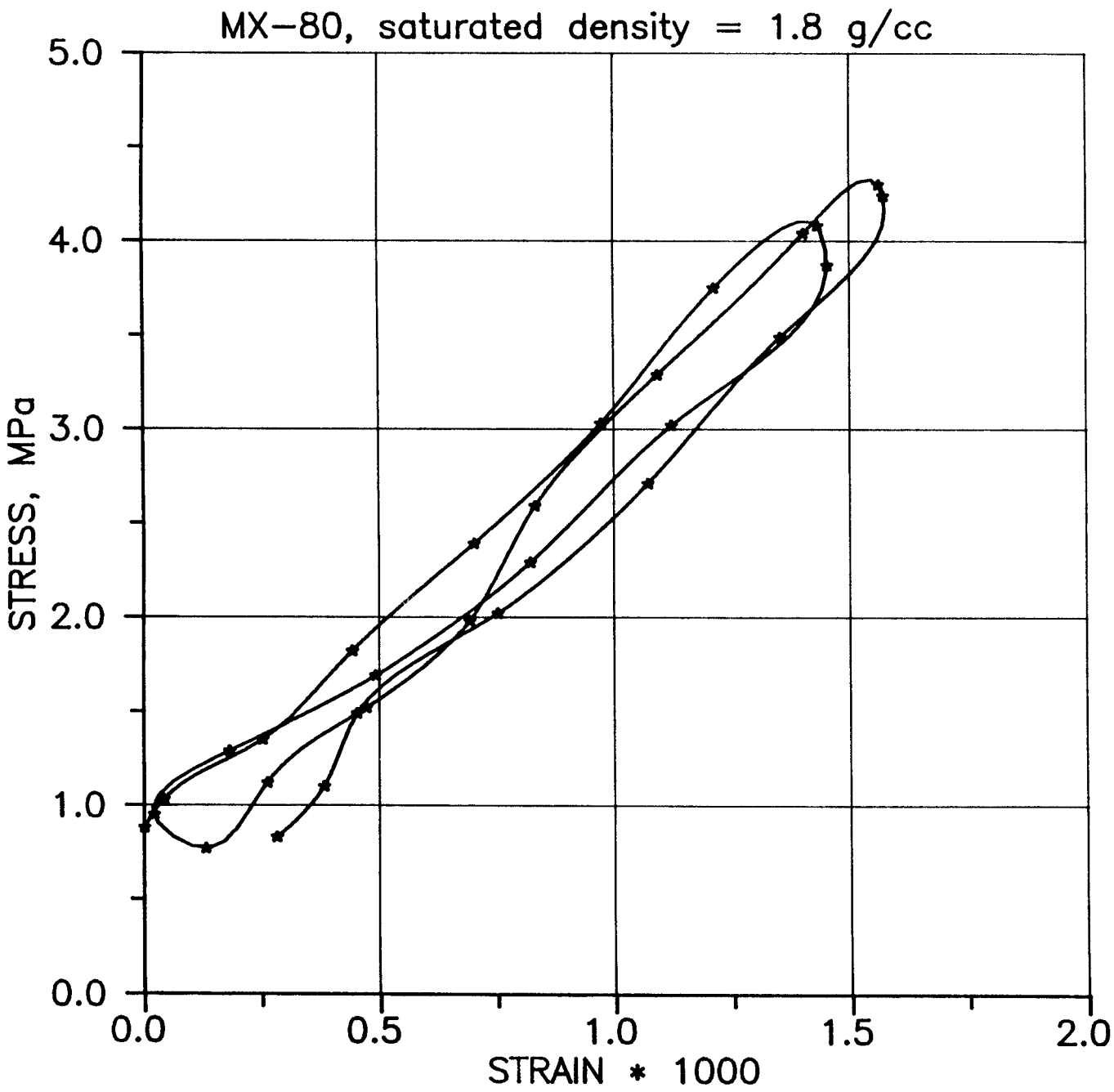
MX–80, saturated density = 1.8 g/cc
5.0
4.0
3.0
2.0
1.0
0.0
STRESS, MPa
0.0
0.5
1.0
1.5
2.0
STRAIN * 1000

List of SKB reports

Annual Reports

1977–78
TR 121
KBS Technical Reports 1 – 120.
Summaries. Stockholm, May 1979.

1979
TR 79–28
The KBS Annual Report 1979.
KBS Technical Reports 79-01 – 79-27.
Summaries. Stockholm, March 1980.

1980
TR 80–26
The KBS Annual Report 1980.
KBS Technical Reports 80-01 – 80-25.
Summaries. Stockholm, March 1981.

1981
TR 81–17
The KBS Annual Report 1981.
KBS Technical Reports 81-01 – 81-16.
Summaries. Stockholm, April 1982.

1982
TR 82–28
The KBS Annual Report 1982.
KBS Technical Reports 82-01 – 82-27.
Summaries. Stockholm, July 1983.

1983
TR 83–77
The KBS Annual Report 1983.
KBS Technical Reports 83-01 – 83-76
Summaries. Stockholm, June 1984.

1984
TR 85–01
Annual Research and Development Report 1984
Including Summaries of Technical Reports Issued during 1984. (Technical Reports 84-01– 84-19)
Stockholm June 1985.

1985
TR 85-20
Annual Research and Development Report 1985
Including Summaries of Technical Reports Issued during 1985. (Technical Reports 85-01-85-19)
Stockholm May 1986.

1986
TR 86-31
SKB Annual Report 1986
Including Summaries of Technical Reports Issued during 1986
Stockholm, May 1987

1987
TR 87-33
SKB Annual Report 1987
Including Summaries of Technical Reports Issued during 1987
Stockholm, May 1988

Technical Reports

1988
TR 88-01
Preliminary investigations of deep ground water microbiology in Swedish granitic rocks
Karsten Pedersen
University of Göteborg
December 1987

TR 88-02
Migration of the fission products strontium, technetium, iodine, cesium and the actinides neptunium, plutonium, americium in granitic rock
Thomas Ittner[1], Börje Torstenfelt[1], Bert Allard[2]
[1]Chalmers University of Technology
[2]University of Linköping
January 1988

TR 88-03
Flow and solute transport in a single fracture. A two-dimensional statistical model
Luis Moreno[1], Yvonne Tsang[2], Chin Fu Tsang[2], Ivars Neretnieks[1]
[1]Royal Institute of Technology, Stockholm, Sweden
[2]Lawrence Berkeley Laboratory, Berkeley, CA, USA
January 1988

TR 88-04
Ion binding by humic and fulvic acids: A computational procedure based on functional site heterogeneity and the physical chemistry of polyelectrolyte solutions
J A Marinsky, M M Reddy, J Ephraim, A Mathuthu
US Geological Survey, Lakewood, CA, USA
Linköping University, Linköping
State University of New York at Buffalo, Buffalo, NY, USA
April 1987

TR 88-05
Description of geophysical data on the SKB database GEOTAB
Stefan Sehlstedt
Swedish Geological Co, Luleå
February 1988

TR 88-06
Description of geological data in SKBs database GEOTAB
Tomas Stark
Swedish Geological Co, Luleå
April 1988

TR 88-07
Tectonic studies in the Lansjärv region
Herbert Henkel
Swedish Geological Survey, Uppsala
October 1987

TR 88-08
Diffusion in the matrix of granitic rock. Field test in the Stripa mine. Final report.
Lars Birgersson, Ivars Neretnieks
Royal Institute of Technology, Stockholm
April 1988

TR 88-09
The kinetics of pitting corrosion of carbon steel. Progress report to June 1987
G P Marsh, K J Taylor, Z Sooi
Materials Development Division
Harwell Laboratory
February 1988

TR 88-10
GWHRT – A flow model for coupled groundwater and heat flow
Version 1.0
Roger Thunvik[1], Carol Braester[2]
[1] Royal Institute of Technology, Stockholm
[2] Israel Institute of Technology, Haifa
April 1988

TR 88-11
Groundwater numerical modelling of the Fjällveden study site – Evaluation of parameter variations
A hydrocoin study – Level 3, case 5A
Nils-Åke Larsson[1], Anders Markström[2]
[1] Swedish Geological Company, Uppsala
[2] Kemakta Consultants Co, Stockholm
October 1987

TR 88-12
Near-distance seismological monitoring of the Lansjärv neotectonic fault region
Rutger Wahlström, Sven-Olof Linder, Conny Holmqvist
Seismological Depertment, Uppsala University, Uppsala
May 1988

TR 88-13
Validation of the rock mechanics HNFEMP code against Colorado school of mines block test data
Ove Stephansson, Tomas Savilahti
University of Luleå, Luleå
May 1988

TR 88-14
Validation of MUDEC against Colorado school of mines block test data
Nick Barton, Panayiotis Chryssanthakis, Karstein Monsen
Norges Geotekniske Institutt, Oslo, Norge
April 1988

TR 88-15
Hydrothermal effects on montmorillonite. A preliminary study
Roland Pusch
Ola Karnland
June 1988

TR 88-16
Swedish Hard Rock Laboratory
First evaluation of preinvestigations 1986-87 and target area characterization
Gunnar Gustafson
Roy Stanfors
Peter Wikberg
June 1988

TR 88-17
On the corrosion of copper in pure water
T E Eriksen[1], P Ndalamba[1], I Grenthe[2]
[1]The Royal Institute of Technology, Stockholm
Department of nuclear chemistry
[2]The Royal Institute of Technology, Stockholm
Department of inorganic chemistry
March 1988

TR 88-18
Geochemical modelling of the evolution of a granite-concrete-water system around a repository for spent nuclear fuel
Bertrand Fritz, Benoit Madé, Yves Tardy
Université Louis Pasteur de Strasbourg
April 1988

TR 88-19
A Bayesian nonparametric estimation of distributions and quantiles
Kurt Pörn
Studsvik AB
November 1988

TR 88-20
Creep properties of welded joints in OFHC copper for nuclear waste containment
Bo Ivarsson, Jan-Olof Österberg
Swedish Institute for Metals Research
August 1988

TR 88-21
Modelling uranium solubilities in aqueous solutions: Validation of a thermodynamic data base for the EQ3/6 geochemical codes
I Puigdomenech[1], J Bruno[2]
[1]Studsvik Nuclear, Nyköping
Environmental Services
[2]Royal Institute of Technology, Stockholm
Department of Inorganic Chemistry
October 1988

TR 88-22
Radiolysis of ground water: influence of carbonate and chloride on the hydrogen peroxide production
T E Eriksen[1], P Ndalamba[2], H Christensen[2], E Bjergbakke[3]
[1]The Royal Institute of Technology, Department of Nuclear Chemistry, S-100 44 Stockholm, Sweden
[2]Studsvik Energiteknik AB, S-611 82 Nyköping, Sweden
[3]Risö National Laboratory, DK-4000 Roskilde, Denmark
December 1988

TR 88-23
Source parameters of major earthquakes near Kiruna, northern Sweden, deduced from synthetic seismogram computation
W T Kim, E Skordas, Y P Zohu, O Kulhanek
Seismological Department, Uppsala University,
Box 12019, S-750 12 UPPSALA
June 1988

TR 88-24
Fission product concentration profiles (Sr, Xe, Cs and Nd) at the individual grain level in power-ramped LWR fuel
R S Forsyth, O Mattsson, D Schrire
Studsvik Nuclear, Nyköping
December 1988

TR 88-25
Postglacial faulting and paleoseismicity in the Lansjärv area, northern Sweden
Robert Lagerbäck
October 1988

TR 88-26
Geological evidence of smectite longevity The Sardinian and Gotland cases
Roland Pusch, Ola Karnland
Clay Technology AB
December 1988

TR 88-27
On the formation of a moving redoc-front by a-radiolysis of compacted water saturated bentonite
Trygve E Eriksen, Pierre Ndalamba
The Royal Institute of Technology, Stockholm
Department of Nuclear Chemistry

TR 88-28
Radionuclide transport in a single fissure A laboratory flow system for transport under reducing conditions
Trygve E Eriksen
The Royal Institute of Technology, Stockholm
Department of Nuclear Chemistry
December 1988

TR 88-29
Modelling of buffer material behaviour. Some examples of matierial models and performance calculations
Lennart Börgesson
Clay Technology AB, Lund, Sweden
December 1988